UNRESTRICTED **OP 02-30011**

Crawling of Pipelines under Cyclic Thermal Loading

Prepared by R. Peek
Reviewed by P.R. Paslay and W.T. Jones
Revised 4th January 2002

UNRESTRICTED

SHELL GLOBAL SOLUTIONS

EXECUTIVE SUMMARY

A pipe can crawl axially through the soil like a worm, if the following conditions prevail:

a) short lines (e.g. 1-5km, depending on size and degree of soil restraint)

b) high temperatures

c) start-up/shut down cycles involving high temperature gradients traveling down the line, especially when the shut-down line is flooded with cold liquid.

Damage due to pipe crawl has been documented in the literature for an on-land line in Canada, as well as for a subsea line in the North Sea. In this report a worst-case temperature history involving a temperature surge traveling down the line is considered. For this case it provides analytical and numerical solutions for the crawl rate, the forces needed to prevent crawl, and the optimal location for restraints provided to stop crawl. The analytical solutions provide insight into the phenomena, and can be used to validate computer models. However they should not be regarded as a substitute, to project-specific finite element analyses. Such analyses needed to be based on temperature and pressure histories from transient simulations of flow conditions during start-up and shut-down. Whereas for lines on sand, simple Coulomb friction models for soil resistance to axial movements appear to be adequate, for soft clay, the cyclic axial force-displacement relation needs to be properly characterised, including the effects of elastic soil deformations before the limiting frictional values of the resistance are reached. This requires attention when planning the soils investigation for the route.

TECHNICAL SUMMARY

Axial crawl of pipe/flowlines by worm action is driven by temperature gradients along the length of the line. Such temperature gradients are largest during transient start-up conditions, especially when start-up involves hot well products flowing into a liquid-filled, cold line. As a worst case, a traveling temperature surge is considered, in which the temperature rises from ambient to full operating conditions over a moving front of negligible length that travels down the line. For such a temperature surge, followed by uniform cooling, the following analytical solutions are derived for elastic pipes undergoing axial movements on a frictional surface:

a) The steady-state axial ratcheting displacement per cycle for an unrestrained pipe of length $L \leq L_{anchor}$ is

$$u_{cycle} = \tfrac{1}{4}\ L^2 f_0 / EA$$

in which L is the length of the line, EA the axial rigidity, f_0 the limiting axial friction force per unit length of the line, and $L_{anchor}=N_0/f_0$, where N_0 is the axial force that would be generated in the line due to the temperature change under axially fully constrained conditions. The crawl direction is downstream.

b) To prevent crawl by applying a constant tensile force at the upstream end, the magnitude of the force must be

$$P = {}^2/_3\, N_0 \{ [1 - L/L_{anchor} + (L/L_{anchor})^2]^{1/2} - 1 + \tfrac{1}{2}\ L/L_{anchor} \}$$

c) To prevent crawl by a unilateral restraint placed at the upstream end, the maximum force that must be resisted by the restraint is given by

$$P = f_0 L$$

This corresponds to the worst imaginable case, with all the available soil friction forces over the entire length acting in the same direction, thereby generating a large force to be resisted by the restraint.

d) The optimal location for a unilateral restraint along a line of length $L \leq L_{anchor}$ is a distance

$$x_{r,optimal} = \tfrac{1}{2} \{ L + L_{anchor} - (L_{anchor}^{\ 2} - L^2)^{1/2} \}$$

from the upstream end. This is a little downstream from the mid-line point.

e) To prevent crawl by a restraint placed at the optimal location, the maximum steady-state restraint force is

$$P = N_0\ [1 - (1-(L/L_{anchor})^2]^{1/2}$$

All the above-quoted analytical solutions have been verified by finite element analyses. One difference between the analytical and finite element solutions is that the former apply for a rigid-plastic soil resistance to axial movements, whereas the latter apply for an elastic-perfectly-plastic soil resistance function, in which the elastic soil displacement that can develop before slip starts is called the mobilisation displacement, and denoted by u_{mob}. A key parameter in this context is the non-dimensional mobilisation displacement, given by

$$[\, u_{mob} \,]_{nd} = u_{mob}\, EA\, f_0 / N_0^{\,2}$$

For a small mobilisation displacement (e.g. $[\, u_{mob} \,]_{nd} = 0.001$), the finite element solutions are in excellent agreement with the analytical ones, as they should be.

Examples show that for a single pipe on sand, the mobilisation displacement is indeed "small" in the sense that the analytical solution (for u_{mob}=0) provides good approximation. However, for a pipe-in-pipe system on soft clay, the soil elasticity strongly affects the behaviour. Indeed for a sufficiently large mobilisation displacement, axial ratcheting ceases.

Both analytical and numerical solutions for longer lines ($L > L_{anchor}$) indicate that crawl can also occur in these cases. Indeed axial forces in excess of N_0 in magnitude can be generated if one attempts to restrain a longer line by a single restraint. However these analyses do not take into account the diffusion of the temperature front. It is this diffusion that dissipates the temperature gradients. Once the temperature gradient falls below a critical value of

$$(dT/dx)_{critical} = f_0 / (\alpha EA)$$

where α is the coefficient of thermal expansion, the temperature gradient by itself is no longer sufficient to cause slip. Slip then occurs only near the ends of the line.

TABLE OF CONTENTS

1. INTRODUCTION

The term "worm action" is to be used here to describe the movement of pipelines in the axial direction, that can occur if the pipeline undergoes a history of axial expansions and contractions like those which a worm uses to push his way through the soil. The phenomenon is associated with spatial gradients in temperature that vary over time in a detrimental way. It is not unknown: Konuk [1] attributed the buckling of a line in Canada to this, with the amplitude of the buckle growing gradually with increasing feed of the pipe into the buckle by such worm action. Koh supported his assessment by analytical and numerical solutions. Not much later Tornes et al. [2] reported the failure of spools connecting a short line due to axial ratcheting. Tornes et al. were able to reproduce this phenomenon by finite element simulation, which they also used to evaluate remediation strategies to prevent further movement of the line after the broken spools had been replaced.

Other terms that have been used to describe such worm action include "pipe crawl" and "axial ratcheting".

In this report analytical and numerical solutions are given for what is probably the most severe loading condition in regard to worm action: a temperature surge that travels down the line, followed by uniform cooling. Formally such a temperature surge can be described as

$$\Delta T(x,\xi) = \begin{cases} \Delta T_0 & \text{if } x < \xi \\ 0 & \text{if } x > \xi \end{cases} \tag{1.1}$$

where

ΔT = temperature rise above ambient conditions

ΔT_0 = maximum temperature rise (constant)

x = the axial coordinate along the length of the pipe,

ξ = time-like parameter with units of length that describes how far the temperature surge has traveled along the line (If time needs to be included explicitly in the formulation then ξ would need to be replaced by ct, where t denotes time and c the speed at which the temperature surge travels).

This type of loading arises for instance for a flowline that is full of cold oil before start-up from a high temperature field.

Eq. 1.1 describes a sharp temperature surge: the temperature change rises sharply from zero to the maximum value over infinitesimal length of pipe. Of course the laws of heat conduction do not allow such infinite temperature gradients. In reality the temperature rise will occur over some length of pipe. This rise length is denoted by X_{rise}. The analytical solutions provided are for the case $X_{rise} = 0$ only, but finite element solutions are also provided to investigate the effect of this parameter in terms of key dimensionless variables.

Another parameter that is investigated in the finite element analyses is the mobilisation displacement, u_{mob}. That is the displacement needed before the axial friction force is developed. It is taken to be $u_{mob}=0$ for the analytical solutions.

The analytical solution can be used as

- a screening criterion,

- to validate finite element simulations of the crawl phenomenon,
- to improve the insight into the phenomena involved,
- to better understand the effect of the various parameters that determine the crawl rate (if any).

However this investigation is not intended to replaced project-specific detailed finite element analyses based temperature histories from transient simulations of start-up/shut-down conditions, where pipe crawl is found to be a potentially critical issue.

2. PROBLEM FORMULATION

2.1. Formulation for Analytical Solutions

For axial loading and deformation only, the response of an elastic pipe laying on a frictional surface is described by the following:

$$N' = f \tag{2.1}$$

$$N = EA\,u' + N_c \tag{2.2}$$

$$\begin{aligned} f &= f_0 && \text{if } v>0 \\ &= -f_0 && \text{if } v<0 \\ -f_0 \le f &\le f_0 && \text{if } v=0 \end{aligned} \tag{2.3}$$

in which a prime as in (.)' denotes differentiation with respect to the axial coordinate x, and

N = effective axial force in the line, positive for tension

N_c = effective axial force due to the temperature and pressure changes for an axially constrained line (this is taken to be a known function of the axial coordinate and the time parameter, which describes the loading)

f = axial friction force per unit length (positive when the friction force arises from movement of the pipe in the positive x direction)

f_0 = limiting value of the friction force ($f = \pm f_0$ when slip occurs)

EA = axial rigidity of the pipe (has units of force)

u = displacement (positive in the positive x direction)

v = velocity (partial derivative of the displacement u with respect to the time parameter for a fixed value of the axial coordinate x)

The first of the above equations is an equilibrium condition derived from the balance of axial forces acting on an infinitesimal pipe element shown in Figure 2.1. Note that the force N includes any axial force transmitted via the pressurised contents of the pipe as well as that transmitted via the pipe wall. As such N is known as the effective axial force.

For a temperature surge traveling along the line, the fully constrained axial force is given by

$$\begin{aligned} N_c &= -N_0 && \text{for } x < \xi \\ &= 0 && \text{for } x > \xi \end{aligned} \tag{2.4}$$

in which

$$N_0 = EA\,\alpha\,\Delta T_0 \tag{2.5}$$

is the fully constrained axial force due to the maximum temperature change, ΔT_0 denotes the maximum temperature change, and α the coefficient of thermal expansion.

For free ends of the pipe the boundary conditions are,

$$N = 0 \qquad \text{at } x = 0, L \tag{2.5}$$

where L denotes the length of the line.

To find the solution for a given loading $N_c=N_c(x,\xi)$, one must find $u=u(x,\xi)$ satisfying the appropriate initial conditions (typically $u(x,0)=0$), such that the axial force $N=N(x,\xi)$

calculated from Eq. 2.2 satisfies the equilibrium condition Eq. 2.1 and the boundary conditions Eq. 2.5.

2.2. Dimensionless Formulation for Analytical Solutions

The analytical solutions are much more easily derived and stated in a dimensionless form. Another advantage of the non-dimensionalisation is that the important dimensionless ratios governing the behaviour of the line emerge automatically, and provide a good framework for a parameter study in which only essential parameters are investigated.

For simplicity the same symbols will be used for the dimensional and dimensionless variables. However, where the intended meaning is not clear from the context, the dimensionless variables will be enclosed in square brackets with a subscript "nd". Thus for instance $[N]_{nd}$ denotes the non-dimensional value of the effective axial force.

The relationship between the dimensional variables and their non-dimensional counterparts is as follows:

$$x = L_{anchor} [x]_{nd} \tag{2.6}$$

$$L = L_{anchor} [L]_{nd} \tag{2.7}$$

$$N = N_0 \; [N]_{nd} \tag{2.8}$$

$$u = \{ N_0^2/(EA\, f_0) \} \; [u]_{nd} \tag{2.9}$$

in which

$$L_{anchor} = N_0 / f_0 \tag{2.10}$$

Henceforth only the non-dimensional variables are used, unless otherwise noted. The formulation of the problem (Eqs. 2.1 to 2.5) then reduces to

$$N' = f \tag{2.11}$$

$$N = u' + N_c \tag{2.12}$$

$$\begin{aligned} f &= 1 && \text{if } v>0 \\ &= -1 && \text{if } v<0 \\ -1 \le f &\le 1 && \text{if } v=0 \end{aligned} \tag{2.13}$$

The loading function becomes

$$\begin{aligned} N_c &= -1 && \text{if } x < \xi \\ &= 0 && \text{otherwise} \end{aligned} \tag{2.14}$$

And the boundary conditions for zero end forces remain:

$$N = 0 \qquad \text{for } x = 0, L \tag{2.15}$$

except that L now becomes the non-dimensional pipe length.

Thus essentially the non-dimensional problem formulation is identical to the original one, but with $EA=N_0=f_0=1$. One can use those values of the problem parameters with no loss of generality, provided that the results are interpreted as the non-dimensional quantities of Eqs. 2.6 to 2.9.

For the solutions presented here, a successful strategy to derive analytical solutions is as follows:

1) Start with a guess in regard to what parts of the pipe slip in what direction. There is a discontinuity in the velocity v at the surge front, and for this reason the surge front is typically (but not necessarily) a location where the direction of slip changes.
2) From the assumed slip directions obtain the soil friction forces f (from Eq. 2.13) and integrate those (using Eq. 2.11) together with the boundary conditions (Eq. 2.15) to obtain a trial axial force diagram (AFD). This can also be done geometrically by using the following rules:
    a) The values of the axial force at the ends are given by the boundary conditions.
    b) The AFD must be continuous everywhere with a slope that does not exceed 1 in magnitude. (Jumps in the AFD are only possible where a concentrated force is applied to the pipe.)
    c) In regions of no slip the change in axial force at any location x is equal to the change in the known fully constrained axial force, N_c .
    d) In the regions of slip, the slope of the AFD is ±1. The AFD slopes upward in the direction of slip.
3) Integrate the AFD (using Eq. 2.12) to obtain a trial displacement history $u=u(x,\xi)$. Differentiate these displacements with respect to ξ to obtain the velocity v.
4) Check that the assumptions made for the direction of the velocity in Step 1 are correct. If not, try again, e.g. using a more general assumption in regard to the slip directions (e.g. involving some unknown parameters that can later be adjusted to satisfy the slip conditions).

Illustrations of this solution strategy for particular cases are given in Section 3.

2.3. Finite Element Formulation

The case of a pipe undergoing axial loading and deformations only is a special case of the more general pipe formulations available in various standard finite element codes. Indeed it is sufficient to use a truss element (bar element) if one constrains the lateral displacements. For the analyses reported here a simple element was developed, with no extra baggage (such as un-used degrees of freedom) that would slow down the execution time. That way simulations could be performed for a large number of cycles relatively quickly. The FORTRAN source code for this element is included in Appendix C.

There are some differences between the finite element and analytical formulations that must be borne in mind: One is the mobilisation displacement u_{mob} which is introduced in the finite element formulation to avoid infinite stiffnesses. "Stick behaviour" occurs as long as the friction force is below the limiting value f_0. For such stick behaviour the soil behaves as a linear spring with stiffness $k_s = f_0 / u_{mob}$. Once the limiting value of the soil friction force is reached, further increases in the displacement no longer affect the soil friction force. However a reversal in the direction of the displacement increments will again give rise to stick behaviour with a linear relationship between the increments in displacement and soil friction force. More formally the algorithm for calculating the soil friction force at each loadstep of an incremental solution procedure is as follows:

1. Start with the soil friction force f at the last converged loadstep, and the displacement increment δu for the current loadstep.

2. Calculate an elastic predictor value of the soil friction force from
   $f_{el} = f + k_s\, \delta u$
3. If $| f_{el} | \le f_0$ then stick behaviour applies for the loadstep, and the new value of the soil friction force is given by
   $f = f_{el}$
   Otherwise the new value of the friction force is given by
   $f = \mathrm{sgn}\,(f_{el})\; f_0$
   in which sgn(.) denotes the sign function, defined by $\mathrm{sgn}(x) = x/\,|x|$ for $x \neq 0$, $\mathrm{sgn}(x)=0$ otherwise.

Another difference between the analytical and finite element solutions is that for the finite element solutions the temperature change is not a sudden step function, but rather the temperature rises linearly over a finite length of pipe denoted by X_{rise}.

2.4. Equivalent Loading

Some physical insight as to why temperature surges produce ratcheting can be achieved by deriving an equivalent (non-thermal) loading as follows:

(a) Consider the pipe undergoing a temperature surge as indicated in Figure 2.2a. (The temperature surge is traveling downstream, from left to right in Figure 2.2a.) This produces displacements $u=u(x,\xi)$ that are unknown.

(b) The external loads that would need to be applied concurrently with the temperature surge to prevent axial displacements are shown in Figure 2.2b. They consists of a compressive force of magnitude N_0 at the upstream end, plus an equal and opposite moving load at the location of the surge.

(c) To recover the loading of Figure 2.2a, one must superpose external forces that are equal and opposite to those in Figure 2.2b.

By applying the principle of superposition[i], it may be concluded that the displacements for loading (a) in Figure 2.2, are the same as those for loading (c). In other words, the temperature surge is equivalent to a moving axial load of magnitude N_0 acting in the downstream direction at the surge front, balanced by an equal and opposite load at the upstream end.

The equivalent moving load reaches the downstream end when the entire line is hot. Uniform cooling is then equivalent to uniformly decreasing the end loads to zero. This history of equivalent loading is then repeated for subsequent cycles. When considering such equivalent loading, it is not surprising that the line tends to “crawl” in the downstream direction.

This equivalent problem also applies for the case when there is a non-zero mobilisation displacement for the soil friction force. If the temperature surge is replaced by a linear

---

[i] In general the principle of superposition does not apply to nonlinear problems, but here the argument only relies on applying the principle to the pipe, while regarding the soil friction forces as given loads. The argument goes as follows: (i) Start with the solution to loading (c). (ii) Apply the temperature and external loads in (b) while regarding the soil friction forces as a given external load. This does not change the displacements. (iii) The solution thus constructed satisfies all the required conditions for loading (a). Hence the displacements for loadings (a) and (c) are the same. The distribution of soil friction forces f are also the same, but the stresses differ by an amount N_0 in the heated portion of the line.

variation of temperature over a length X_{rise} , then the equivalent moving load N_0 must be spread out over the rise length X_{rise}.

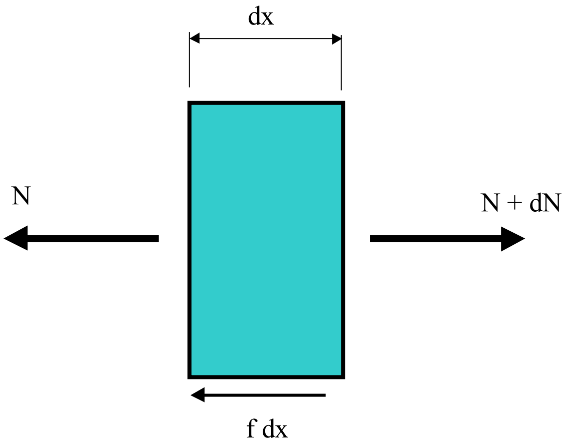

Figure 2.1: **Forces acting on an infinitesimal element of the pipe. (The element shown includes the fluid within the pipe.)**

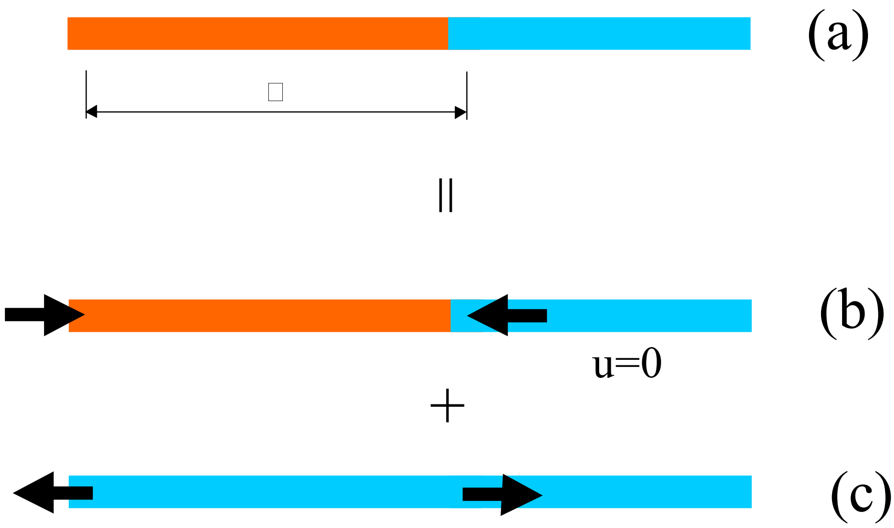

Figure 2.2: **Application of superposition principle, to determine external forces that are equivalent to the temperature surge in the sense that they produce the same displacements. (The forces in (c) are equivalent to the temperature surge in (a).)**

3. SHORT LINE – ANALYTICAL SOLUTION

The problem solved in this section is that of a line of length L, that is free to move axially at both ends, but at the upstream end a constant axial tensile force P is applied. Each cycle of loading consists of passage of the temperature surge followed by uniform cooling. The solution derived in this section applies for a sufficiently short pipe. It will be seen that in this case, the solution of this problem is simple, and the 3rd and subsequent cycles are identical to the 2nd one. Throughout this section all symbols refer to the dimensionless values of the variables. The time-like parameter used to describe the process is denoted by ξ during heating, and by ζ during cooling. There is no single expression for the stresses and displacements that is valid throughout the entire heating or cooling of the line. Instead both the heating and cooling processes are divided into different stages. In what follows a separate sub-section is devoted to each of these stages.

First Heating with $0 < \xi < P$

The application of the axial tensile load P will produce upstream slip. This means an AFD that slopes downward in the downstream direction. Also from the boundary condition the AFD must start with N=P at the upstream end. This results in the AFD shown in Figure 3.1. This AFD does not change at the start of heating, as long as $\xi < P$. The heating merely increases the amount of upstream slip in the region $0<x<\xi$.

Integration of Eq. 2.12 using the condition that the displacement is zero at point B in Figure 3.1, leads to the conclusion that the displacement at any location $\xi < x < P$ is negative (i.e. upstream) and equal in magnitude to the area under the AFD to the right of the location considered. Thus

$$u = -\tfrac{1}{2}(P - x)^2 \qquad \text{for } \xi < x < P \tag{3.1}$$

Within the heated part of the line the displacement will also be affected by the temperature rise in the hot portion of the line to the right of the location considered. This contributes a displacement increment $-(\xi\text{-}x)$, so that

$$u = x - \xi - \tfrac{1}{2}(P - x)^2 \qquad \text{for } 0 < x < \xi \tag{3.2}$$

Differentiating these expressions with respect to ξ gives the following expressions for the velocity

$$v = 0 \qquad \text{for } \xi < x < P \tag{3.3}$$

$$v = -1 \qquad \text{for } 0 < x < \xi \tag{3.4}$$

Thus the slip conditions (Eqs. 2.13) are also satisfied.

First Heating with $P < \xi < a$

This stage starts when the heating front goes beyond point B in Figure 3.1. At $\xi = P$, the velocity just upstream of the heating front is $v = -1$, and this is not expected to jump to a zero or negative value. Therefore the axial force will have to become compressive at the surge front. This in turn implies downstream slip at the downstream side of the surge, which then gives rise to the trial AFD of Figure 3.2. Again there are two contributions to the displacements:

- those due to axial forces in the line equal to the area under the AFD to the right of the location where the displacement is to be determined, and
- those due to the temperature change, equal to the length of hot line to the downstream side of the location considered

Thus one obtains

$$
\begin{aligned}
u &= 0 && \text{for } x_D \le x \le L \text{ (region DE in Fig. 3.2)}\\
&= \tfrac{1}{2}(x_D - x)^2 && \text{for } \xi \le x \le x_D \text{ (region CD in Fig. 3.2)}\\
&= \tfrac{1}{2}(\xi - P)^2 + (\xi - x)(\xi - P - 1) - \tfrac{1}{2}(\xi - x)^2 && \text{for } 0 \le x \le \xi \text{ (region AC in Fig. 3.2)} \quad (3.5)
\end{aligned}
$$

in which

$$x_D = 2\,\xi - P \tag{3.6}$$

represents the coordinate of point D in Fig. 3.2. Considering this in the differentiation of the displacement with respect to the time parameter ξ gives,

$$
\begin{aligned}
v &= 0 && \text{for } x_D \le x \le L \text{ (region DE in Fig. 3.2)}\\
&= 2\,(x_D - x) && \text{for } \xi \le x \le x_D \text{ (region CD in Fig. 3.2)}\\
&= 2\,(\xi - P) - 1 && \text{for } 0 \le x \le \xi \text{ (region AC in Fig. 3.2)} \quad (3.7)
\end{aligned}
$$

It is clear that in region CD the slip condition $v \ge 0$ is satisfied, since $x \le x_D$ in that region. In region AC, the slip condition $v \le 0$ can be reduced to

$$\xi \le P + \tfrac{1}{2} \tag{3.8}$$

This heating stage continues until the slip front (point D_ξ in Fig. 3.2) reaches the end of the line, which occurs when $\xi = a$, where

$$a = \tfrac{1}{2}(L + P) \tag{3.9}$$

Thus in order for the solution for this stage to be valid, the line must be sufficiently short so that

$$L \le 1 + P \tag{3.10}$$

The end displacements at the end of this heating stage can be calculated by substituting $x=0$, L and $\xi=a$ into Eq. 3.5, to obtain

$$u_{ends(\xi=a)} = \{\, -\tfrac{1}{4}\,[\,2L - L^2 + 2P(1+L) + P^2\,]\,,\ \ 0\ \} \tag{3.11}$$

where the first expression in the brackets denotes the displacement at the upstream end, and the second (after the comma) denotes the displacement at the downstream end.

The above expression for the displacement at the upstream end can also be derived more simply from the geometry of the AFD when $\xi=a$ to obtain

$$u_{ends(\xi=a)} = \{\, b^2 - \tfrac{1}{2}P^2 - a\ \ ,\ \ 0\ \} \tag{3.12}$$

where

$$b = \tfrac{1}{2}(L - P) \tag{3.13}$$

By substituting for a and b it can be verified that both expressions are equivalent, as they should be.

First Heating with $a < \xi < L$

This stage is initiated when the slip front (point D in Figure 3.2) reaches the end of the line. Thereafter, further movement of the temperature surge from $\xi = a$ to $\xi = L$ produces no change in the AFD. This AFD is shown in Figure 3.3. The progression of the heating front is accommodated by slip in the part of the line that is still cold ($\xi < x \leq L$), with a velocity v=1. Throughout the hot part the velocity is zero. Thus during this stage the displacement at the downstream end (x=L) goes from u=0 to u=b. The increment in end displacements during this stage of heating is given by

$$\begin{aligned} \Delta u_{ends} &= \{ 0 , \ b \} \\ &= \tfrac{1}{2} (L - P) \{ 0 , 1 \} \end{aligned} \tag{3.14}$$

The end of this stage is the end of the first heating cycle. The total end displacements at the end of this stage are given by

$$\begin{aligned} u_{ends(\xi=L)} &= u_{ends(\xi=a)} + \Delta u_{ends} \\ &= \{ b^2 - \tfrac{1}{2} P^2 - a , \ b \} \end{aligned} \tag{3.15}$$

Cooling, $0 < \zeta < 2b$

The cooling is assumed uniform. Thus during cooling, the constrained axial load can be written as

$$N_c(x,\zeta) = 1 - \zeta \tag{3.16}$$

in which ζ is the time-like parameter used to describe the cooling process. It ranges from $\zeta=0$ when the entire line is hot to $\zeta=1$ when the line is fully cooled to ambient conditions. In absence of slip, such cooling simply moves the AFD upwards. However to satisfy the force boundary conditions at the ends of the line, some regions of slip develop there, resulting in the AFD shown in Figure 3.4. The displacements arise due to the difference between the actual AFD and the translated AFD. More specifically the increment in the end displacement due to cooling is the area between the actual and translated AFD's. This implies inward displacement increments of $\tfrac{1}{4} \zeta^2$ at each end, due to cooling. This stage continues until $\zeta=2b$. At that point the total inward displacement increment of b^2 at each end, and the AFD is that of Figure 3.5. Thus the end displacement increments during this stage can be written as

$$\Delta u_{ends} = b^2 \{ 1 , -1 \} \tag{3.17}$$

Cooling, $2b < \zeta < 1$

During this stage the uniform thermal contraction can be accommodated with slip in opposite directions at each side of the apex of the AFD (Point H), and no change in the AFD. The displacement increments that develop during this stage are

$$\Delta u_{ends} = (1\text{-}2b) \{ b, -a \} \tag{3.18}$$

The end of this stage is also the end of the cooling cycle. By adding the end displacement increments for both cooling stages, one obtains:

$$\Delta u_{ends,\ cooling} = \{ b - b^2 \ , \ -a (1 - 2b) - b^2 \} \tag{3.19}$$

The total end displacements at the end of the first cycle (including application of the load P, heating and cooling) can then be calculated as

$$
\begin{aligned}
u_{ends(\zeta=1)} &= u_{ends(\xi=L)} + \Delta u_{ends,\ cooling} \\
&= \{ -P\,(1 + P/2)\ ,\ \tfrac{1}{4}\ L^2 - P\,(1 - L/2) - \tfrac{3}{4}\,P^2\ \}
\end{aligned} \tag{3.20}
$$

The final AFD at the end of the first cycle is shown in Figure 3.6. The maximum axial force is N=a (in tension). These are the residual stresses due to reversal of axial slip.

Second Heating, $0 \le \xi \le a$

For the second cycle it is cumbersome to work with expressions for the total displacement u. Instead the additional displacement that occurs after the end of the first cycle will be used, and denoted by $w=w(x, \xi)$. The velocity is then the derivative of w with respect to the time parameter ξ. The displacements w arise due to

a) the strain increments due to the change in the AFD diagram after the end of the first cycle, and

b) the thermal strains due to heating of part of the line

Again a reasonable guess is that heating will produce upstream slip on the upstream side of the heating front and downstream slip on the downstream side. This then results in the AFD in Figure 3.7. The regions of slip are also indicated in Figure 3.7. There is no slip (w=0) in region JD of Figure 3.7.

For a location x upstream of point J in Figure 3.7, the contributions to the displacement increment $w=w(x,\xi)$ are

a) a positive contribution equal to the area of the portion of the rectangle AIJH in Figure 3.7 that is downstream of the location x, and

b) a negative contribution consisting of the length of heated pipe downstream from the location x

To obtain expressions for the displacements in the same manner as before, one would need to distinguish between different stages depending on whether point I in Figure 3.7 is upstream or downstream of point H (i.e. depending on whether $\xi < b$ or not). However this can be avoided by using a step function H(.) and its integrals to obtain the following expression for $w=w(x,\xi)$ valid for $0 \le \xi \le a$:

$$
w = 2\ \{ H^{(-2)}(b + \xi - x) - H^{(-2)}(b - x) - H^{(-2)}(\xi - x) \} - H^{(-1)}(\xi - x) \tag{3.21}
$$

in which for any argument, x,

$$
\begin{aligned}
H(x) &= 1 \qquad && \text{for } x > 0 \\
&= 0 && \text{otherwise}
\end{aligned} \tag{3.22}
$$

and $H^{(-n)}(x)$ denotes the n^{th} integral of H(x), so that

$$
\begin{aligned}
H^{(-1)}(x) &= x \qquad && \text{for } x > 0 \\
&= 0 && \text{otherwise}
\end{aligned} \tag{3.23}
$$

$$
\begin{aligned}
H^{(-2)}(x) &= \tfrac{1}{2}\,x^2 \qquad && \text{for } x > 0 \\
&= 0 && \text{otherwise}
\end{aligned} \tag{3.24}
$$

Differentiating the expression for the displacement with respect to ξ gives the following expressions for the velocity:

$$
\begin{aligned}
v &= 2\{ H^{(-1)}(b + \xi - x) - H^{(-1)}(\xi - x) \} - H(\xi - x) \\
&= 2b - 1 \qquad \text{for } 0 \le x < \xi \\
&= 2 (b + \xi - x) \qquad \text{for } \xi < x \le b + \xi \\
&= 0 \qquad \text{for } b + \xi \le x \le L
\end{aligned} \tag{3.25a-d}
$$

It follows directly from Eq. 3.25b that the slip condition $v \ge 0$ downstream from the heating front (where $\xi < x \le b+\xi$) is satisfied. For the heated portion of the line ($0 \le x < \xi$), the slip condition $v \le 0$ can be reduced to

$$L \le 1 + P \tag{3.26}$$

which again is satisfied for a sufficiently short line.

This heating stage continues until point J (in Figure 3.7) reaches the end of the line. When that happens, the AFD is that shown in Figure 3.8, and the end displacement increments are given by

$$w_{ends(\xi=a)} = \{ 2ab - a \;,\; 0 \} \tag{3.27}$$

Comparing the AFD's in Figure 3.3 and Figure 3.8 reveals that they are identical. Hence the subsequent stages will be identical to those for the first cycle with respect to the axial force diagrams, and the displacement increments for each stage.

Subsequent Stages (As for First Cycle)

The AFD at $\xi=a$ for the second cycle is the same as that for the first cycle at the same value of ξ. Therefore subsequent stages are essentially repetitions of previous stages. In particular the axial forces and displacement increments are the same. Thus the total end displacement increment for the second heating and cooling cycles are

$$
\begin{aligned}
w_{ends(\xi=L)} &= w_{ends(\xi=a)} + \{ 0 , b \} \\
&= \{ a (2b - 1) \;,\; b \}
\end{aligned} \tag{3.28}
$$

$$
\begin{aligned}
\Delta w_{ends,\ cooling} &= \Delta u_{ends,\ cooling} \\
&= \{ b - b^2 \;,\; - a (1 - 2b) - b^2 \}
\end{aligned} \tag{3.29}
$$

so that the total end displacement increments for the second cycle are

$$
\begin{aligned}
w_{ends(\zeta=1)} &= w_{ends(\xi=L)} + \Delta w_{ends,\ cooling} \\
&= [\, \tfrac{1}{4} L^2 - P (1 - L/2) - \tfrac{3}{4} P^2 \,] \; \{ 1 , 1 \}
\end{aligned} \tag{3.30}
$$

The equality of these displacement increments at both ends of the line is not a coincidence, but a necessary consequence of having reached a steady state ratcheting condition: Since the line always returns to the same AFD at the end of each cycle, there can be no change in length. Indeed the displacement increments per cycle must be the same at any location x along the line.

All the results given for the second cycle also apply for all subsequent cycles. The axial ratcheting displacement per cycle is given by

$$u_{cycle} = \tfrac{1}{4} L^2 - P (1 - L/2) - \tfrac{3}{4} P^2 \tag{3.31}$$

This displacement can be positive (i.e. downstream) or negative (i.e. upstream) depending on the value of the tension force P at the upstream end. For no applied load, the displacement per cycle is ¼ L^2 in the downstream direction. The value of this force for which the ratcheting displacement vanishes is given by

$$P = {}^{2}/_{3} \{ [1 - L + L^2]^{1/2} - 1 + L/2 \} \tag{3.32}$$

Typical values of this force are shown in Table 3.1. For instance if the length of the line is half the anchor length (L_{anchor} of Eq.2.10), a constant force of 7.7% of the temperature-induced axial force under fully constrained conditions is enough to prevent ratcheting. For short lengths the force needed is rather small. What is remarkable is that the solution remains valid for arbitrarily large lengths: Inequality 3.10 remains valid because the increase in the length L is followed by a corresponding increase in the required axial force P to prevent ratcheting. Extended validity of the solution does not imply extended validity of the assumptions on which this solution relies, however. In particular the assumption of a sharp temperature surge cannot remain valid for a long line, since the heating front will become increasingly diffuse as it travels along the line.

Table 3.1: Magnitude of a constant force at the upstream end needed to prevent ratcheting.

Dimensionless Length of Line, L	0.1	0.2	0.5	1	2	5
Dimensionless Tensile force at upstream, P	0.003	0.011	0.077	0.333	1.15	4.06

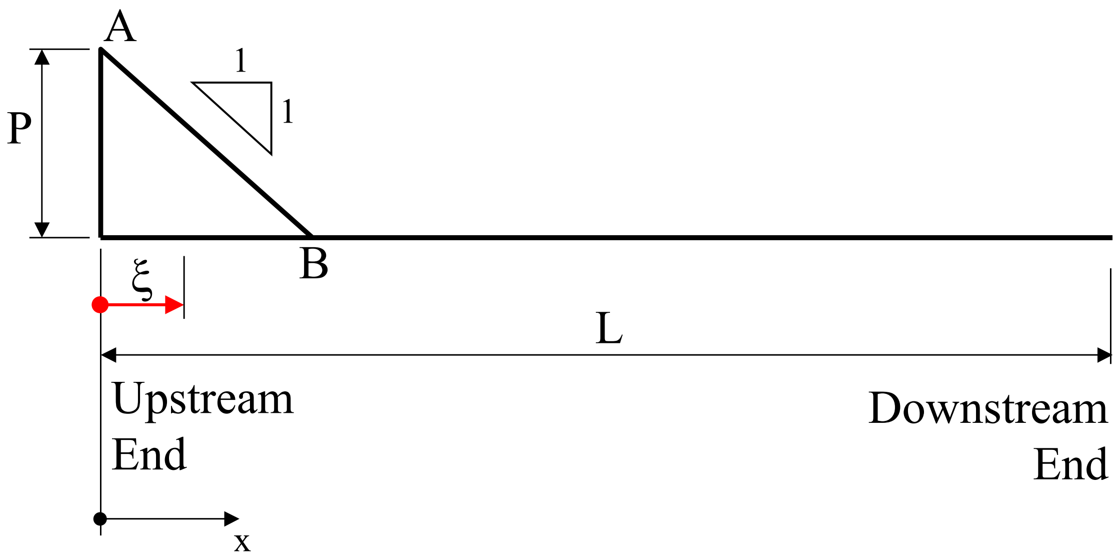

Figure 3.1: **Axial force diagram (AFD) during first cycle heating in the range 0≤ξ≤P for a short line with a tensile force P applied at the upstream end.**

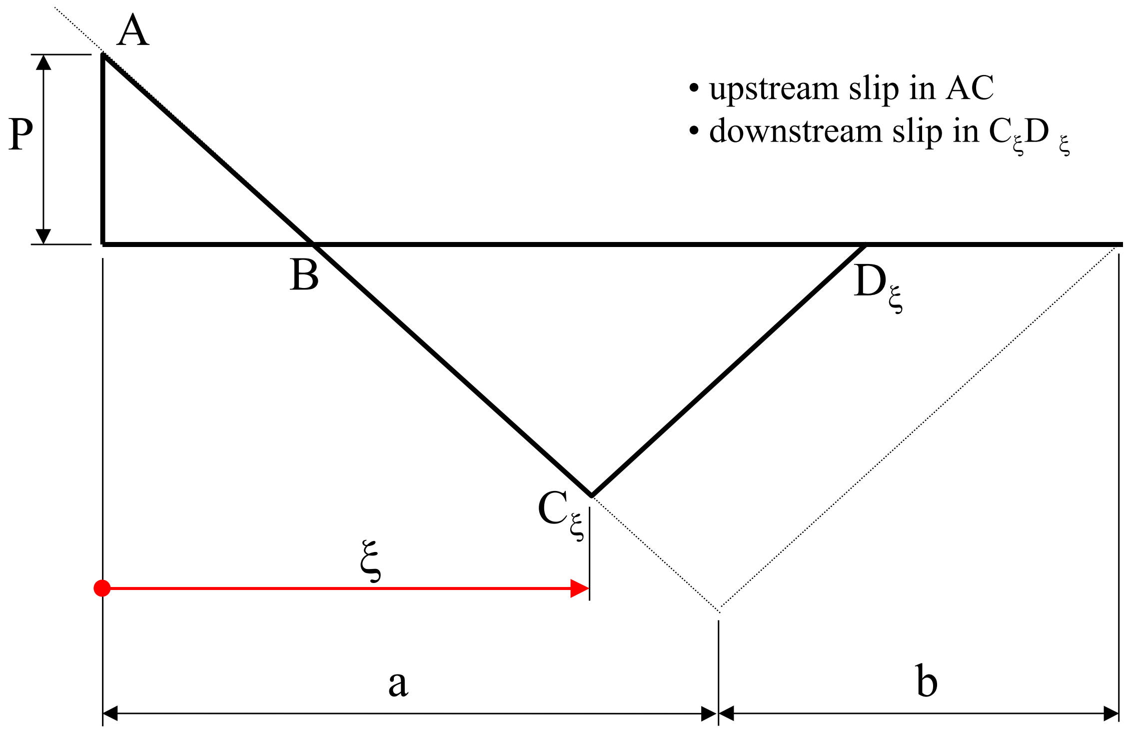

Figure 3.2: **AFD for first cycle heating in the range P ≤ ξ ≤ a.**

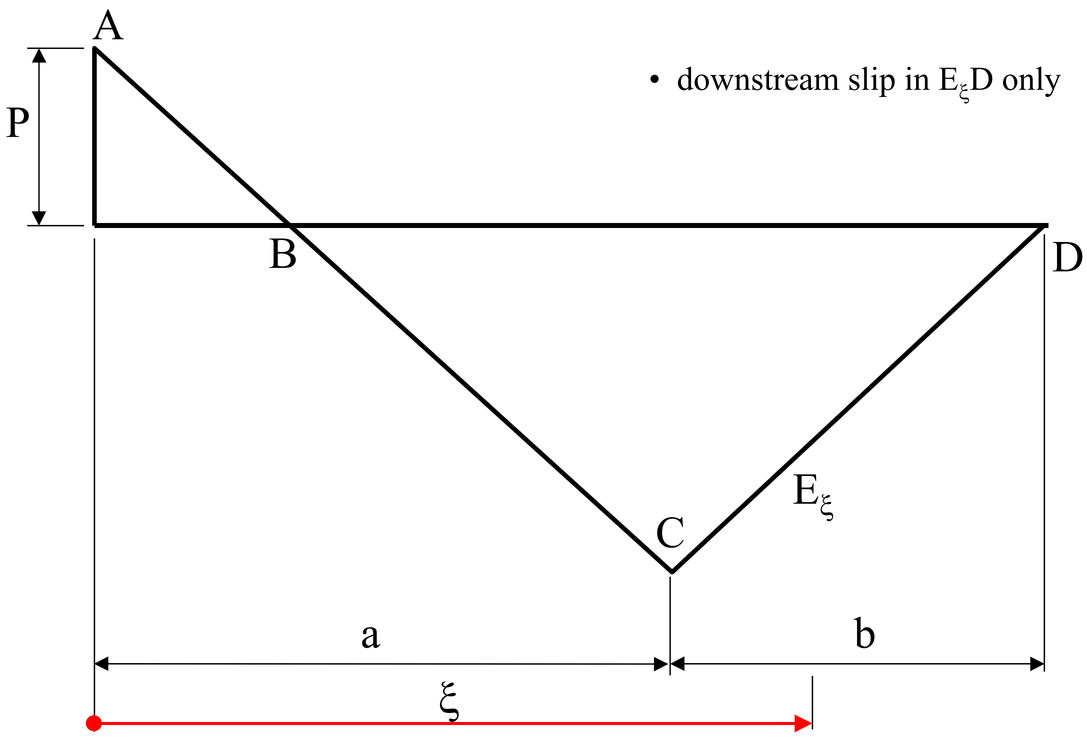

Figure 3.3: AFD during first cycle heating in the range a < ξ < L.

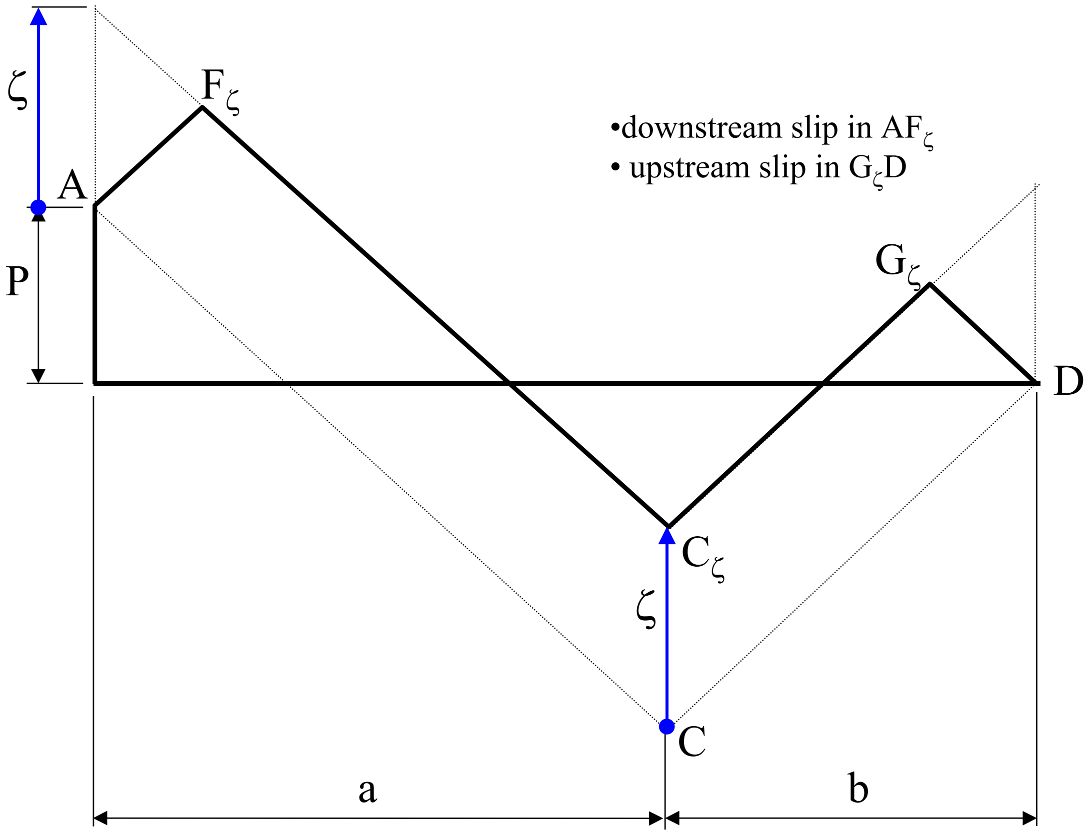

Figure 3.4: AFD during uniform cooling in the range 0≤ζ≤2b.

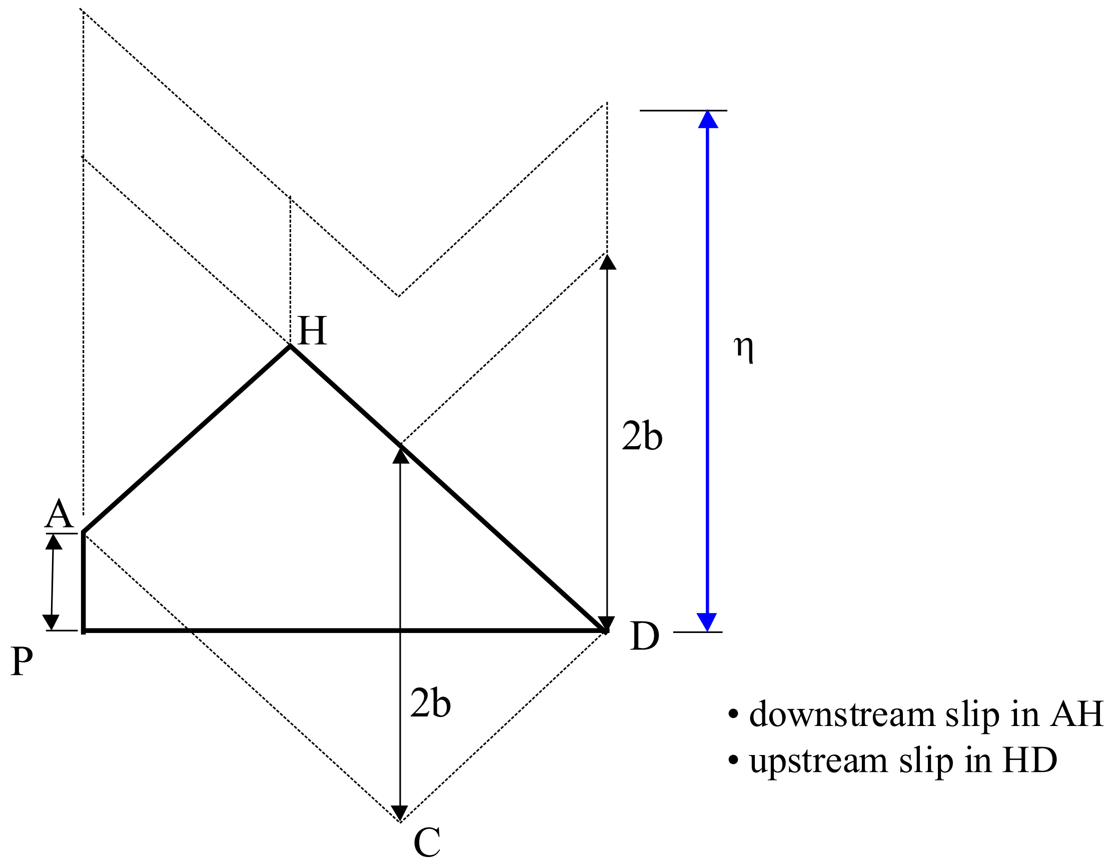

Figure 3.5: AFD during uniform cooling in the range 2b≤ζ≤1.

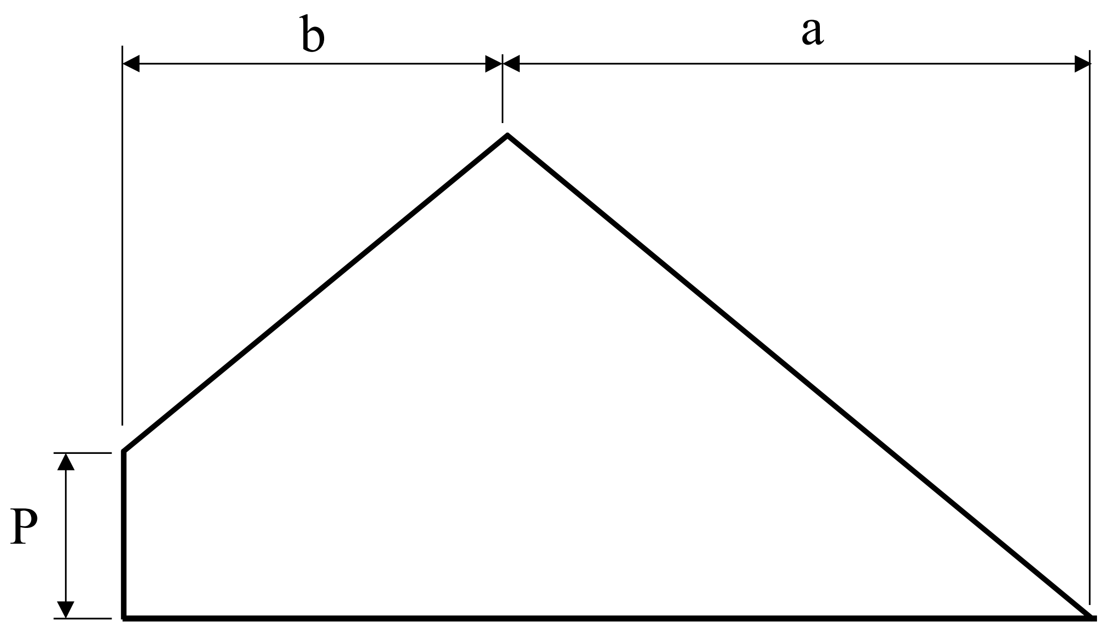

Figure 3.6: Residual AFD at end of one or more heating and cooling cycles. (ζ=1, ξ=0.)

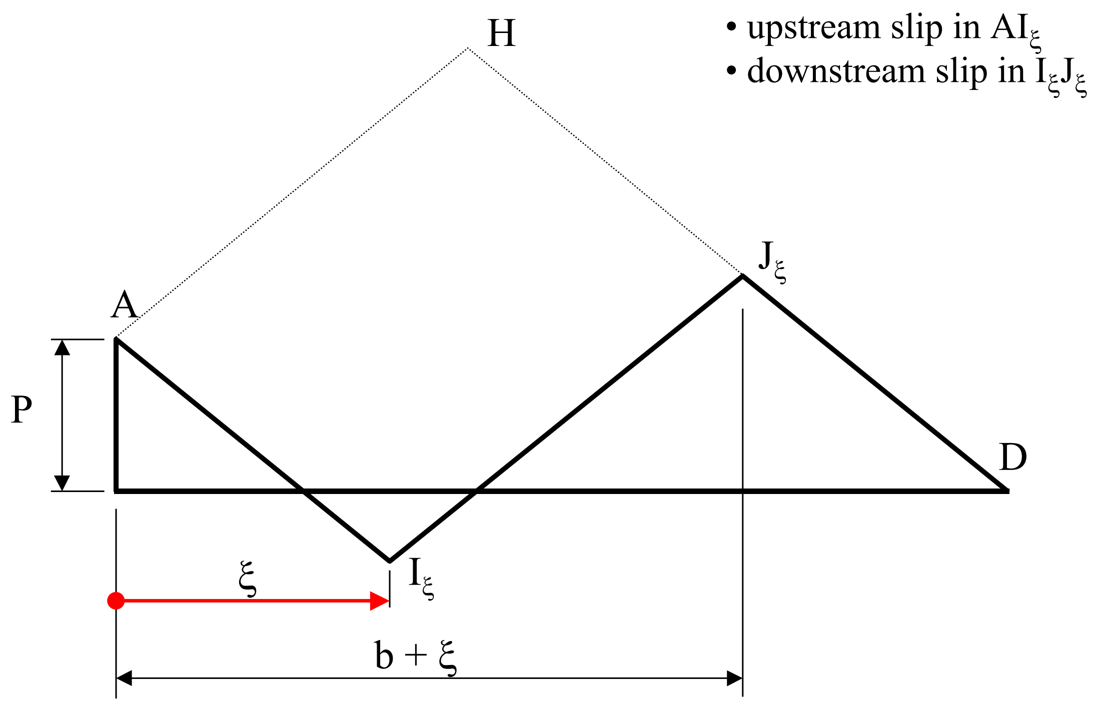

Figure 3.7: **AFD during 2nd cycle heating in the range $0 \le \xi \le a$.**

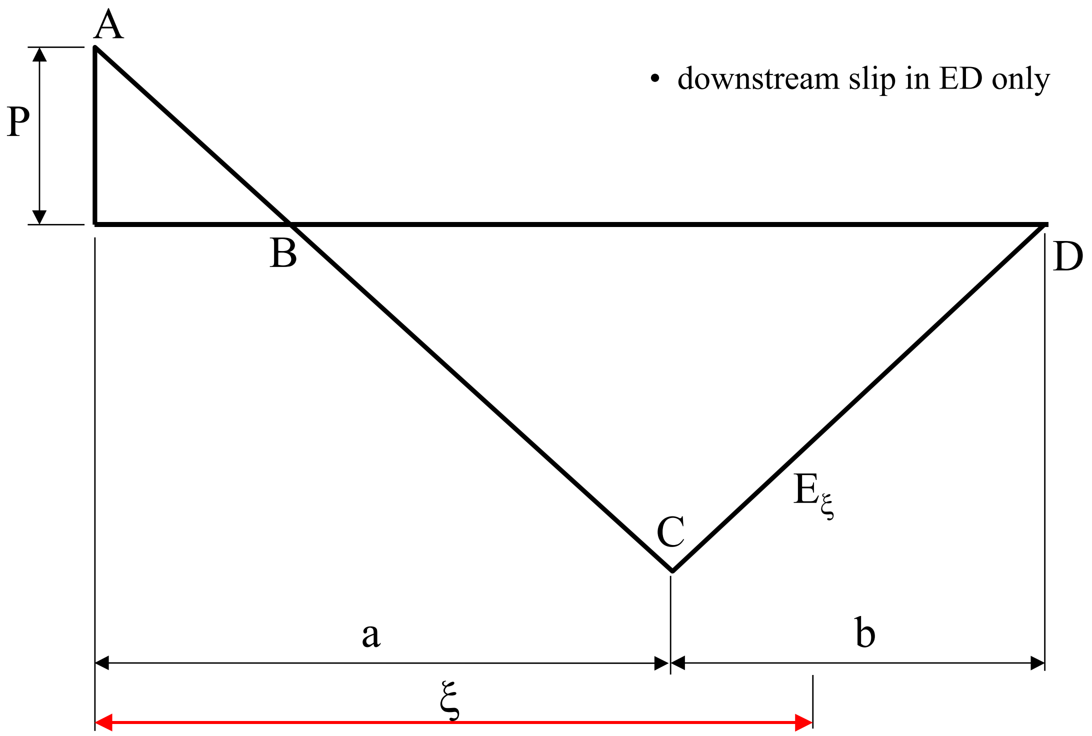

Figure 3.8: **AFD during 2nd cycle heating in the range $a \le \xi \le L$.**

4. SHORT LINE – VERIFICATION BY FINITE ELEMENT ANALYSIS

For the analytical solution, the mobilisation displacement required to develop the friction force is $u_{mob}=0$, and the length of pipe over which the temperature rises from ambient to the maximum temperature is $X_{rise}=0$. In the finite element solution, these parameters cannot be set to exactly zero, since this would result in dividing by zero. Therefore small values are initially chosen, of $u_{mob} = 0.001$ and $X_{rise} = 0.001$ (dimensionless values). This corresponds to actual values of 0.001 $(N_0^2/(EA\ f_0)$ for the mobilisation displacement, and 0.001 L_{anchor} for the rise length. The resulting end displacement histories for a line of dimensionless length L=0.4 and P=0 are shown in Figure 4.1. Therein the solid lines represent the finite element results, and open circles represent the analytical solution. The finite element results were computed using 400 loadsteps for each heating cycle, and also 400 for each cooling cycle to give a total of 800 load steps per cycle. Clearly the agreement between the analytical and finite element solutions is as good as it should be. (Both solutions should converge to the same answer in the limit as $u_{mob} \rightarrow 0$, $X_{rise} \rightarrow 0$, and $L_{element} \rightarrow 0$, where $L_{element}$ is the length of the finite elements, which was taken to be $L_{element}$ = 0.0013.)

The results in Figure 4.1 apply for free ends. Repeating the analysis for different values of a constant force P at the upstream end leads to the results shown in Figure 4.2. Again these show excellent agreement between the analytical and finite element results for small values of the mobilisation displacement. A larger mobilisation displacement leads to less ratcheting per cycle if no force is applied to prevent it, but the level of force to prevent ratcheting is also larger for a larger mobilisation displacement.

A second example serves to verify the analytical result that for longer pipes the force needed to prevent crawl is larger than the axial force that develops under fully constrained conditions. For this purpose, a pipe with L=3 is chosen. From the analytical solution, a constant[ii] tensile force at the upstream end needed to prevent crawling of the pipe is P = 2.097 (from Eq. 3.32). This corresponds a tensile force of 2.097 times the magnitude of the compressive force that would develop in the line under axially fully constrained conditions. Thereafter the axial forces is kept constant. The comparison of the finite element and analytical solutions for this case are shown in Figure 4.3 to Figure 4.4. In Figure 4.3 the analytical solution (open circles) has been evaluated only for key stages in the heating and cooling cycles, whereas the finite element solution (continuous lines) is available for very closely spaced values of the time-like parameter. In Figure 4.4, the axial forces from the finite element solution have been plotted for the first 4 cycles when the line is cooled. As expected from the analytical solution, there is no difference between the AFD's at the end of different cycles. Indeed the agreement is excellent in all cases. The only discernible difference between the analytical and FE solutions is a slight drift in the end displacements from the finite element solution in Figure 4.3. This corresponds to a ratcheting displacement of 0.0125 per cycle in the upstream direction. This ratcheting displacement from the finite element solution vanishes, if one decreases the applied load at the end by 0.2% from P = 2.097 to P = 2.092. Thus from the FE analysis the force

---

[ii] According to the analytical solution this force was applied before any heating and then kept constant. However applying the force during the first heating cycle does affect the analytical solution provided that the specified value is reached soon enough. In the finite element simulation, the end force was increased from zero to the stated value during the first heating cycle, while the time-like parameter ξ increases from $\xi=0$ to $\xi=1$, and kept constant thereafter.

needed to prevent ratcheting from the finite element solution is about 0.2% lower than that from the analytical solution. This is consistent with small differences that might be expected due to discretisation ($L_{element}$=0.01 in this case), and due to finite values of the mobilisation displacement u_{mob} and rise time X_{rise}. Thus the finite element solution confirms that to prevent crawl in a longer line, the magnitude of the force needed can exceed the magnitude of the compressive force that develops under fully constrained conditions.

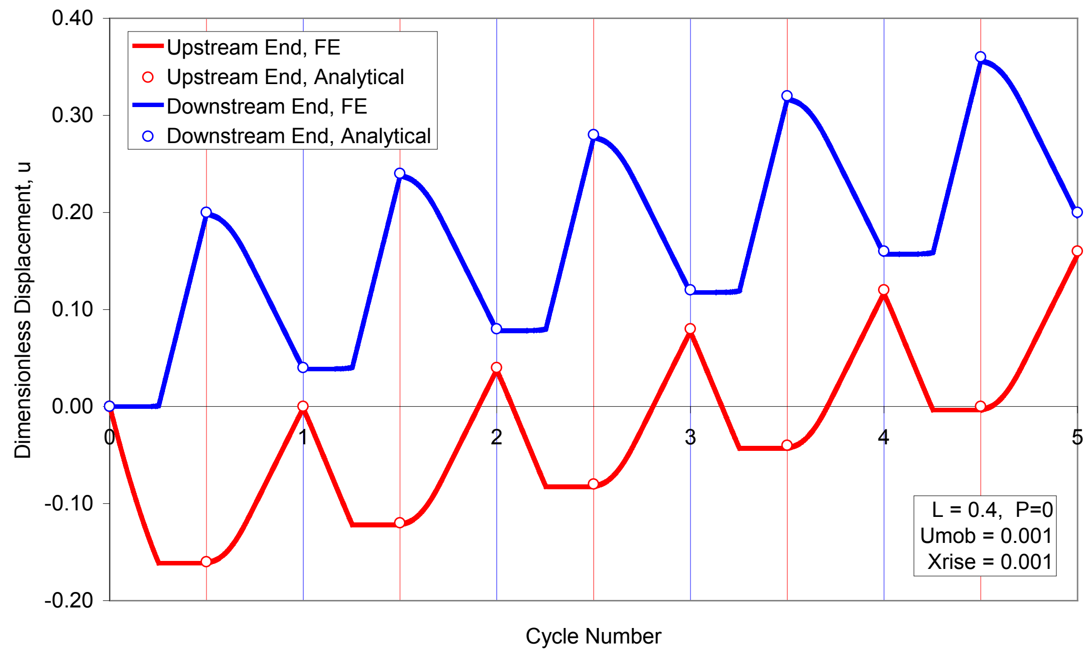

Figure 4.1: **Comparison of dimensionless end displacement histories from finite element analysis (solid lines) with analytical results (hollow circles appearing at the end of the heating and cooling cycles). All the values given correspond to the dimensionless values defined in Eqs. 2.6 to 2.10.**

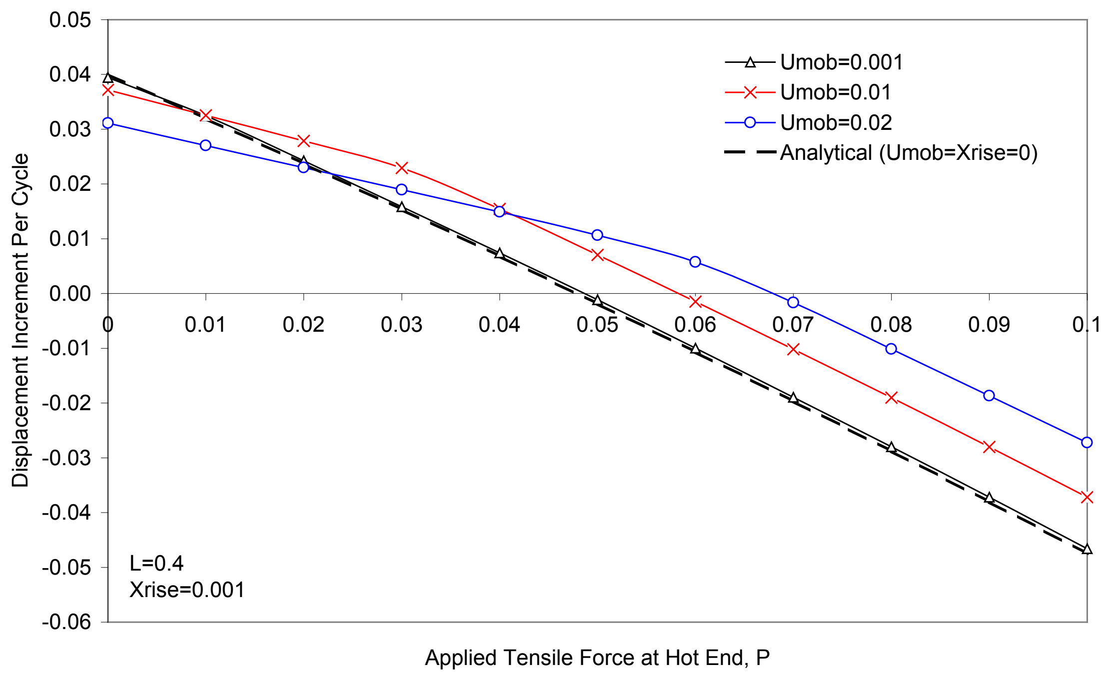

Figure 4.2: **Dimensionless ratcheting displacement increments per cycle from the finite element analysis as a function of the applied constant axial tension P at the upstream end, and the dimensionless mobilisation displacement u_{mob} for the axial soil friction force.**

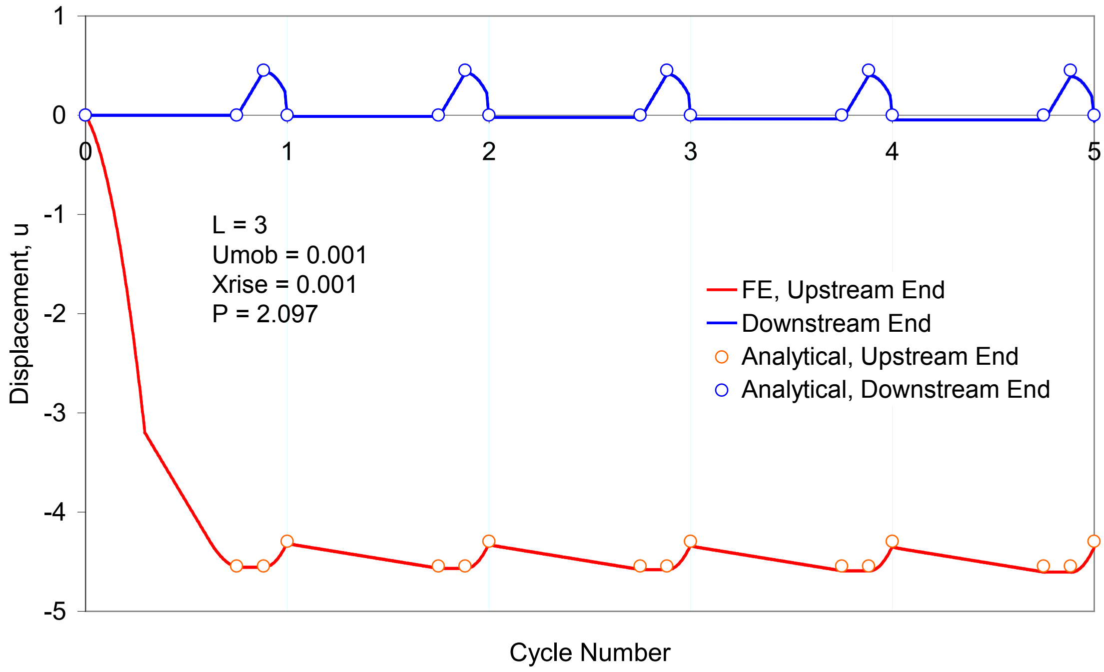

Figure 4.3: **Comparison of dimensionless end displacement histories from finite element analysis (solid lines) with analytical results (hollow circles) for a pipe of length L=3 with a constant tensile force P=2.097 applied at the upstream end. All the parameters given or plotted correspond to the dimensionless values defined in Eqs. 2.6 to 2.10.**

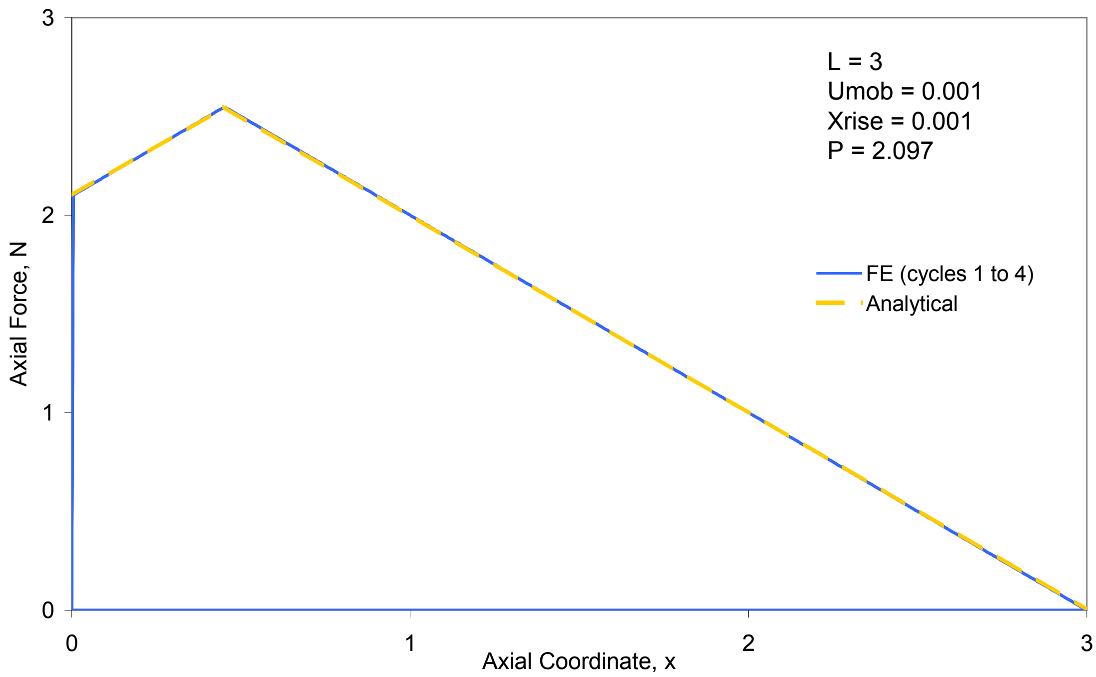

Figure 4.4: **Comparison of axial force diagrams at the end of each cooling cycle from the finite element and analytical solutions, for a pipe of length L=3 with a constant axial tensile force P=2.097 applied at the upstream end.**

5. SHORT LINE WITH RIGID UNILATERAL RESTRAINT AT THE UPSTREAM END

Consider again a line of a sufficiently short length L, but this time a rigid unilateral restraint is provided at the upstream end instead of a constant force. This means that either $u<0$ at the upstream end, and there is no end force, or the displacement is kept at $u=0$ at the upstream end with whatever tensile force P is required to achieve this. The downstream end is taken to be unrestrained, as before.

From the previous analytical solution (of Section 3) with $P=0$, as well as from Figure 4.1, it is clear that the displacements at the upstream end are negative throughout the first cycle. This means that the unilateral restraint remains slack throughout the first cycle.

For subsequent cycles it is assumed that the AFD for the fully cooled line coincides with that for the constant force P at the upstream end (shown in Figure 3.6). However in this case P denotes the unknown force exerted by the unilateral restraint when the line is fully cooled, rather than a constant given applied force.

Certainly the assumption in regard to the shape of the AFD for the fully cooled line applies for the fully cooled line at the end of the first cycle. In this case, $P=0$, and the AFD reduces to a simple triangle with zero forces at the ends.

By starting with the assumed AFD (of Figure 3.6), and carrying the analysis through all stages of heating by the traveling heating front followed by uniform cooling, it is shown in Appendix A that at the end of the cycle one returns to an AFD that is of the same form (as Fig. 3.6), except for a different value of P. The relationship between the value of P at the beginning of the cycle and that at the end is given by

$$P_{n+1} / L = 1 - \tfrac{1}{2} (1 - P_n / L)^2 \qquad (5.1)$$

in which P_n and P_{n+1} denote the restraint forces at the end of the n^{th} and $(n+1)^{th}$ cycles, respectively. This result is valid as long as

$$L \leq \tfrac{1}{2} \qquad (5.2)$$

It implies that the assumption in regard to the form of the axial force diagram at the beginning/end of each cycle is indeed correct. The values of P/L for each cycle calculated from Eq.5.1 are shown in Table 5.1. Clearly rapid convergence to $P=L$ is achieved. This means that when the line is cooled after only a few cycles, the limiting axial friction force will be acting on the pipe in the downstream direction over its entire length. All of this needs to be resisted by the restraint at the upstream end, giving rise to the restraint force $P=L$, in terms of the dimensionless values of the variables, or $P = f_0 L$ in terms of the actual (dimensional) values. In summary, the worst conceivable loading on the restraint does indeed materialise, after only a few cycles.

Table 5.1: Normalised restraint force exerted by a unilateral restraint at the upstream end of a line as a function of the cycle number. [Using the actual rather than dimensionless values of the variables, the second row of this table provides the values of P/(f L).]

Cycle Number n	1	2	3	4	5
Restraint Force P/L	0	0.5	0.875	0.992	0.99997

6. SHORT LINE – OPTIMAL LOCATION OF A UNILATERAL RESTRAINT

It was seen in the previous section that a unilateral restraint provided at the upstream end to stop pipe crawl can be subject to quite large forces. In this section other restraint locations are examined with the objective of minimising the required restraint resistance.

At first, the optimal location is found by finite element analyses (Section 6.1). Then a feature of the finite element solution with the restraint at the optimal location is used to aid the derivation of the analytical solution for the optimal restraint location (Section 6.2).

As before the restraint allows only upstream (i.e. negative) displacement. Such displacements open a gap at the restraint, which needs to be closed again before the restraint becomes active.

6.1. Results from Finite Element Simulations

Typical histories of the gap size and the restraint reaction are shown in Figure 6.1 to Figure 6.6 for various locations of the unilateral restraint. Therein x_r denotes the value of the axial coordinate at the restraint, measured from the upstream end. For integer values of the "cycle number" in Figure 6.1 to Figure 6.6 , the line is fully cooled. If n denotes the integer cycle number, and η denotes the real-valued cycle number, as plotted in Figure 6.1 to Figure 6.6, then heating for the n^{th} cycle occurs in the range $n \leq \eta \leq n+0.8$, while cooling occurs in the range $n+0.8\leq\eta\leq n+1$. As before heating is by passage of a temperature surge down the line, and cooling is uniform, with spatially constant temperature.

With the restraint at the upstream end (x_r=0, Figure 6.1), the restraint remains slack during all of the first cycle and most of the second. It is only towards the end of the second cooling cycle that the restraint becomes active, but when that happens, the restraint force grows rapidly, and continues to grow when the line is fully cooled. This results in a high and sharp peak. Subsequent cooling cycles bring about even higher peaks, reaching a steady-state condition reached after only 3-4 cycles. So far this only replicates the results of Section 5, but different behaviours are obtained for different locations of the restraint.

For the restraint in at mid-line (x_r=0.5 L, Figure 6.2), the restraint remains active at all times. (I.e. a gap never opens.) This results in a very high peak restraint force, almost equal to the maximum that could possibly be generated by the axial soil friction forces on the pipe.

With the restraint slightly downstream from mid-line (x_r = 0.6L, Figure 6.3), the peaks of the restraint force during the first cycles exceed those at steady-state. This has implications for the required restraint capacity: a brittle restraint must be able to withstand the highest restraint force, so that it is not damaged. On the other hand a ductile restraint will simply yield if it is overloaded, ideally with no loss in load-carrying capacity. Under such circumstances a small amount of crawl occurs over the first few cycles, but, as long as the restraint capacity exceeds the maximum force at steady state, crawl stops when steady state is reached.

Figure 6.4 shows a magnified version of a typical steady state cycle from Figure 6.3. Therein key stages of the steady state cycle are identified. The sharp peak in the restraint force occurs when the heating front passes the restraint. This is because heating upstream of the restraint generates compressive forces there, thus transferring additional load to the restraint. On the other hand, heating at the downstream tends to relieve the restraint, by generating compressive forces just downstream of the restraint. However, if no more compressive forces can be generated downstream of the restraint (because the available friction forces have already been fully mobilised), then there is no further change in the restraint force. This results in the flat portion DE of the restraint force history in Figure 6.4.

Moving the restraint a bit further downstream (to $x_r/L = 0.62$, see Figure 6.5), the sharp peak in the restraint force disappears. In this case the maximum possible compressive force downstream of the restraint has already been reached before the heating front reaches the restraint. Thus no further change in axial forces or the restraint force is possible, after the heating front crosses the restraint.

The maximum restraint forces for the various locations of the restraint are plotted in Figure 6.7 for the case L=0.4. Therein two types of maxima are plotted:

(a) the maximum restraint force over all cycles (i.e. including the first few cycles before steady state is reached, and

(b) the maximum restraint force for a cycle at steady state.

For restraints in the upstream half of the line ($x_r/L \leq 0.5$), the peaks during the first few cycles are lower than the steady state peaks. This means that the steady-state peaks also correspond to global maxima. However for a range of restraint locations the first few cycles result in higher peaks. This is then reflected by the difference between the blue and pink lines in Figure 6.7. (Where only a pink line is seen, it is because the blue and pink lines coincide exactly.) The first type of maximum is what needs to be considered for the design of a brittle restraint, whereas the second type applies for a ductile restraint.

Observations from Figure 6.7 include:

- There is a well-defined optimum location for the restraint, which occurs just downstream of the midway point.
- The required restraint capacity for an optimally located ductile restraint is about half that for a brittle restraint.

Whereas Figure 6.7 applies only for L=0.4, similar results are shown in Figure 6.8 for various values of the dimensionless length L. Key observations from this are:

- The optimal restraint location moves downstream for larger values of the dimensionless length parameter L.
- For shorter lines, more is to be gained by optimally locating the restraint.
- For L=1.0, the restraint force is always equal to the maximum force that could possibly be developed by limiting friction forces over the entire length of the line pulling the line against the restraint. Although not shown in Figure 6.8, this was also found to be the case for L=1.5, and is presumed to be so for other $L \geq 1$ as well.

As in Section 3, it becomes again clear that the walking of longer lines is difficult to restrain, if the heating front remains sharp over the length of the line. However the heating front will always tend to diffuse over longer distances, thus reducing the tendency towards crawl in a manner that is not accounted for in these analyses.

6.2 Analytical Solution for Optimal Restraint Location

Normally, finding the analytical solution for the optimal restraint locations would require first finding the analytical solution for an arbitrary location of the restraint, and then solving the optimisation problem. However it turns out that the analytical solution for the optimal location can be found directly based on the following observation from the finite element solutions of the previous section:

For an optimally located unilateral restraint, the closing of the gap at the restraint during heating coincides with the development of downstream slip over the entire length of the line downstream of the restraint.

In Appendix B an analytical solution is derived for which the above optimality condition holds. This is then referred to as the "optimal" solution. According to this solution the optimal location of the restraint is given by

$$x_{r,optimal} = \tfrac{1}{2} \{ L + 1 - (1-L^2)^{1/2} \} \tag{6.1}$$

$$P = 1 - (1-L^2)^{1/2} \tag{6.2}$$

It applies for

$$L \leq 1 \tag{6.3}$$

The values of P and x_r calculated from Eqs. 6.1 and 6.2 are shown in Figure 6.8 as open red circles. There is one such open circle corresponding to each of the L values. The agreement with the optimal solution from the finite element analysis is seen to be good, especially for larger values of L.

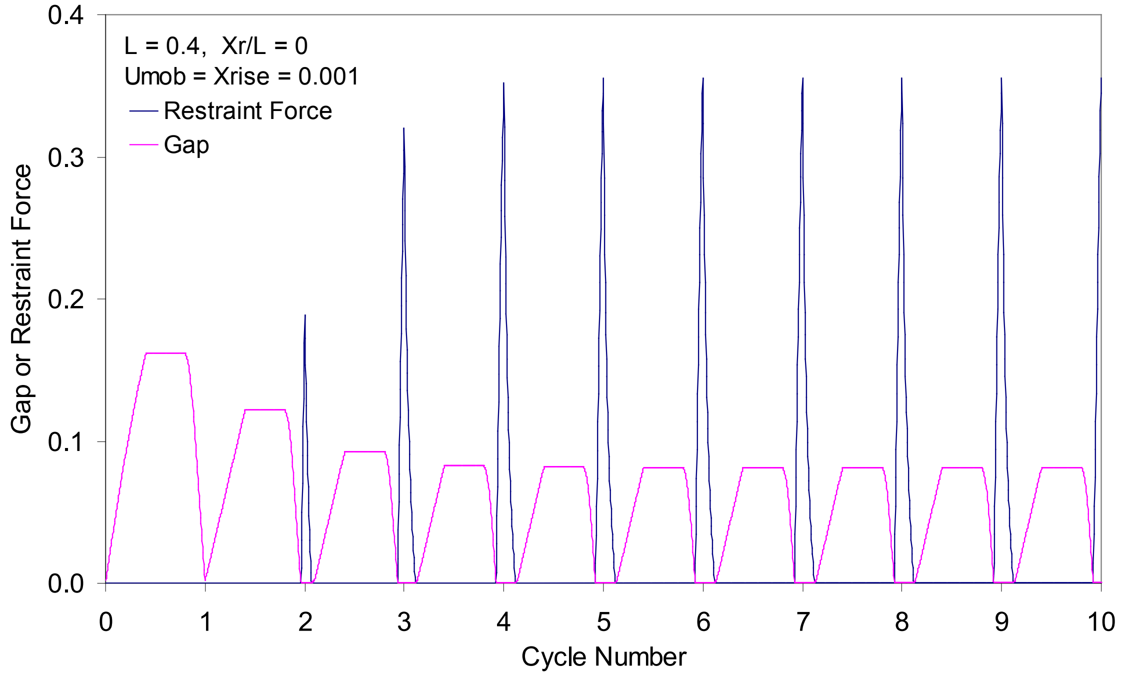

Figure 6.1: **History of the restraint force (blue line) and the gap at the restraint (pink line), for a unilateral restraint at x_r=0 (i.e. at upstream end).**

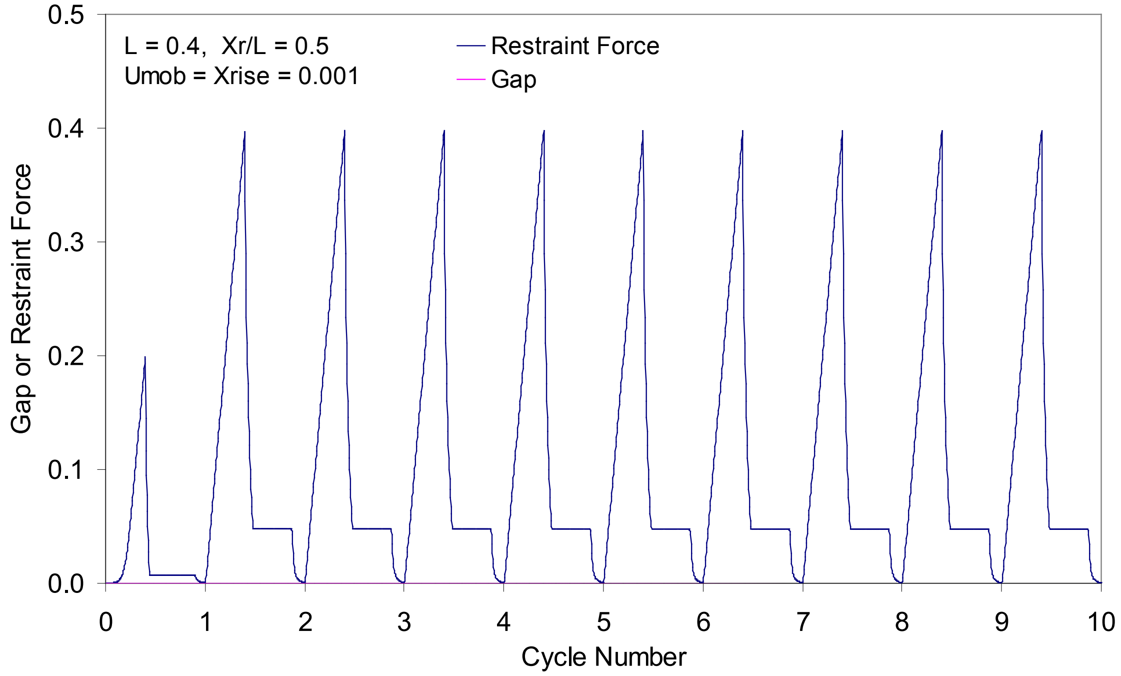

Figure 6.2: **History of the restraint force (blue line) and the gap at the restraint (pink line), for a unilateral restraint at x_r=0.5 L (i.e. at the midpoint).**

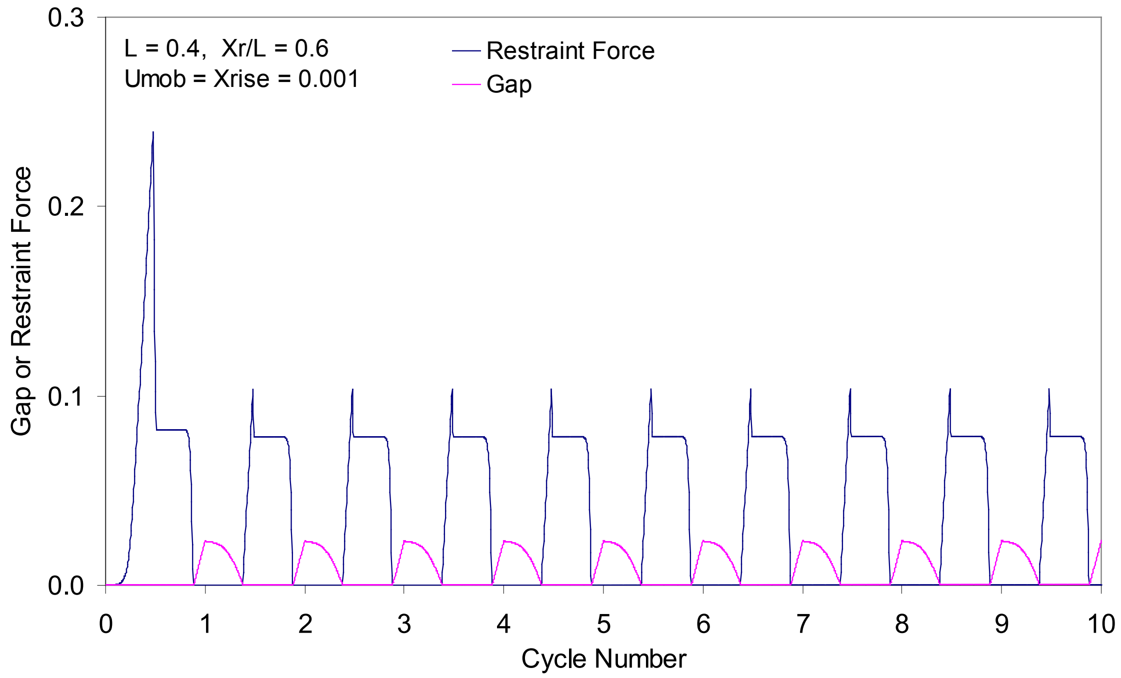

Figure 6.3: **History of the restraint force (blue line) and the gap at the restraint (pink line), for a unilateral restraint at x_r=0.6 L (slightly upstream of optimal location).**

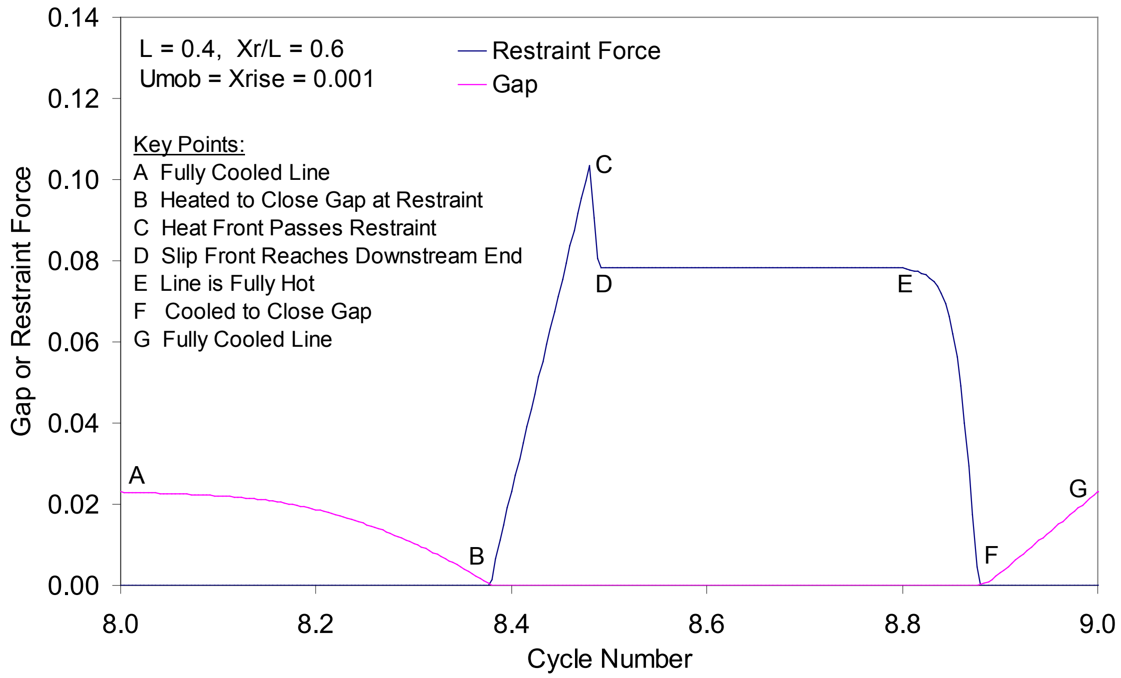

Figure 6.4: **Magnification of Fig. 6.3 showing the 9^{th} cycle as an example of a steady-state cycle. Heating occurs the range 8.0 < n < 8.8, and Cooling in the range 8.8 < n < 9.0, where n denotes the cycle number, as plotted. Gap at restraint closes at point B and re-opens at point F. Restraint is just downstream from the optimal location. For the restraint at the optimal location points C and D become coincident.**

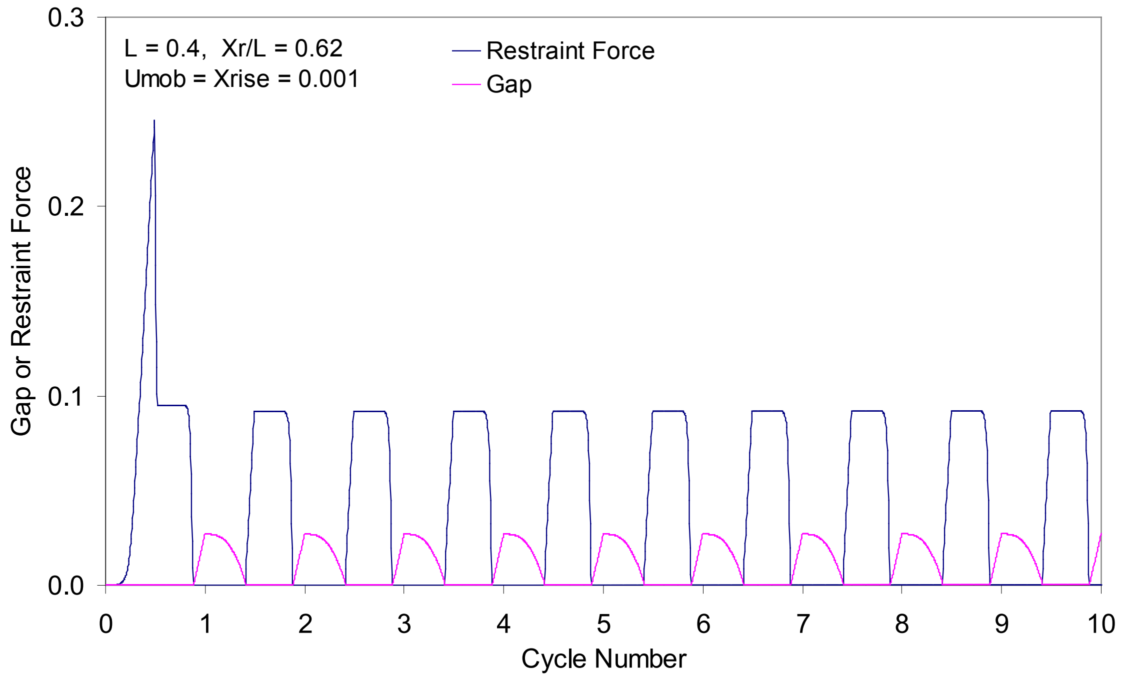

Figure 6.5: **History of the restraint force (blue line) and the gap at the restraint (pink line), for a unilateral restraint at x_r=0.62 L (at optimal location).**

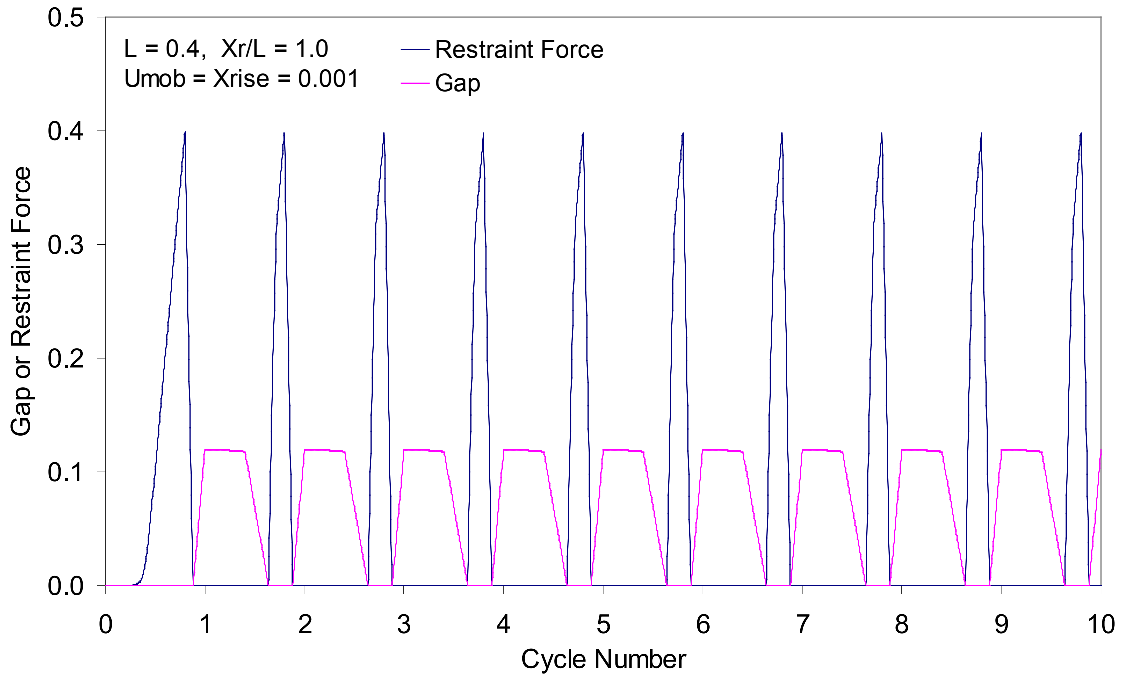

Figure 6.6: **History of the restraint force (blue line) and the gap at the restraint (pink line), for a unilateral restraint at x_r=L (downstream end).**

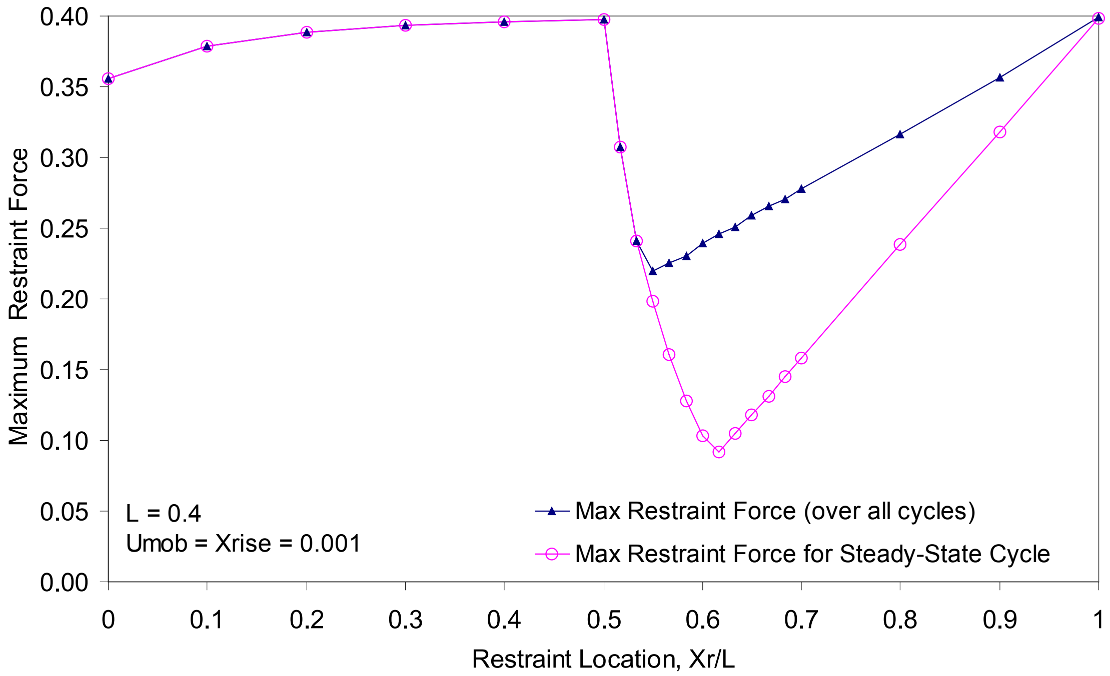

Figure 6.7: **Influence of restraint location on the maximum force that needs to be resisted by the restraint.**

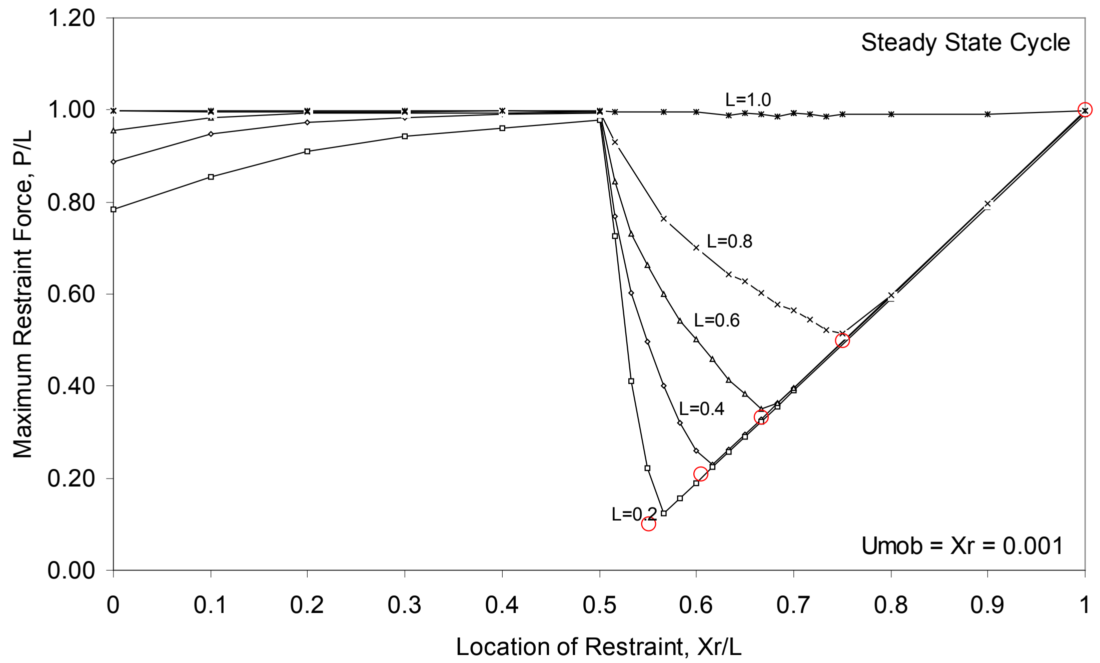

Figure 6.8: **Maximum restraint forces during a steady-state cycles as a function of the dimensionless length of the line, L, and the location of the unilateral restraint. (Applies for the design of a ductile restraint. Red circles correspond to the analytical solution for the optimal location of the restraint.)**

7. ILLUSTRATIVE EXAMPLES

Two examples are considered: The first is for a single pipe on sand, the second for a pipe-in-pipe system on soft clay. In both cases the lines are subsea (in seawater with a specific density of 1.025), and carry oil of a specific density of 0.85. Furthermore they are made of carbon steel, which has a specific density of 7.84, a coefficient of thermal expansion of $\alpha = 1.17 \times 10^{-5}/°C$, and a modulus of elasticity of E=200GPa. The lines are subjected to a temperature surge of $\Delta T=80°C$ traveling down the line with a sharp heating front ($X_{rise} = 0$, unless otherwise noted), followed by uniform cooling.

7.1. Example 1 – Single Pipe on Sand

Consider a 3km-long, 16-inch diameter pipe, with a wall thickness of 0.75" insulated by 2inches (50mm) of a polypropylene coating of a specific density of 0.78. The line is resting on a sandy seabed. A friction factor of μ=0.5 applies between the polypropylene coating and the seabed. The currents are sufficiently low so that embedment and/or self-burial may be neglected. The mobilisation displacement (to develop the axial soil resistance) is u_{mob} = 5mm. The following quantities need to be determined: (a) the ratcheting displacement per cycle, if the line is not restrained, (b) the maximum force needed to restrain the line by a unilateral restraint at the upstream end, and (c) the maximum force required to restrain the line by a unilateral restraint at the optimal location.

The basic derived problem parameters are:

Submerged weight per unit length	$W = 1.19$ kN/m
Soil force per unit length	$f_0 = \mu W = 0.60$ kN/m
Axial Rigidity	$EA = 4.64$ GN
Axial force under fully constrained conditions	$N_0 = EA\,\alpha\,\Delta T = 4.34$ MN

The non-dimensionalisation scheme of Section 2.2 gives:

Anchor length	$L_{anchor} = N_0 / f_0 = 7.3$ km
Non dimensional length	$[L]_{nd} = L / L_{anchor} = 0.41$
Unit displacement[iii]	$u_1 = N_0^2 / (EA\, f_0) = 6.8$ m
Dimensionless Mobilisation Displacement	$[u_{mob}]_{nd} = u_{mob} / u_1 = 0.0007$

This dimensionless mobilisation displacement is lower than any of the ones used in the finite element simulations reported so far. Therefore the approximation of zero mobilisation displacement used in the analytical solution is a good one. We proceed to evaluate the analytical solutions.

For the case when there are no restraints, or external applied forces, the non-dimensional ratcheting displacement per cycle is given by Eq. 3.31 with P=0. This gives

$$[u_{cycle}]_{nd} = \tfrac{1}{4}[L]_{nd}^2 = \tfrac{1}{4}(0.41)^2 = 0.0426$$

The corresponding actual value is

[iii] The unit value of a quantity is the actual value corresponding to a unit non-dimensional value. It is the factor by which the non-dimensional value needs to be multiplied to get the actual value.

$$u_{cycle} = [\, u_{cycle} \,]_{nd} \;\; u_1 \;=\; 0.0426\ (6.8) \;=\; 0.29 \text{ m} \approx 1\text{ft}$$

Thus the crawl rate is about 1 foot per cycle, if unrestrained.

If it were possible to apply an external tensile force at the upstream end that remains constant despite the cycling movements associated with temperature changes, then the magnitude of the force needed to stop crawl can be calculated from Eq. 3.32, to obtain:

$$[\, P \,]_{nd} = {}^{2}/_{3}\, [\, [\, 1 - L + L^2 \,]^{1/2} - 1 + L/2 \,]_{nd} \;=\; 0.0512$$

$$P \;=\; [\, P \,]_{nd} \;\; N_0 \;=\; (0.0512)\ (4.34 \text{ MN}) \;=\; 222 \text{ kN}$$

Thus 222kN (23 tonnes, or 50kips) would be sufficient if a constant force could be maintained. The cyclic end displacements are calculated as follows:

Eq. 3.9 $\Rightarrow$ $[\, a \,]_{nd} = \tfrac{1}{2}\, [\, L + P \,]_{nd} = \; 0.23$

Eq. 3.13 $\Rightarrow$ $[\, b \,]_{nd} \; = \tfrac{1}{2}\, [\, L - P \,]_{nd} = \; 0.18$

Eq. 3.28 $\Rightarrow$ $[\, w_{ends(\xi=L)} \,]_{nd} = \; [\{ \, a\,(\,2b - 1) \;,\; b \;\}]_{nd} = \{ \, -0.15, 0.18 \,\}$

$\Rightarrow$ $w_{ends(\xi=L)} \;=\; [\, w_{ends(\xi=L)} \,]_{nd} \;\; u_1 = \{ \, -1.0 \text{ m} \,,\, 1.2 \text{ m} \,\}$

Thus the cyclic displacements at the ends are 1.0m and 1.2m at the upstream and downstream ends, respectively. A restraint would need to be very flexible to maintain a constant force despite up and down displacements of 1.0m.

If instead of being very flexible the restraint is a unilateral one, i.e. one that allows upstream displacements, but not downstream displacements, then the maximum restraint force depends on the location of the unilateral restraint. If the restraint is at the upstream end, the maximum restraint force is given from Table 5.1 as

$$[\, P \,]_{nd} = [\, L \,]_{nd} = 0.41$$

$$P \;=\; [\, P \,]_{nd} \;\; N_0 \;=\; 0.41\ (4.34 \text{ MN}) = 1.79 \text{ MN}$$

Thus the maximum restraint force is 1790 kN (182 tonnes, 400 kips). This is a very large force indeed. It can be reduced by placing the restraint at the optimal location. The distance of this optimal location from the upstream end is given by

Eq. 6.1 $\Rightarrow$ $[\, x_{r,optimal} \,]_{nd} = \tfrac{1}{2}\, [\, L + 1 - (1 - L^2)^{1/2} \,]_{nd} = \; 0.25$

$\Rightarrow$ $x_{r,optimal} = [\, x_{r,optimal} \,]_{nd} \; L_{anchor} \;=\; 1.824 \text{ km}$

Thus the optimal restraint location is 324m (about 1000ft) downstream of the mid-line point. The restraint force for this case is given by

Eq. 6.2 $\Rightarrow$ $[\, P \,]_{nd} = \; [\, 1 - (1 - L^2)^{1/2} \,]_{nd} \;=\; 0.089$

$\Rightarrow$ $P \;=\; [\, P \,]_{nd} \;\; N_0 \;=\; 387 \text{ kN}$

Thus for an optimally located unilateral restraint the maximum restraint force during a steady-state cycle is 387 kN (39 tonnes, 87 kips). In order for a restraint of this capacity to stop crawl, it must be able to give a bit in the first few cycles, while still being able to resist the 387 kN during subsequent cycles.

Thus in summary the required restraint forces are:

- 222kN for a very flexible restraint at the upstream end that maintains a constant force despite cyclic movements of 1m,
- 1790 kN for a unilateral restraint at the upstream end, and

- 387 kN for a ductile unilateral restraint at the upstream end

For design, the most practical proposition is likely to be the unilateral restraint at the optimal location. If the restraint has some flexibility, it is likely that the required restraint force could be brought below the 387 kN.

Finally it must be emphasised that the above analysis applies only if the line does not buckle laterally due to the induced compressive forces. Lateral buckling should not be a problem, if the restraint is at the upstream end. At least in that case any buckle should not grow with the cycles. However it could become a problem for the restraint at the optimal location. If there is a possibility that a buckle might form, one needs to check that the buckle will not grow as a result of the cyclic temperature changes. This requires a finite element analysis simulating the lateral as well as the axial response.

7.2. Example 2 – Pipe-in-Pipe System on Soft Clay

For a 1.5 km-long deepwater pipe-in-pipe system, the outer diameters of the pipes are 16" and 12", and wall thicknesses of 0.75" and 0.875", respectively. As for the previous example the line is subject to a temperature surge of 80°C above ambient conditions, followed by uniform cooling. Only the inner pipe is affected by the temperature changes. Regularly spaced bulkheads ensure that any differences between the axial displacements of the inner and outer pipes are negligible.

The soil is a soft clay, with an undrained shear strength of about 2kPa (50psf) at the surface, increasing with depth. Good adhesion between the clay and the pipe is expected. In this case the slip mechanism is not friction. Rather it involves permanent plastic deformations of the clay near the pipe. Based on the weight of the pipe, the soil properties, and the expected embedment the maximum axial resistance is expected to be f_0=1.9 kN/m, and the mobilisation displacement u_{mob} = 50mm (2 inches). Furthermore the clay is not sensitive, so that those f_0 and u_{mob} values can also provide a reasonable first approximation for subsequent cycles, as is assumed in the frictional model.

Proceeding as for the previous example, one obtains:

Axial Rigidity (includes both pipes)	EA = 8.58 GN
Axial force under fully constrained conditions[iv]	$N_0 = EA_{ip}\,\alpha\,\Delta T$ = 3.69 MN

The non-dimensionalisation scheme of Section 2.2 gives:

Anchor length	$L_{anchor} = N_0 / f_0$ = 1.94 km
Non dimensional length	$[L]_{nd} = L / L_{anchor}$ = 0.77
Unit displacement[v]	$u_1 = N_0^2 / (EA\, f_0)$ = 0.84 m
Dimensionless Mobilisation Displacement	$[u_{mob}]_{nd} = u_{mob} / u_1$ = 0.060

In Figure 4.2 it was seen that a dimensionless mobilisation displacement of 0.02 already had a significant influence on the results. This mobilisation displacement is 3 time higher.

---

iv Includes contribution from inner pipe only, since the temperature rise for the outer pipe is expected to be negligible. (This is a good approximation as long at the outer pipe remains exposed to the seawater, but significant heating of the outer pipe can develop if the pipe becomes buried, due to the insulation provided by the soil.)

v The unit value is a factor to be applied to the non-dimensional value to get the actual value.

Therefore the analytical solution based on zero mobilisation displacement will not be a good approximation. Nevertheless, for the sake of completeness, the analytical solution is computed below, and later compared with finite element solutions.

For the case when there are no restraints, or external applied forces, the non-dimensional ratcheting displacement per cycle is

Eq. 3.31 (with P=0) $\Rightarrow$ $[\,u_{cycle}\,]_{nd} = \frac{1}{4}\,[\,L\,]_{nd}^{2} = \frac{1}{4}\,(0.77)^2 = 0.15$

$\Rightarrow$ $u_{cycle} = [\,u_{cycle}\,]_{nd}\; u_1 = 0.125 \text{ m} = 5 \text{ inches}$

Thus the crawl rate is about 12cm (5 inches) per cycle, if unrestrained.

The magnitude of a constant tensile force at the upstream end that is needed to prevent crawl is

Eq. 3.32 $\Rightarrow$ $[\,P\,]_{nd} = {}^{2}/_{3}\,[\,[\,1 - L + L^2\,]^{1/2} - 1 + L/2\,]_{nd} = 0.196$

$\Rightarrow$ $P = [\,P\,]_{nd}\; N_0 = (0.196)\,(3.69 \text{ MN}) = 725 \text{ kN}$

Thus 725kN (74 tonnes, or 163 kips) is sufficient if this force can be kept constant despite the cyclic movements of the pipe. The cyclic end displacements are calculated as follows:

Eq. 3.9 $\Rightarrow$ $[\,a\,]_{nd} = \frac{1}{2}\,[\,L + P\,]_{nd} = 0.48$

Eq. 3.13 $\Rightarrow$ $[\,b\,]_{nd} = \frac{1}{2}\,[\,L - P\,]_{nd} = 0.29$

Eq. 3.28 $\Rightarrow$ $[\,w_{ends(\xi=L)}\,]_{nd} = [\{\,a\,(\,2b - 1)\,,\; b\,\}]_{nd} = \{\,-0.21, 0.29\,\}$

$\Rightarrow$ $w_{ends(\xi=L)} = [\,w_{ends(\xi=L)}\,]_{nd}\; u_1 = \{\,-0.17\text{m}, 0.24 \text{ m}\,\}$

In this case the restraint would need to accommodate cyclic displacements of 17cm (7 inches) with no change in force.

For a unilateral restraint at the upstream end, the maximum force is

$[\,P\,]_{nd} = [\,L\,]_{nd} = 0.77$

$P = [\,P\,]_{nd}\; N_0 = 0.77\,(3.69 \text{ MN}) = 2.85 \text{ MN}$

Thus the maximum restraint force is 2,850 kN (291 tonnes, 641 kips).

This force can be reduced by placing the restraint at the optimal location. The distance of this optimal location from the upstream end is given by

Eq. 6.1 $\Rightarrow$ $[\,x_{r,optimal}\,]_{nd} = \frac{1}{2}\,[\,L + 1 - (1{-}L^2)^{1/2}\,]_{nd} = 0.57$

$\Rightarrow$ $x_{r,optimal} = [\,x_{r,optimal}\,]_{nd}\; L_{anchor} = 1.1 \text{ km}$

The corresponding maximum restraint force at steady-state is

Eq. 6.2 $\Rightarrow$ $[\,P\,]_{nd} = [\,1 - (1{-}L^2)^{1/2}\,]_{nd} = 0.37$

$\Rightarrow$ $P = [\,P\,]_{nd}\; N_0 = 1.35 \text{ MN}$

Thus for an optimally located unilateral restraint, the maximum restraint force during a steady-state cycle is 1.35 MN (138 tonnes, 303 kips).

The above analytical results apply only for zero mobilisation displacement. To account for the mobilisation displacement u_{mob} = 50 mm (2 in), one must resort to finite element calculations. The results for a constant tensile force applied at the upstream end are shown in Figure 7.1. Therein the finite element solution is also compared with the analytical one for zero mobilisation displacement. Due to the finite mobilisation displacement of 50mm, the ratcheting displacement for zero applied force decreases from 126mm/cycle (5in/cycle) to 26mm/cycle (1in/cycle). Much of the crawling action of the pipe is being absorbed by elastic deformations of the soil. Also, due to the elastic deformation capability of the soil, there is not just one value of the end force P for which the ratcheting displacement is zero, but rather a range of values for which no ratcheting occurs.

The axial force diagrams for the cooled line from the finite element analysis are shown in Figure 7.2. For comparison, Figure 3.6 shows the AFD from the analytical solution, for zero mobilisation displacement. The effect of soil elasticity is to round off the corners in the AFD. (The corners in the AFD imply an inmediate transition from slip on one direction to slip in the opposite direction, but the soil elasticity introduces a stick region, in which there are only elastic soil deformations, with no slip.)

For a unilateral restraint, the maximum restraint force at steady-state is shown in Figure 7.3 as a function of restraint location and mobilisation displacement. The applicable mobilisation displacement for this example is "u_{mob}=50mm".

If the mobilisation displacement is sufficiently large, the unrestrained pipe will not crawl. This is the reason why for u_{mob}=100mm, the restraint force in Figure 7.3 is zero for the restraint near the upstream end. The restraint simply does not become active in this case. The gap that opens during heating never closes. However if the restraint is placed further downstream, a high restraint force is generated even though the restraint is not needed to prevent crawl. This suggests that it is important to consider yielding restraints, as well as the rigid restraints considered so far.

To model a ductile yielding restraint, an elastic-perfectly-plastic relationship is used between the force on the unilateral restraint and the restraint displacement. This model yielded the following results for this example:

A) For the essentially zero mobilisation displacement (u_{mob}=1mm, in Figure 7.3) it is found that a restraint with a yield force of 99% of the maximum restraint force at steady state (given in Figure 7.3) is not sufficient to stop crawl. After a few cycles a steady-state condition is reached involving a constant plastic displacement increment for the restraint per cycle. This confirms the assessment in Section 6 that for zero mobilisation displacement, the required capacity of a ductile unilateral restraint is equal to the maximum load experienced by a rigid restraint at steady-state.

B) For a restraint located at x_{res} = 1.1km, and u_{mob}=50mm (2in), it is found by trial and error simulations[vi] that the required yield force of the restraint is about 1.47MN, whereas the maximum restraint force at steady state for a rigid restraint is 2.1MN. Thus when significant soil elasticity is involved, one can no longer determine the required capacity of a ductile restraint from an analysis involving a rigid restraint.

Finally it is worth while to consider the force transfer between the inner and outer pipes. If instead of having closely spaced bulk heads the pipes are free to slide with respect to one another, the behaviour will be drastically altered. Indeed if the friction between the inner and outer pipes is reduced to zero, there can be no crawl, as the inner pipe will only transfer equal and opposite forces to both ends of the outer pipe. Thus one of the ways to

---

[vi] For a restraint capacity of 1.46MN crawl continues at steady-state, whereas for a 1.48MN restraint crawl is eventually arrested. Such simulations are time consuming, because close to the required restraint capacity it takes longer for reach a steady-state condition. E.g. 50 cycles were needed for the 1.48MN restraint, to ascertain that crawl had indeed stopped.

combat crawl could be to leave out the structural bulk heads between the pipes, or increase their spacing.

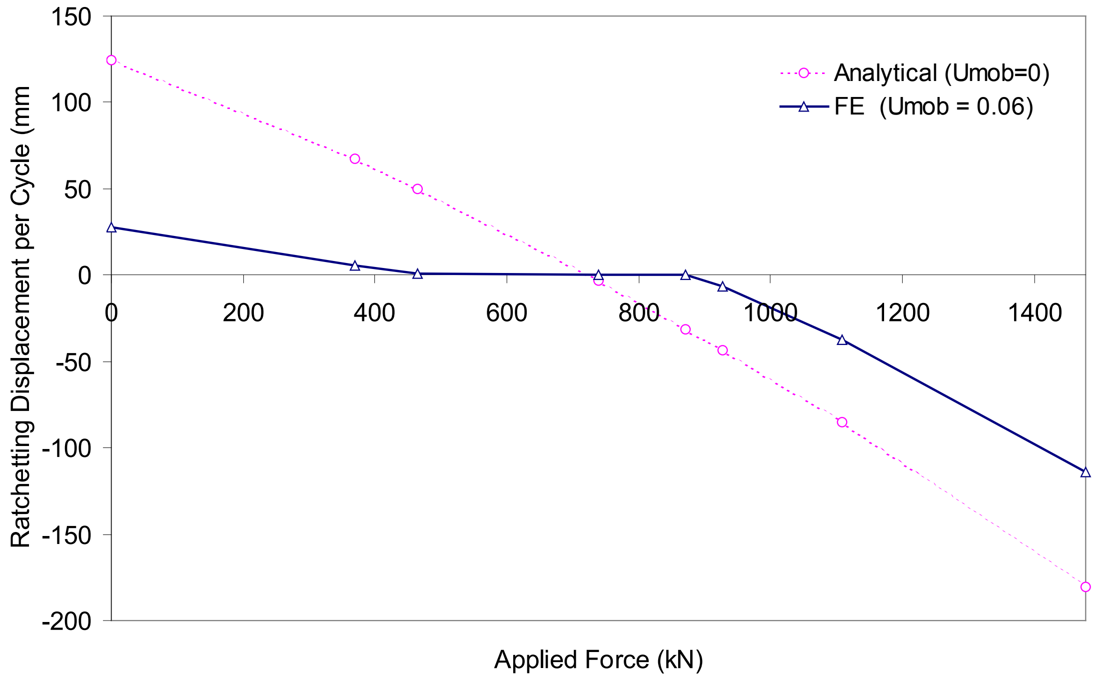

Figure 7.1: **Ratcheting displacements per cycle for pipe-in-pipe system on soft clay (Example 2), for a constant force applied at the upstream end.**

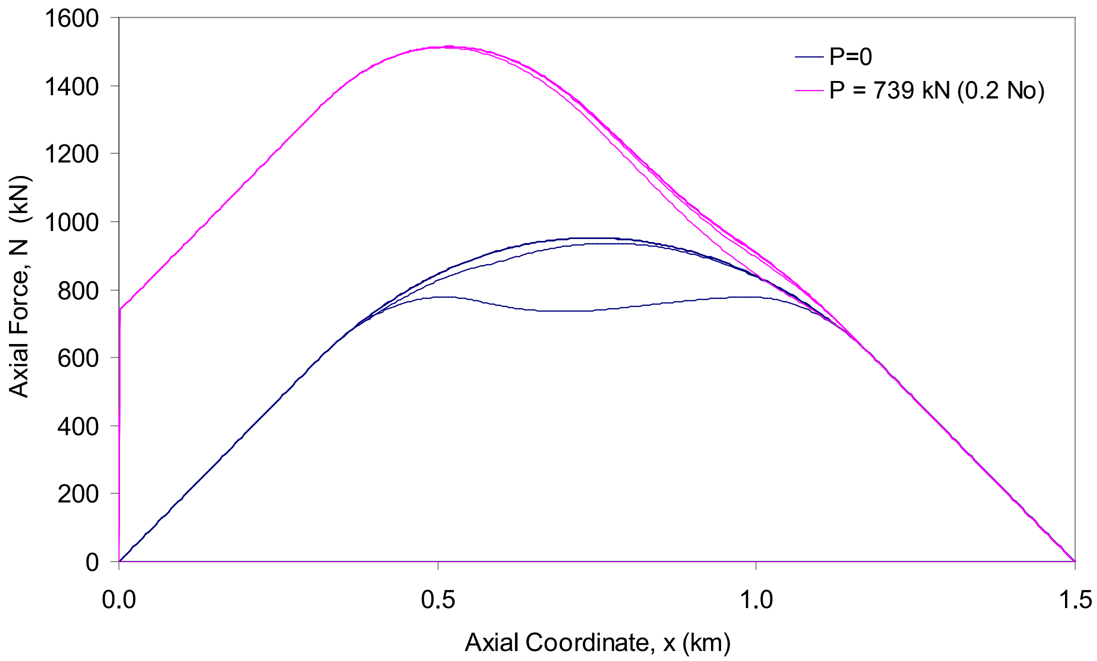

Figure 7.2: **Pipe-in-pipe on soft clay (Example 2), axial force diagrams for fully cooled line with a constant tensile force P applied at the upstream end. (The AFD's are shown for the first 10 cycles, but for cycles 7 to 10, the curves fall on top of each other, and can therefore not be distinguished. The AFD for the first cycle lies slightly lower than for the steady-state cycles.)**

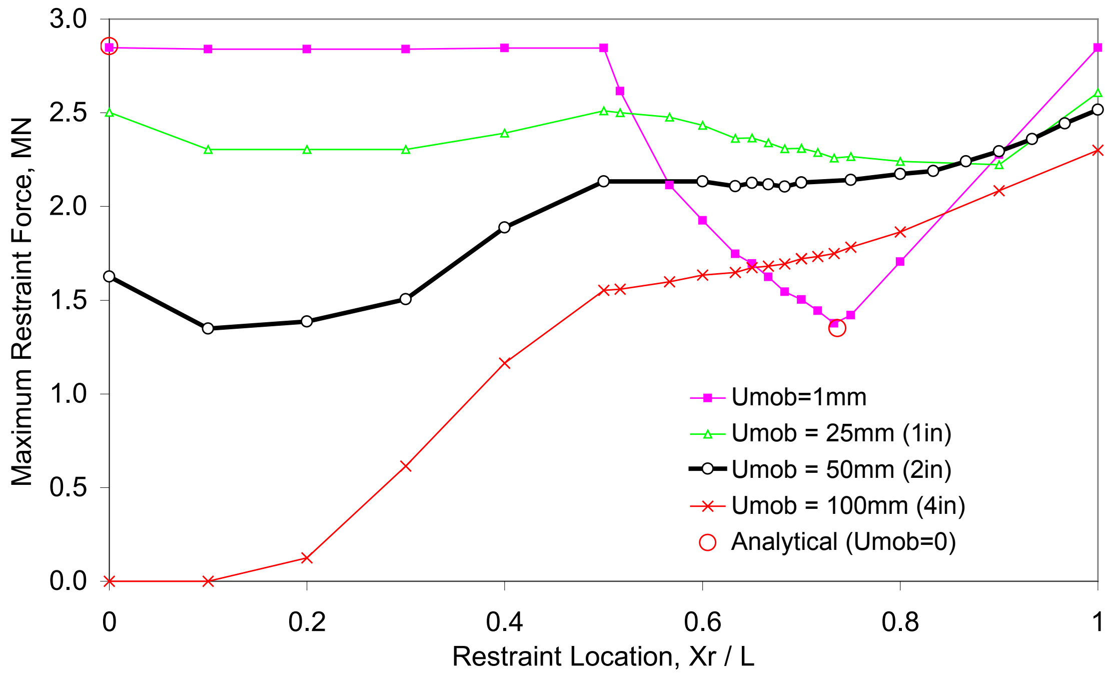

Figure 7.3: **Pipe-in-pipe on soft clay (Example 2), restraint force exerted by the pipe on a unilateral restraint during a steady-state cycle as a function of restraint location (in terms of the distance x_r from the upstream end) and mobilisation displacement (u_{mob}).**

8. BEHAVIOUR OF LONG LINES

So far all the analytical solutions calculated have involved axial force diagrams (AFD's) that consist of segments of straight lines. For longer lines ($L>L_{anchor}$, with no end loads applied), it will be seen that the AFD's can contain non-linear segments. Furthermore it can take considerably longer to reach a steady-state ratcheting condition. However the length of the line in itself is not sufficient to prevent crawl. One also needs the temperature front to diffuse sufficiently so that the temperature gradients fall below a critical level that causes slip every time the temperature front passes by.

First an analytical solution for heating and cooling of a long line free of any end forces or restraints is derived (Section 8.1). This is then compared with finite element solutions (Section 8.2), and finally the effect of key parameters for the finite element solution is examined (Section 8.3).

Throughout this section all symbols refer to the non-dimensional values of the parameters, as defined in Section 2.2.

8.1. Analytical Solution for the First Cycle

A line with L > 1, and no end forces or restraints is considered. As before, the loading consists of passage of a heating front followed by uniform cooling. In what follows, the solutions for different stages of heating and cooling during the first cycle are given in separate sub-sections.

Heating with $0 \le \xi \le ½$

As before ξ is the time-like parameter that describes the distance that the heating front has traveled from the upstream end. For this stage ($0 \le \xi \le ½$), the same solution as for the short line (Section 3, with P=0) applies. The AFD is shown in Figure 8.1. The displacements are given by:

$$
\begin{aligned}
u &= ½\,(2\xi - x)^2 - (\xi - x)^2 - (\xi - x) && \text{for } 0 \le x \le \xi \\
&= ½\,(2\xi - x)^2 && \text{for } \xi \le x \le 2\xi \\
&= 0 && \text{for } 2\xi \le x \le L
\end{aligned}
\tag{8.1}
$$

and the corresponding velocities by

$$
\begin{aligned}
v &= 2\xi - 1 && \text{for } 0 \le x \le \xi \\
&= 2\,(2\xi - x) && \text{for } \xi \le x \le 2\xi \\
&= 0 && \text{for } 2\xi \le x \le L
\end{aligned}
\tag{8.2}
$$

Thus clearly the assumed slip directions are satisfied as long as $\xi \le ½$. However at $\xi=1/2$ slip at the upstream side of the heating front ceases (v=0 where $0 \le x \le \xi$). For larger values of ξ this solution would indicate the wrong slip direction, and therefore does not apply. Therefore, for the next stage, we seek a solution involving no slip on the upstream side of the heating front.

Heating, $\frac{1}{2} \le \xi \le \xi_1$

At this stage the slip region upstream of the heating front has become so long, that the compressive force at the heating front can no longer increase as rapidly as before. There is not enough thermal expansion being generated for this. Therefore the axial force beyond x = ½ can be expected to increase more slowly, as shown in the AFD of Figure 8.2. Since there is no slip or temperature change downstream of the heating front the AFD remains frozen there. The slip region downstream of the heating front is much the same as in the previous stage, only a bit longer. In Figure 8.2, the dimension b depends on ξ, as in

$$b = b(\xi) \tag{8.3}$$

Furthermore, at point D in Figure 8.2 the axial force is negative and equal to b in magnitude, so that

$$N(\xi,\xi) = -b(\xi) \tag{8.4}$$

where $N=N(x,\xi)$ denotes the axial force at location x and time ξ. Since the AFD remains frozen downstream of the heating front, we have

$$\begin{aligned} N(x,\xi) &= -\tfrac{1}{2}x && \text{for } 0 \le x \le \tfrac{1}{2} \\ &= N(x,x) && \text{for } \tfrac{1}{2} \le x \le \xi \\ &= -(\xi + b(\xi) - x) && \text{for } \xi \le x \le \xi + b(\xi) \end{aligned} \tag{8.5}$$

Furthermore it follows from Eq. 8.4 that $N(x,x)= -b(x)$, so that Eq. 8.5 now becomes:

$$\begin{aligned} N(x,\xi) &= -\tfrac{1}{2}x && \text{for } 0 \le x \le \tfrac{1}{2} \\ &= -b(x) && \text{for } \tfrac{1}{2} \le x \le \xi \\ &= -(\xi + b(\xi) - x) && \text{for } \xi \le x \le \xi + b(\xi) \end{aligned} \tag{8.6}$$

Since the displacement at point E in Figure 8.2 must vanish, the displacement at some point $x \le \xi$ can be obtained from the area under the AFD in Figure 8.2 downstream of the dashed line, plus a contribution due to the thermal strain. This gives

$$u(x,\xi) = \tfrac{1}{2}\, b(\xi)^2 + \int_x^{\xi} [-N(y,\xi)]\, dy - (\xi - x) \tag{8.7}$$

Differentiating this with respect to ξ while noting that for the integrand in Eq. 8.7, $\partial N/\partial\xi=0$, gives

$$v = b(\xi)\,(db/d\xi) - N(\xi,\xi) - 1 \tag{8.8}$$

$$\;\; = b(\xi)\,(db/d\xi) + b(\xi) - 1 \tag{8.9}$$

The condition of no slip (v=0) then gives an ordinary differential equation for $b=b(\xi)$, which is subject to the initial condition $b(\tfrac{1}{2})=\tfrac{1}{2}$ (since at $x = \xi= \tfrac{1}{2}$, $N= -\tfrac{1}{2}$). The solution satisfying the initial condition is

$$\xi = 1 - b - \ln[\, 2(1-b)\,] \tag{8.10}$$

where ln[.] denotes the natural logarithm function. This implicitly defines the function $b=b(\xi)$. Unfortunately no explicit expression for b as a function of ξ appears to be available. However if the objective is to plot the AFD, this presents no difficulty whatsoever: One simply calculates ξ for a range of values of b, instead of proceeding the other way around. For $b \rightarrow 1$ (from below), it is clear from Eq. 8.10 that $\xi \rightarrow \infty$. This means that as the heating front travels down the line, the maximum compressive force asymptotically approaches the fully constrained axial compressive force.

The values of ξ and b when the heating front reaches the downstream end will be denoted by ξ_1 and b_1, respectively. They must satisfy the condition

$$\xi_1 + b_1 = L \tag{8.11}$$

which upon substitution from Eq. 8.10 gives

$$b_1 = 1 - \tfrac{1}{2} e^{-(L-1)} \tag{8.12}$$

$$\xi_1 = L - b_1 \tag{8.13}$$

The end displacements remain at

$$u_{ends} = \{ -\tfrac{1}{4} \ , \ 0 \} \tag{8.14}$$

throughout this stage.

Heating, $\xi_1 \le \xi \le L$

This stage starts when the slip front (point E in Figure 8.2) reaches the downstream end. This results in the AFD of Figure 8.3. There is no change in the AFD during the remainder of the heating cycle. The additional heating is simply accommodated by slip with velocity v=1 downstream of the heating front only, so that at the end of this stage the end displacements are given by,

$$u_{ends,\,\xi=L} = \{ -\tfrac{1}{4} \ , \quad b_1 \ \}$$

which for large L converge to

$$u_{ends,\,\xi=L} = \{ -\tfrac{1}{4} \ , \ 1 \ \} \qquad \text{as} \qquad L \rightarrow \infty \tag{8.15}$$

Cooling, $0 \le \zeta \le 1$

Assuming no slip uniform cooling makes the AFD move upwards. Then some adjustments need to be made to account for slip at the ends, so that the force boundary conditions satisfied. This gives rise to the AFD in Figure 8.4. Therein slip occurs only in regions AG and FH. The change in end displacements during this stage is

$$\Delta u_{ends} = \tfrac{1}{4} \zeta^2 \{ 1 \ , -1 \} \tag{8.16}$$

Once the line is fully cooled (ζ=1), the axial forces are tensile everywhere, as shown in Figure 8.5, and the total displacement increment during cooling is ¼ inward at each end. Thus the total end displacements at the end of the first cycle are:

$$u_{ends(\zeta=1)} = \{ \ 0 \ , \quad b_1 - \tfrac{1}{4} \ \}$$

which converges to

$$u_{ends(\zeta=1)} = \{ \ 0 \ , \ \tfrac{3}{4} \ \} \qquad \text{as} \qquad L \rightarrow \infty \tag{8.17}$$

Although in principle the analysis for the second cycle could proceed in much the same way as for the short line, the more complicated parametric description of the residual axial force diagram in this case makes this more complicated. Therefore, for the second and subsequent cycles, the finite element solutions are relied upon.

8.2. Finite Element Solutions

A comparison of the finite element and analytical solutions for the first cycle is shown in Figure 8.6 to Figure 8.11 for a line of dimensionless length L=3 with no restraints or end forces. As expected the finite element solution converges to the analytical one for small values of the mobilisation displacement. Indeed the curve for the smallest mobilisation displacement (u_{mob}=0.0001) is for the most part indistinguishable from the analytical solution. This validates both the finite element as well as the analytical solution. It also indicates that the element length used (L_e=0.01) is sufficiently small to ensure converged results. The rise length over which the temperature change rises linearly from zero to the maximum value was taken to be X_{rise}=0.01 for the finite element solution. (It is zero for the analytical solution.)

Finite element solutions for subsequent cycles are shown in Figure 8.12 to Figure 8.21 for a line of dimensionless length L=10. In all cases the dimensionless mobilisation displacement is taken as u_{mob}=0.001 (i.e. essentially zero, but large enough to avoid convergence difficulties). However the rise length X_{rise} over which the temperature rises is varied. For X_{rise}<1, the temperature gradients are supercritical. In such cases passage of the heating front invariably produces slip of an initially stress-free line. On the other hand for X_{rise}>1 the gradients are subcritical. The results of Figure 8.12 to Figure 8.21 include:

a) the axial force diagram for the fully cooled line at the end of cycles 1,2,3,…,10,20,30,…,100,

b) the end displacement increment that occurs after each full cycles of heating and cooling,

c) the total end displacements for critical (X_{rise}=1.0) and sub-critical (X_{rise}=1.5) cases.

Key observations from these figures are as follows:

1. For the cases with super-critical temperature gradients (X_{rise}=0.01 and X_{rise}=0.5), ratcheting continues with a constant displacement increment per cycle. The axial force diagram (AFD) for the cooled line seems to converge to a steady state value, involving higher axial tension near the upstream end.

2. The ratcheting displacement for X_{rise}=0.5 is about half that for $X_{rise}\approx 0$. (The actual dimensionless values are 0.21 and 0.43, respectively.)

3. For the case with a critical temperature gradient (X_{rise}=1.0), convergence to a steady-state condition has not been achieved after 100 cycles. The AFD's are still changing significantly, and the end displacement increments have not equalised: they are zero at the upstream end, but remain non-zero at the downstream end. Extending the analysis for the critical case to 300 cycles leads to the total end displacements of Figure 8.20. This shows that after 150 cycles ratcheting displacements start to develop at the upstream end as well, but there is still no clear evidence that a steady-state condition has been reached.

4. For the sub-critical case (X_{rise}=1.5), residual axial force develops only near the ends. Although initially there is some ratcheting at the downstream end, the displacement increments decay to zero fairly rapidly, so that at the end the total displacement is about double that at the first cycle.

Of course all of the above applies for idealised temperature histories. More realistically, gradients at the heating front do not remain constant. Rather the heating front may start off fairly sharp (i.e. with super-critical gradients), but then diffuse to become sub-critical as the hot product travels far enough down the line. Therefore, it is essential to determine the actual history of temperatures for every point along the line, and use that as input to the finite element simulation of pipe crawl. Even if the drive from the temperature gradients is not strong enough to move the whole line forward, the possibility of pipe crawl feeding into lateral buckles near the upstream end must be addressed.

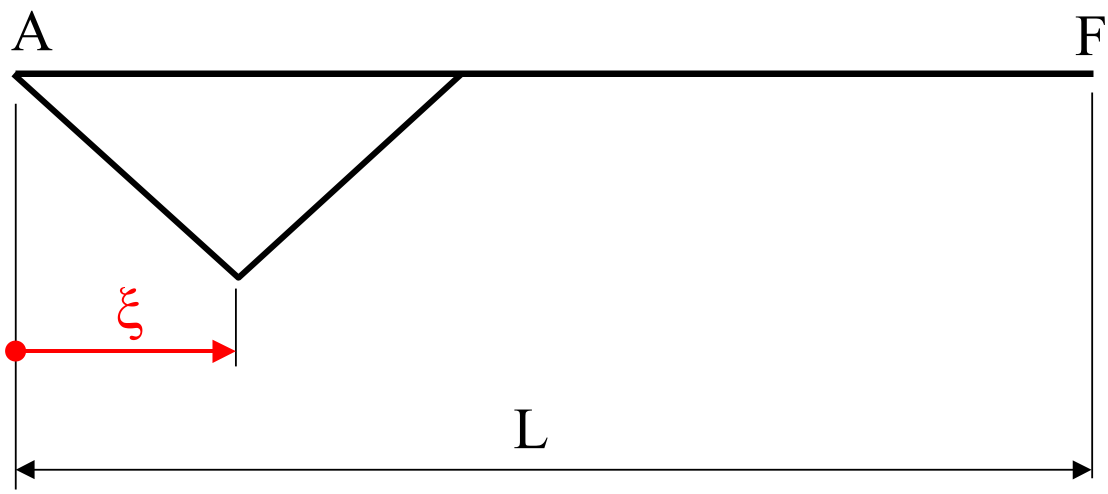

Figure 8.1: **Axial force diagram for a long line during the first cycle of heating in the range $0 \leq \xi \leq ½$.**

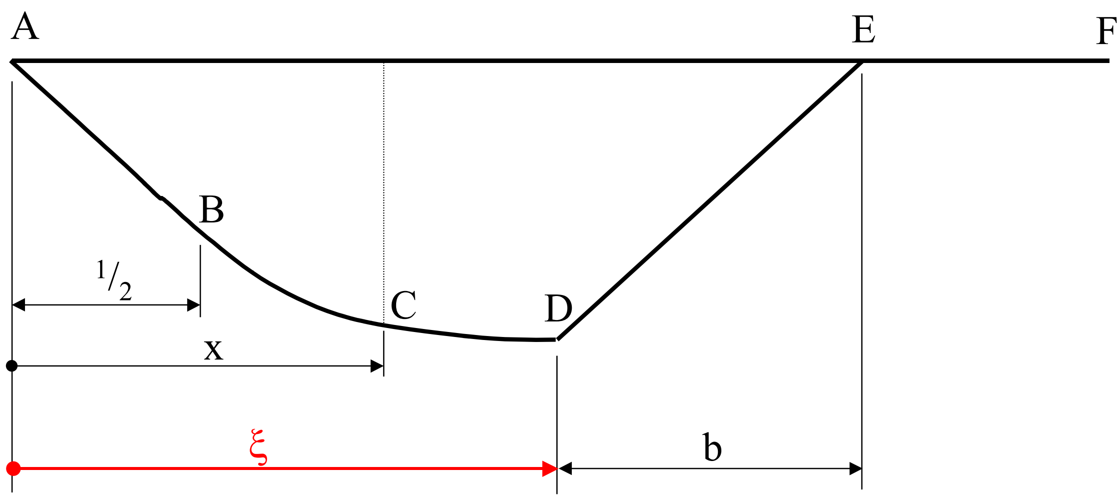

Figure 8.2: **Axial force diagram for a long line during the first cycle of heating for $½ \leq \xi \leq \xi_1$.**

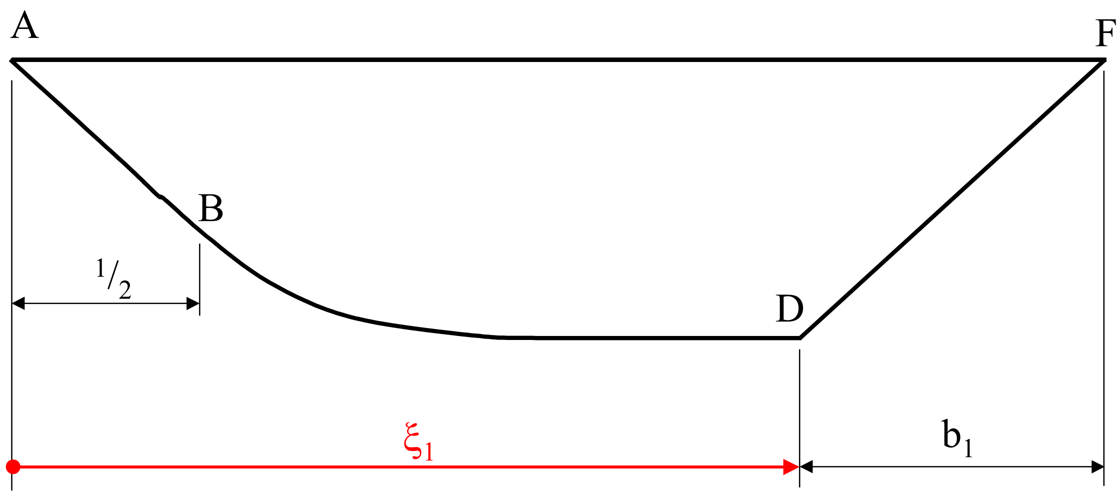

Figure 8.3: **Axial force diagram for a long line during the first cycle of heating in the range $\xi_1 \leq \xi \leq L$.**

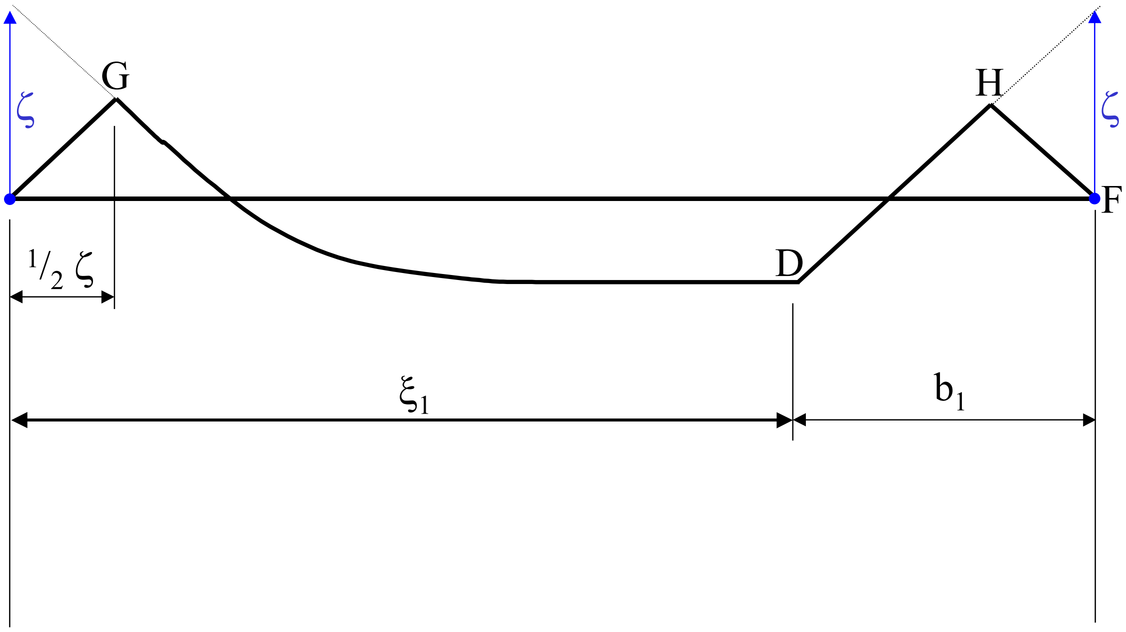

Figure 8.4: **Axial force diagram for a long line during the first cycle of cooling in the range $0 \le \zeta \le 1$.**

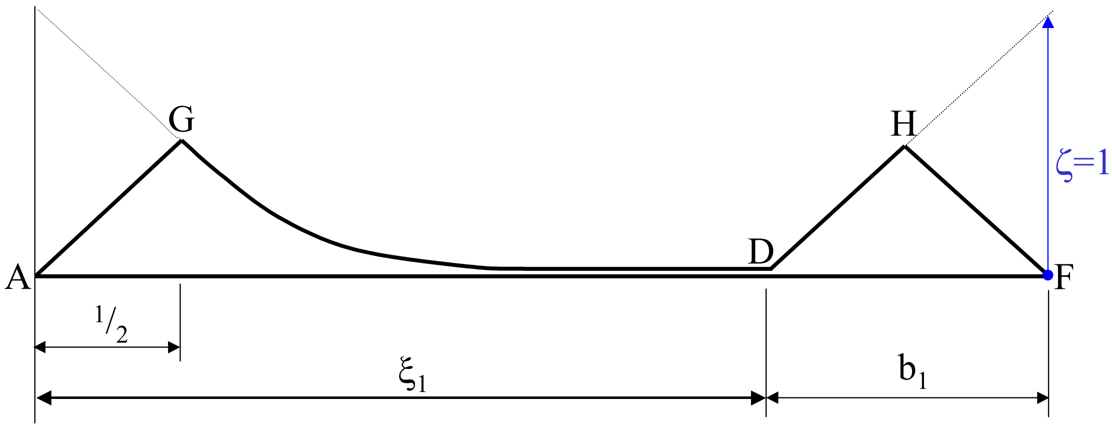

Figure 8.5: **Axial force diagram for a long line at the end of the first cooling cycle, i.e. when ζ=1.**

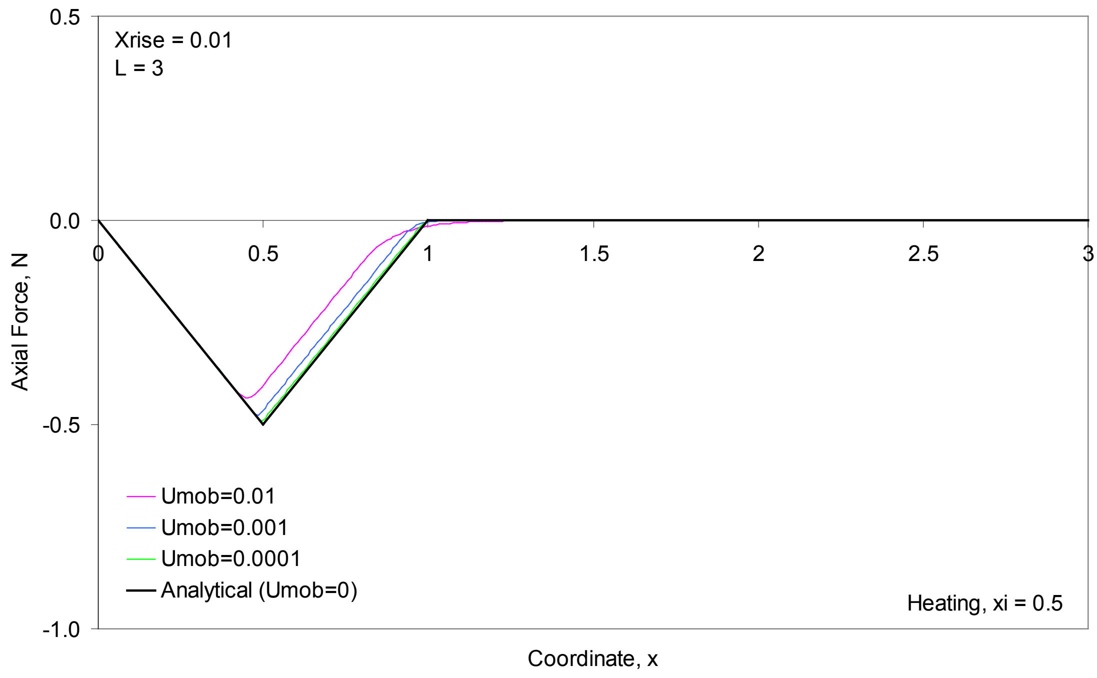

Figure 8.6: **Comparison of axial force diagrams from the finite element solution for various values of the dimensionless mobilisation displacement ("Umob") with the analytical solution during heating at ξ=0.5.**

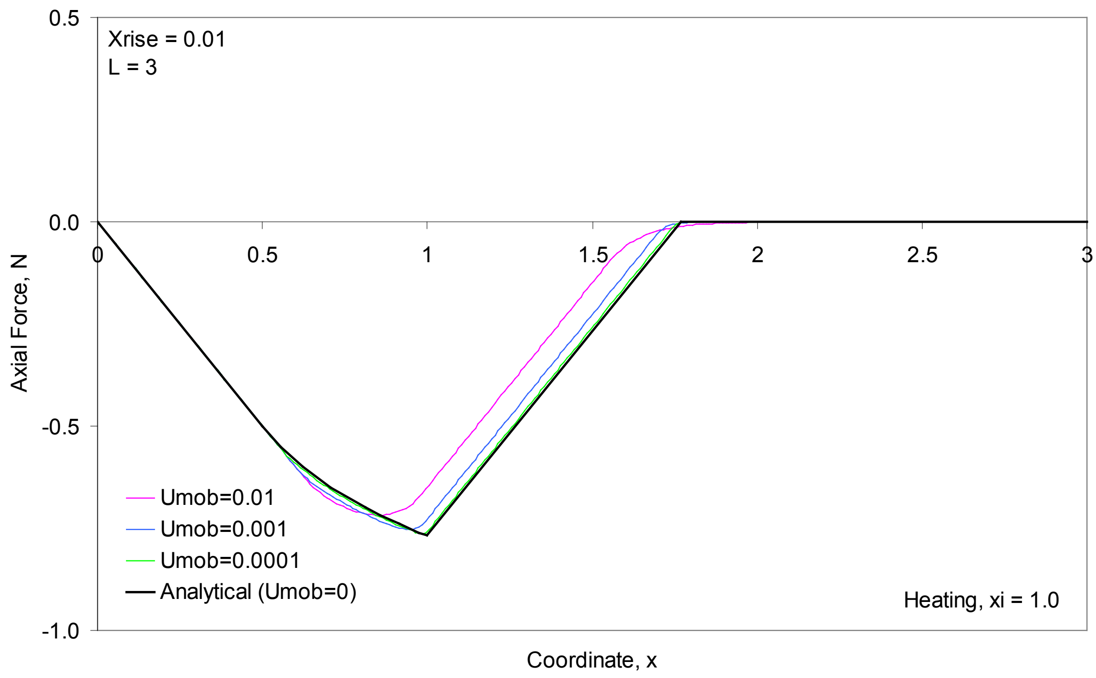

Figure 8.7: **Comparison of axial force diagrams from the finite element solution for various values of the dimensionless mobilisation displacement ("Umob") with the analytical solution during heating at ξ=1.0.**

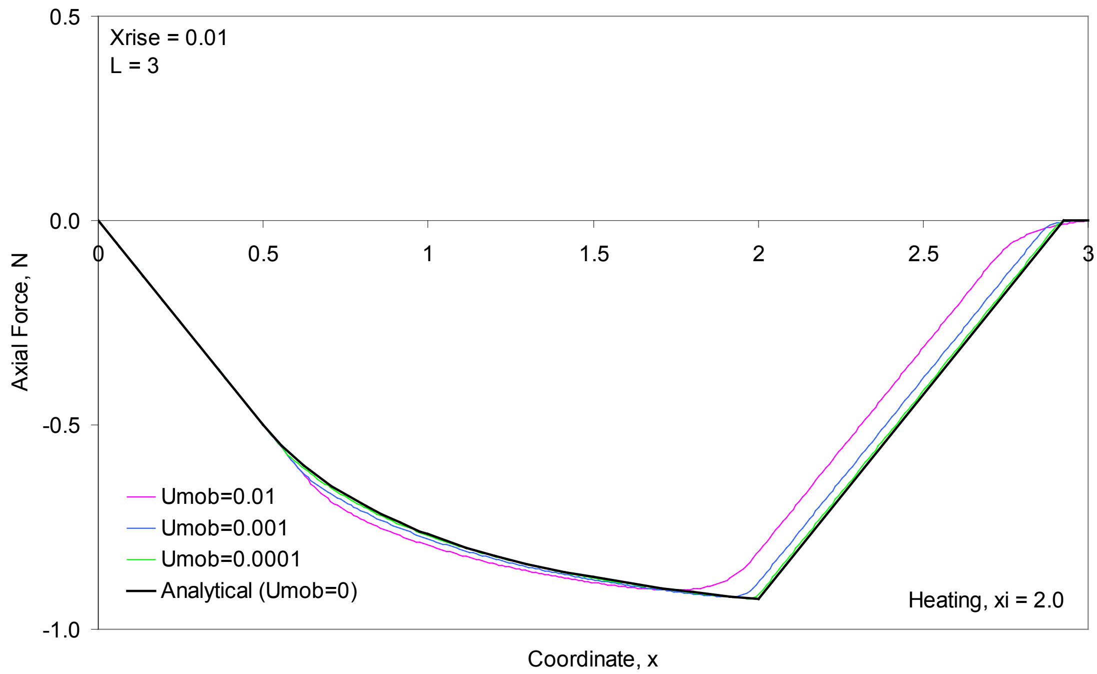

Figure 8.8: **Comparison of axial force diagrams from the finite element solution for various values of the dimensionless mobilisation displacement ("Umob") with the analytical solution during heating at ξ=2.0.**

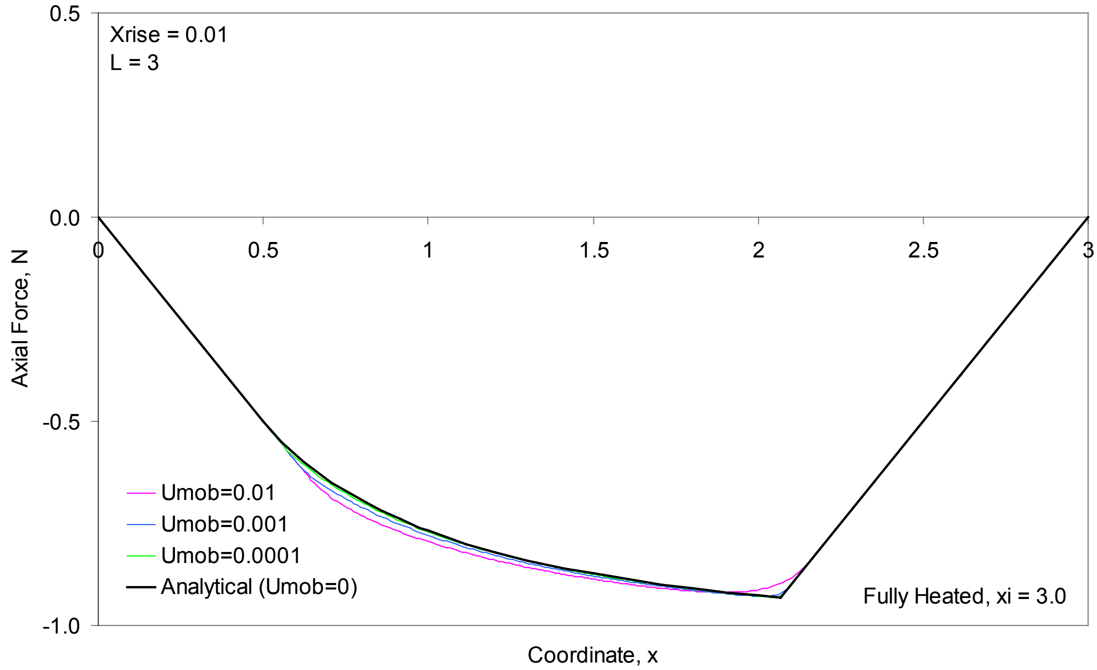

Figure 8.9: **Comparison of axial force diagrams from the finite element solution for various values of the dimensionless mobilisation displacement ("Umob") with the analytical solution when fully heated (ξ=3.0).**

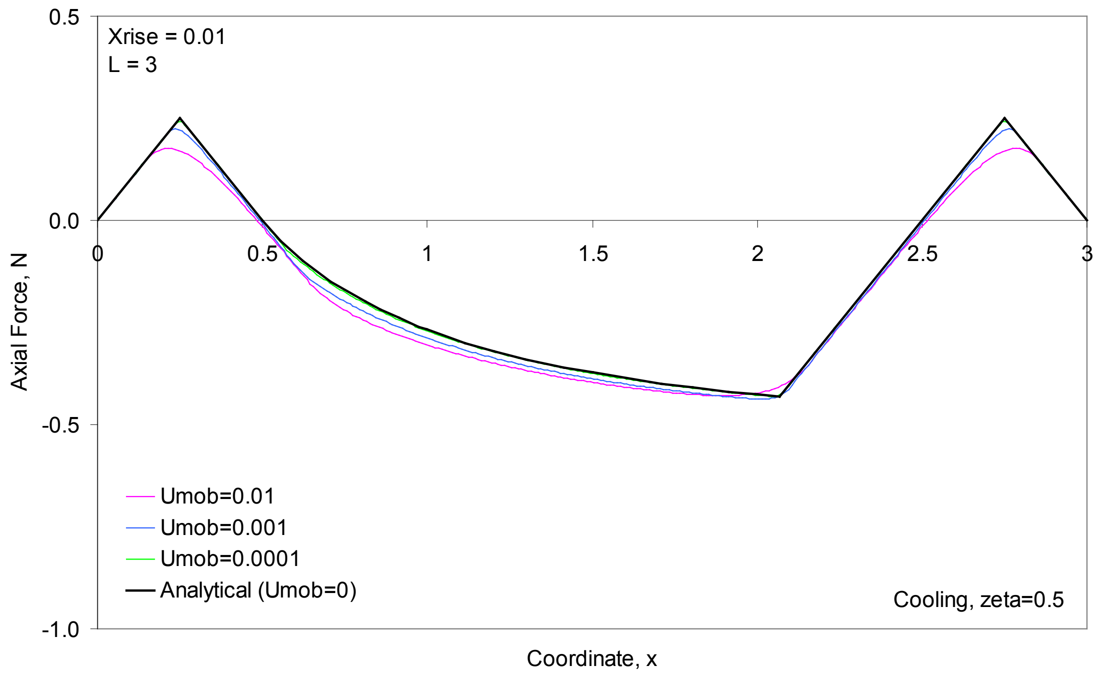

Figure 8.10: **Comparison of axial force diagrams from the finite element solution for various values of the dimensionless mobilisation displacement ("Umob") with the analytical solution when line is half-cooled (ζ=0.5).**

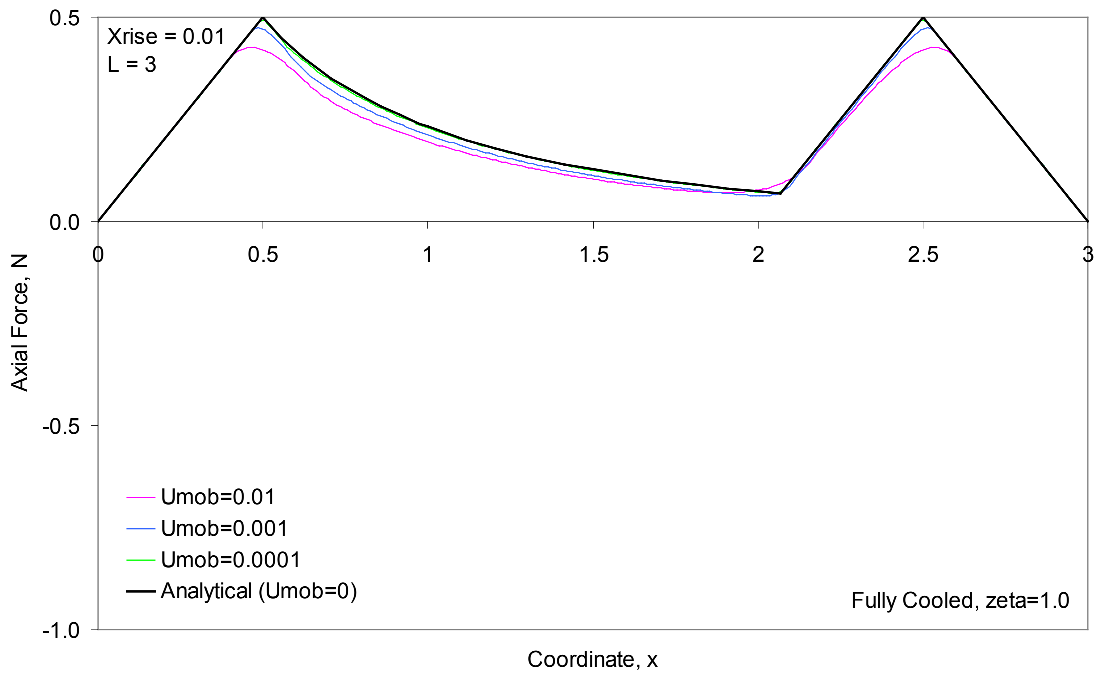

Figure 8.11: **Comparison of axial force diagrams from the finite element solution for various values of the dimensionless mobilisation displacement ("Umob") with the analytical solution when line is fully cooled (ζ=1.0).**

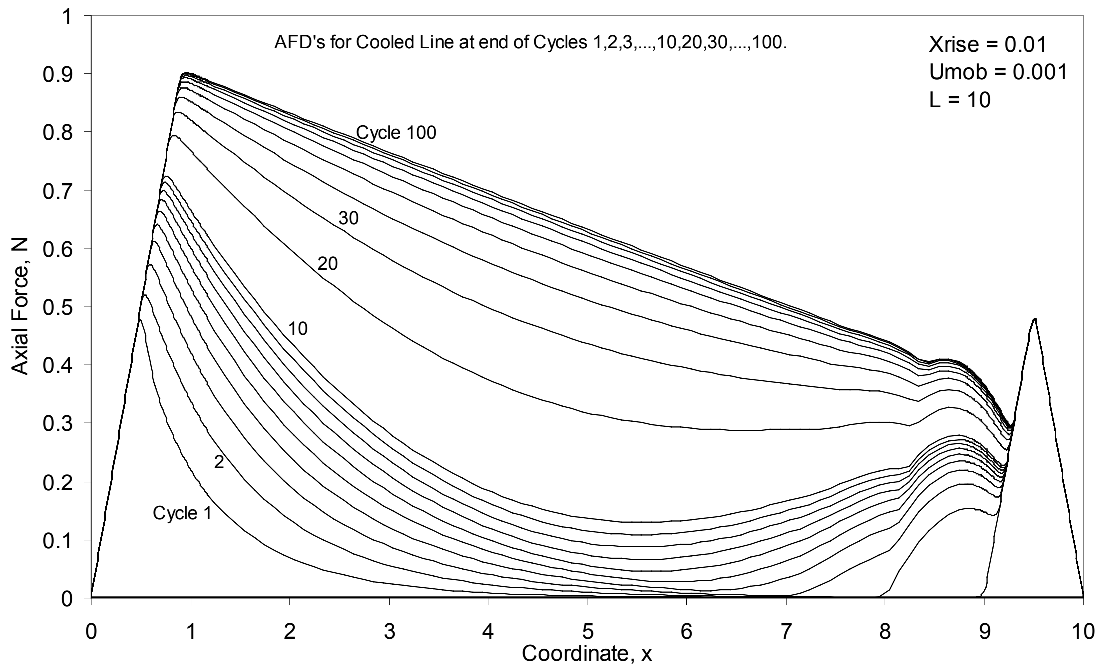

Figure 8.12: **Axial force diagrams for the cooled line at the end of cycles 1,2,3,…,10,20,30,…,100, for a temperature rise length of X_{rise}=0.01 (involves supercritical temperature gradients traveling over the entire line).**

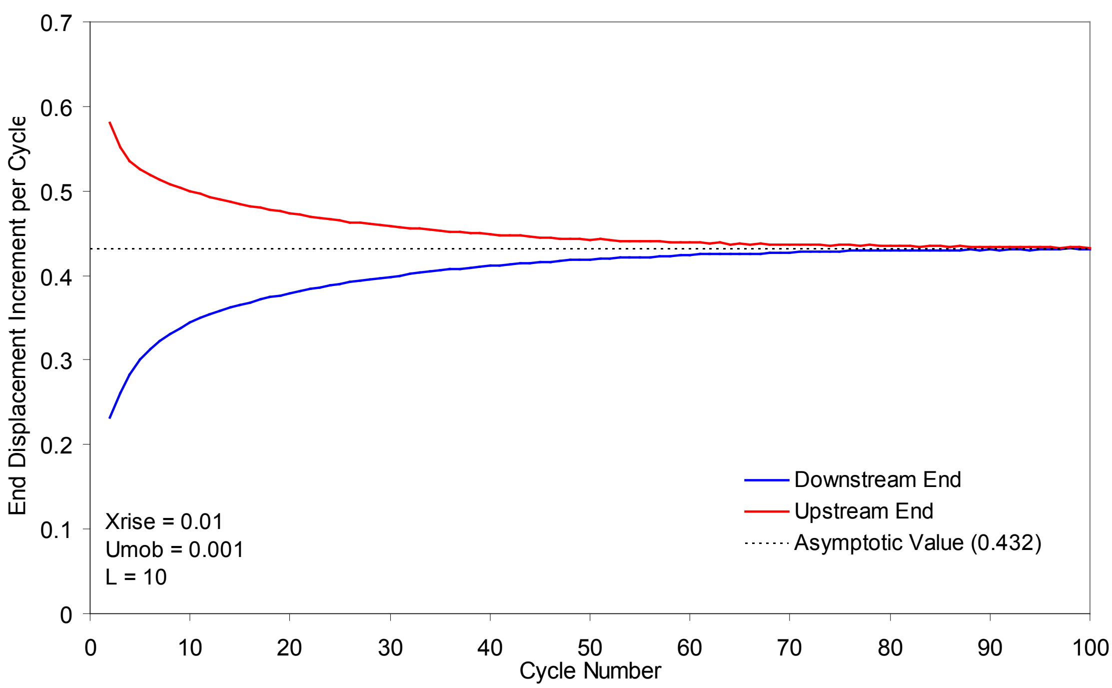

Figure 8.13: **End displacement increments per cycle for case X_{rise}=0.01.**

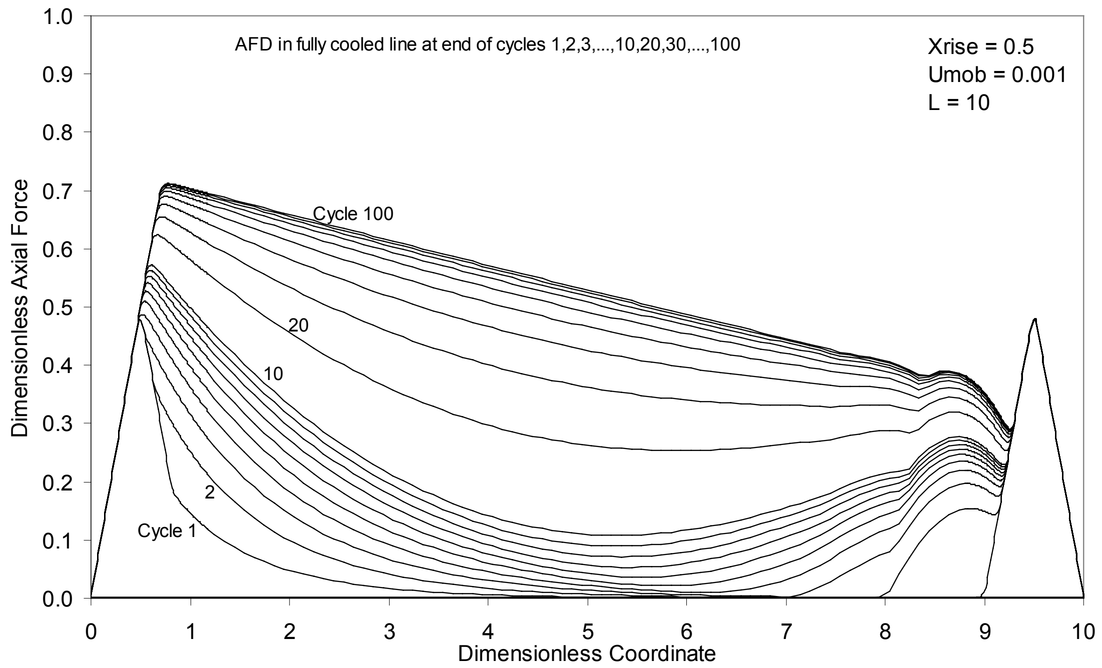

Figure 8.14: Axial force diagrams for the cooled line at the end of cycles 1,2,3,…,10,20,30,…,100, for a temperature rise length of X_{rise}=0.5 (involves super-critical temperature gradients traveling over the entire line).

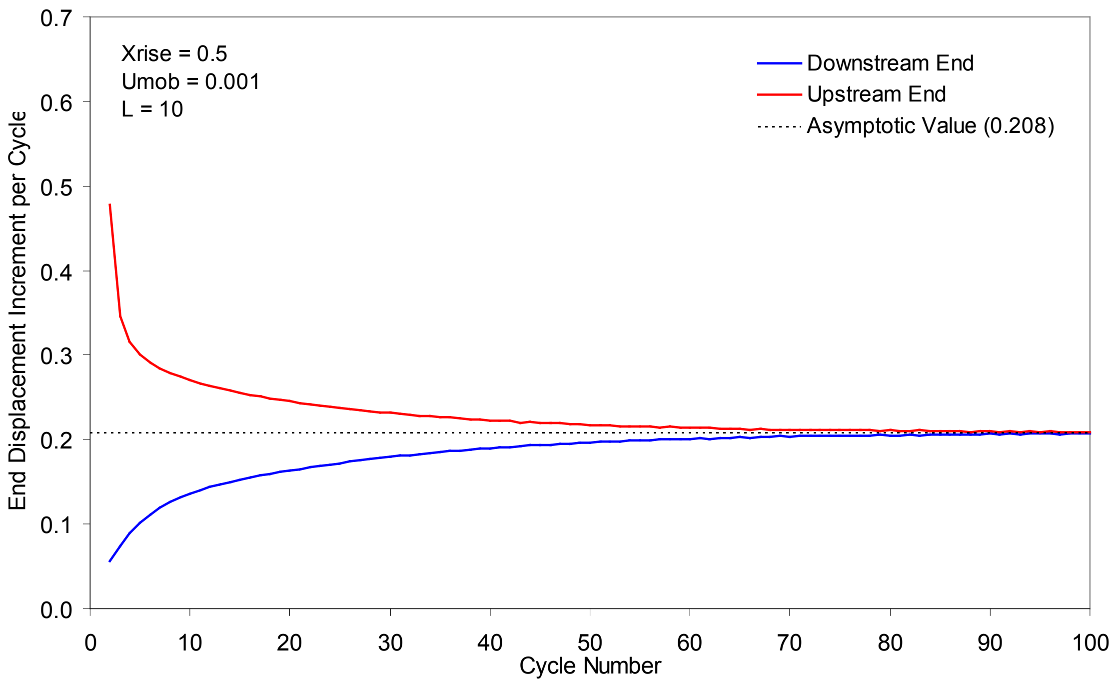

Figure 8.15: End displacement increments per cycle for case X_{rise}=0.5.

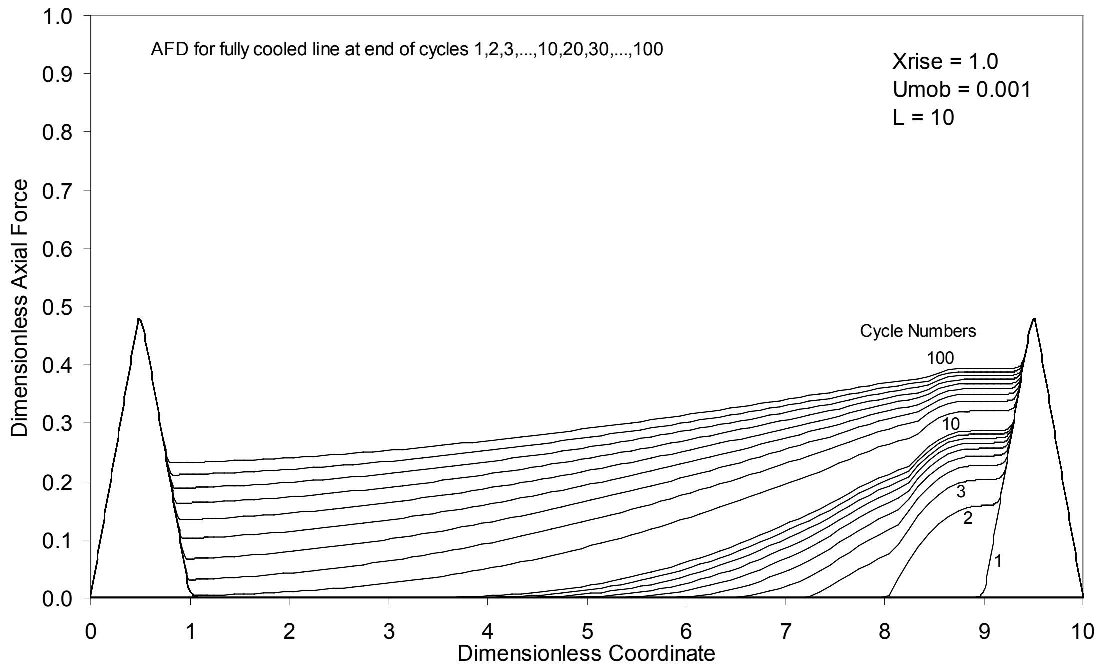

Figure 8.16: **Axial force diagrams for the cooled line at the end of cycles 1,2,3,…,10,20,30,…,100, for a temperature rise length of X_{rise}=1.0 (involves critical temperature gradient).**

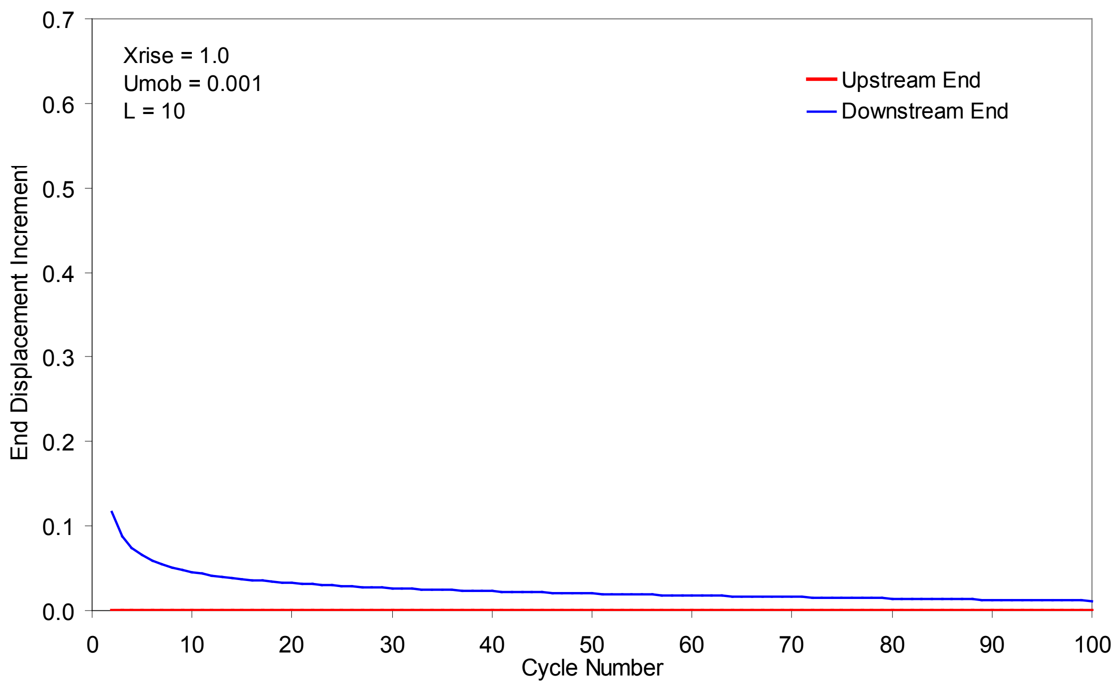

Figure 8.17: **End displacement increments per cycle for case X_{rise}=1.0.**

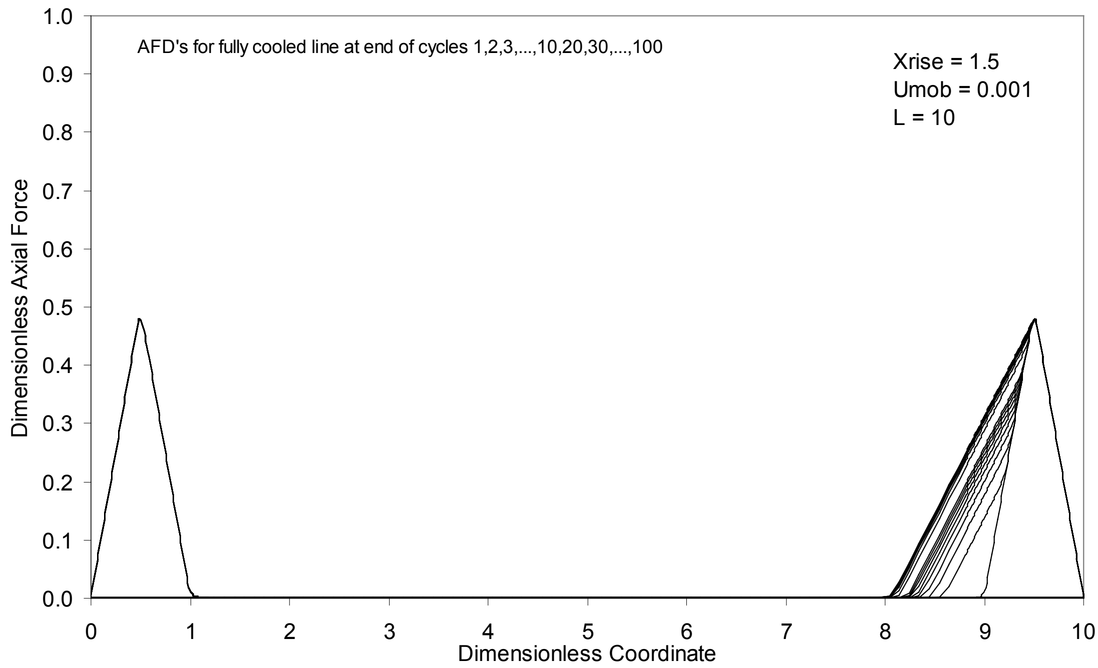

Figure 8.18: **Axial force diagrams for the cooled line at the end of cycles 1,2,3,…,10,20,30,…,100, for a temperature rise length of X_{rise}=1.5 (involves sub-critical temperature gradients).**

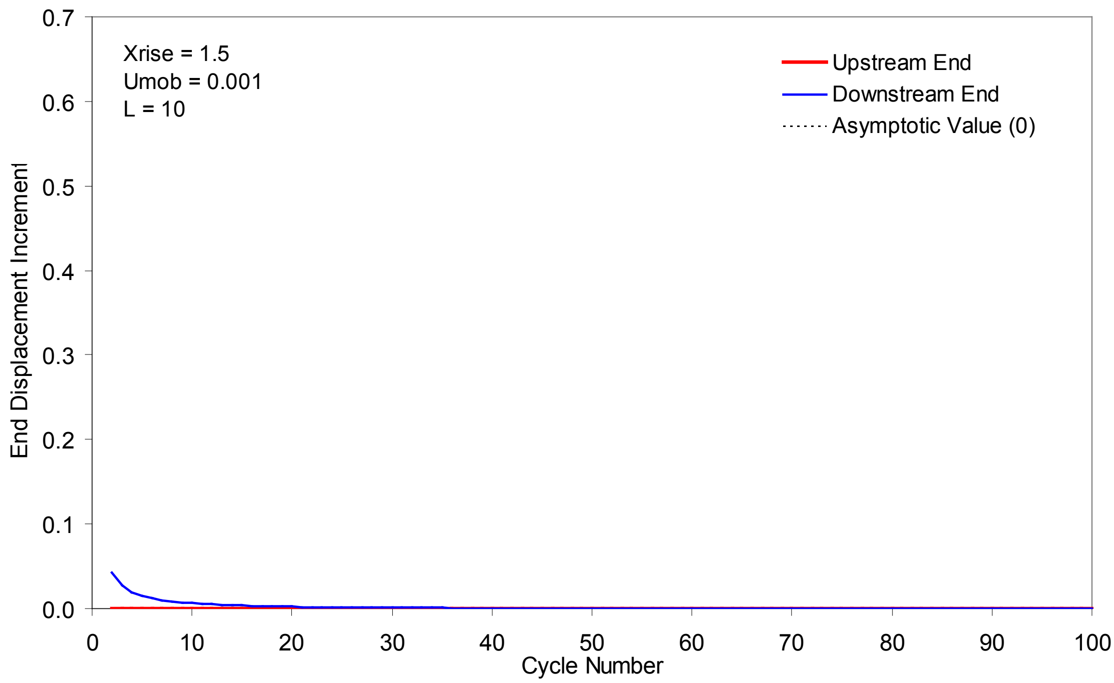

Figure 8.19: **End displacements increments per cycle for case X_{rise}=1.5.**

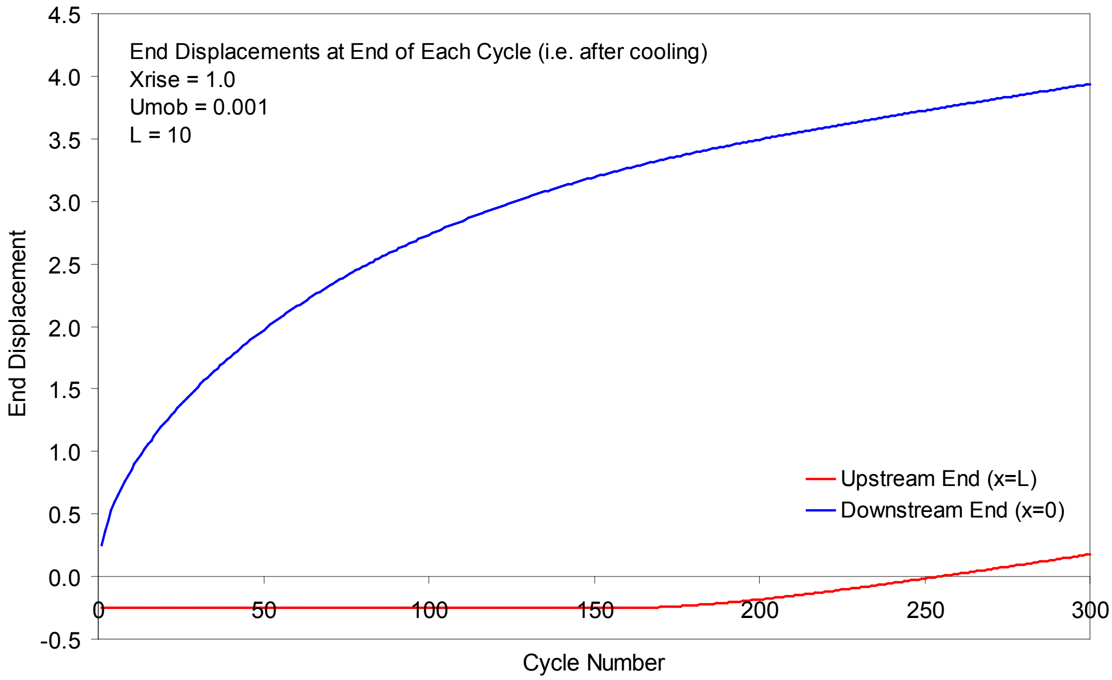

Figure 8.20: Total displacements at end of each heating and cooling cycle for case X_{rise}=1 (critical case).

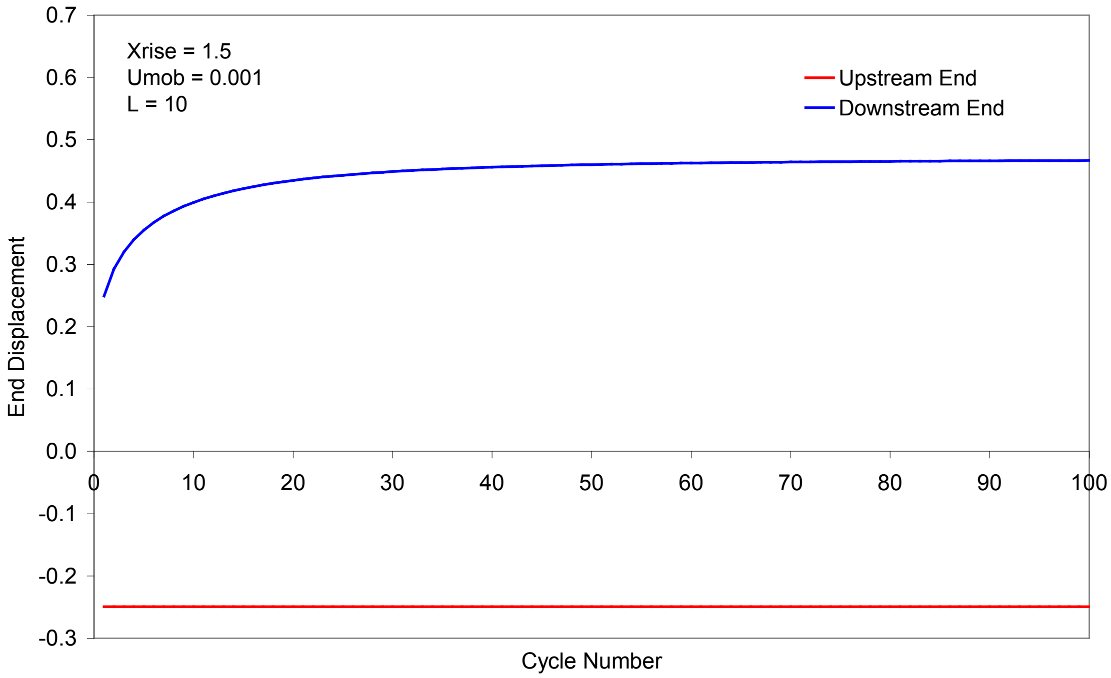

Figure 8.21: Total displacements at end of each heating and cooling cycle for case X_{rise}=1.5 (sub-critical case).

REFERENCES

[1] Konuk, I., (1998), "Expansion of Pipelines under Cyclic Operational Conditions: Formulation of Problem and Development of Solution Algorithm," 17th International Conference on Offshore Mechanics and Arctic Engineering, ASME, paper OMAE98-1103.

[2] Tornes,K., Ose, B.A., Jury, J. and Thomson, P., (2000), "Axial Creeping of High Temperature Flowlines Caused by Soil Ratcheting," OMAE 2000, Paper No. 5055.Konuk, I., (1998), "Expansion of Pipelines under Cyclic Operational Conditions: Formulation of Problem and Development of Solution Algorithm," 17th International Conference on Offshore Mechanics and Arctic Engineering, ASME, paper OMAE98-1103.

APPENDIX A. ANALYTICAL SOLUTION FOR A RIGID UNILATERAL RESTRAINT AT THE UPSTREAM END

The assumed axial force diagram (AFD) for the fully cooled line with a rigid unilateral restraint at the upstream end is shown in Figure A.1, where P denotes the tensile force exerted by the unilateral restraint at the upstream end. It is shown in this Appendix that applying a temperature surge followed by uniform cooling of the line results again in an AFD that is of the same form of that from Figure A.1, but with a different value of P. To do so, a number of different stages of heating and cooling are considered. For each of these stages different expressions for the analytical solution apply. A separate sub-section being devoted below to each one of these.

Heating, $0 \le \xi \le c$ (To Slackening of Restraint)

As the line is heated, the restraint force will decrease. Whereas P denotes the value of the restraint force when the line is fully cooled, the value during heating will be denoted by $p=p(\xi)$, where $p(\xi)\le P$, and $p(0)=P$. Again it is reasonable to expect upstream slip on the upstream side of the heating front and downstream slip downstream side. This gives rise to the AFD of Figure A.2. The corresponding displacements are

$$w(x,\xi) = 2 \{ H^{(-2)}(x_J - x) - H^{(-2)}(B-x) - H^{(-2)}(\xi - x)\} - H^{(-1)}(\xi - x) \quad \text{(A.1)}$$

in which $w=w(x,\xi)$ denotes the displacement increment from the beginning of the cycle, $H^{(-n)}$ is the n^{th} integral of a step function, as defined in Eqs. 3.22 to 3.24, and

$$x_J = \xi - \tfrac{1}{2} (L - p) \quad \text{(A.2)}$$

represents the x-coordinate of point J in Figure A.2. In particular the displacement at the upstream end is

$$w(0,\xi) = x_J^2 - B^2 - \xi^2 - \xi \quad \text{(A.3)}$$

in which $B=(L - P)/2$. Requiring this to be zero, in view of the rigid constraint gives

$$\xi = \tfrac{1}{4} [(L - p)^2 - (L - P)^2]/(1 - L + p) \quad \text{(A.4)}$$

which implicitly defines the time dependence $p=p(\xi)$ of the restraint force. Of particular interest is the value of the time parameter ξ at which the restraint force drops to zero. This value will be denoted by c and is given by substituting $p=0$ into Eq. A.4, to obtain

$$c = \tfrac{1}{4} P (2L - P)/(1 - L) \quad \text{(A.5)}$$

A condition for the solution to remain valid until $p=0$ is that point J in Figure A.2 may not reach the end of the line. This requires that

$$c \le L/2 \quad \text{(A.6)}$$

However c depends on P. The maximum value occurs at $P=L$ and is given by

$$c_{max} = \tfrac{1}{4} L^2 /(1 - L) \quad \text{(A.7)}$$

This means that the solution remains valid until $p=0$ for all values of P, provided that $c_{max} \le L/2$, which means that

$$L \le 2/3 \quad \text{(A.8)}$$

By differentiating the displacements with respect to ξ one can also verify after some effort that the assumed slip directions are correct provided that $L<1$. This then also validates the AFD of Figure A.2.

Heating, $c \leq \xi \leq L/2$

Beyond ξ=c, the unilateral restraint slackens, and the pipe behaves again as if both ends were free. Indeed the intricacies of the solution of the previous stage become irrelevant to the solution at the end of this stage, which is identical to that for the case when both ends are fully unrestrained. In other words the presence of the unilateral restraint during the previous stage affected the AFD then, but it has no influence on the solution during this stage. During the previous stage the axial force did not help in preventing crawling of the pipe. The AFD at the end of the this stage is shown in Figure A.3, and the end displacements are given by

$$w_{ends(\xi=L/2)} = \{\ \tfrac{3}{4} L^2 - B^2 - \tfrac{1}{2} L\ ,\ 0\ \} \qquad \text{(A.9)}$$

Heating, $L/2 \leq \xi \leq L$

During this stage:

- there continues to be no contact at the restraint, so that the solution continues to coincide with that for the case when both ends are fully free;
- there is no change in the axial force diagram (Figure A.3 still applies); and
- slip occurs only in the cold portion of the line.

The end of this heating stage is also the end of the entire heating cycle. At that point the end displacements are given by:

$$w_{ends(\xi = L)} = \{\ \tfrac{3}{4} L^2 - B^2 - \tfrac{1}{2} L\ ,\ \tfrac{1}{2} L\ \} \qquad \text{(A.10)}$$

Cooling, $0 \leq \zeta \leq L$

While the restraint remains slack, the solution continues to coincide with that for a fully free line. The AFD for this stage is shown in Figure A.4. The end displacement increments are $\tfrac{1}{4}\zeta^2$ inward at each end, resulting in total end displacements given by

$$w_{ends} = \{\ \tfrac{3}{4} L^2 - B^2 - \tfrac{1}{2} L - \tfrac{1}{4}\zeta^2\ ,\ \tfrac{1}{2} L + \tfrac{1}{4}\zeta^2\ \} \qquad \text{(A.11)}$$

This solution remains valid until either

(a) AFD becomes triangular (at shown in Figure A.5), which happens at $\zeta = L$, or

(b) the restraint becomes active again,

whichever occurs first. It can be shown that as long as $L \leq 1/2$, the former always happens first. In the range $\tfrac{1}{2} \leq L \leq {}^{2}/_{3}$, it depends on the value of P, whereas for $L > 2/3$ the latter happens first. Here we consider the case when

$$L \leq \tfrac{1}{2} \qquad \text{(A.12)}$$

so that the above solution remains valid until ζ=L, with the restraint remaining slack throughout this stage, and displacements at the end of this stage are given by

$$w_{ends(\zeta=L)} = \{\ \tfrac{1}{2} L^2 - B^2 - \tfrac{1}{2} L\ ,\ \tfrac{1}{2} L + \tfrac{1}{4} L^2\ \} \qquad \text{(A.13)}$$

Cooling, $L \le \zeta \le \zeta_c$

During this stage cooling occurs with no change in the AFD (Figure A.5 continues to apply), and the change in end displacements is given by

$$\Delta w_{ends} = \tfrac{1}{2}\,\zeta\, L \ \{1, -1\} \tag{A.14}$$

which results in end displacements given by

$$w_{ends} = \{ \tfrac{1}{2} L^2 - B^2 - \tfrac{1}{2} L + \tfrac{1}{2}\zeta L,\ \tfrac{1}{2} L + \tfrac{1}{4} L^2 - \tfrac{1}{2}\zeta L \} \tag{A.15}$$

From this it is seen that the displacement at the upstream end vanishes when

$$\zeta = \zeta_c = 1 + 2B^2/L - L \tag{A.16}$$

Thus at the end of this stage the end displacements are given by

$$w_{ends(\zeta=\zeta c)} = \{ 0 ,\ \tfrac{3}{4} L^2 - B^2 \} \tag{A.17}$$

Cooling, $\zeta_c \le \zeta \le 1$

If both ends were restrained during this cooling, the AFD would be the one shown as a dashed line in Figure A.6. However only the upstream end is restrained. Therefore slip can be expected at the downstream end. It is reasonable to assume that such slip extends over region BC in Figure A.6, resulting in the AFD shown, where

$$p = \zeta - \zeta_c \tag{A.18}$$

$$a = (L+p)/2 \tag{A.19}$$

$$b = (L - p)/2 \tag{A.20}$$

The corresponding displacement increments from the beginning of this stage can be written as

$$\begin{aligned} \Delta u &= 0 && \text{for } 0 \le x \le b \\ &= -(x - b)^2 && \text{for } b \le x \le L/2 \\ &= -(L/2 - b)^2 - (\zeta - \zeta_c)(x - L/2) && \text{for } L/2 \le x \le L \end{aligned} \tag{A.21a-c}$$

By differentiating this expression with respect to ζ (noting that $\partial b/\partial\zeta = -\tfrac{1}{2}$) one can verify that the assumed slip directions are satisfied.

Cooling is complete when $\zeta=1$. At that point the tensile force exerted by the restraint is given by

$$P^* = 1 - \zeta_c \tag{A.22}$$

Thus at the end of the cycle the AFD has the same shape it started off with, except that the end force at the end of the cycle is P^* given by Eq. A.22, instead of the end force P at the beginning of the cycle. Eq. A.22 can be made more explicit by substituting for ζ_C from Eq. A.16, and then for B from the expression following Eq. A.3 to obtain

$$\begin{aligned} P^* &= L - 2B^2/L \\ &= L - (L - P)^2/(2L) \end{aligned} \tag{A.22}$$

This can then be re-written in the form of Eq. 5.1. The steady-state value of the restraint forces at the end of each cycle is found by substituting $P^*=P$ into Eq. A.22. This gives P=L.

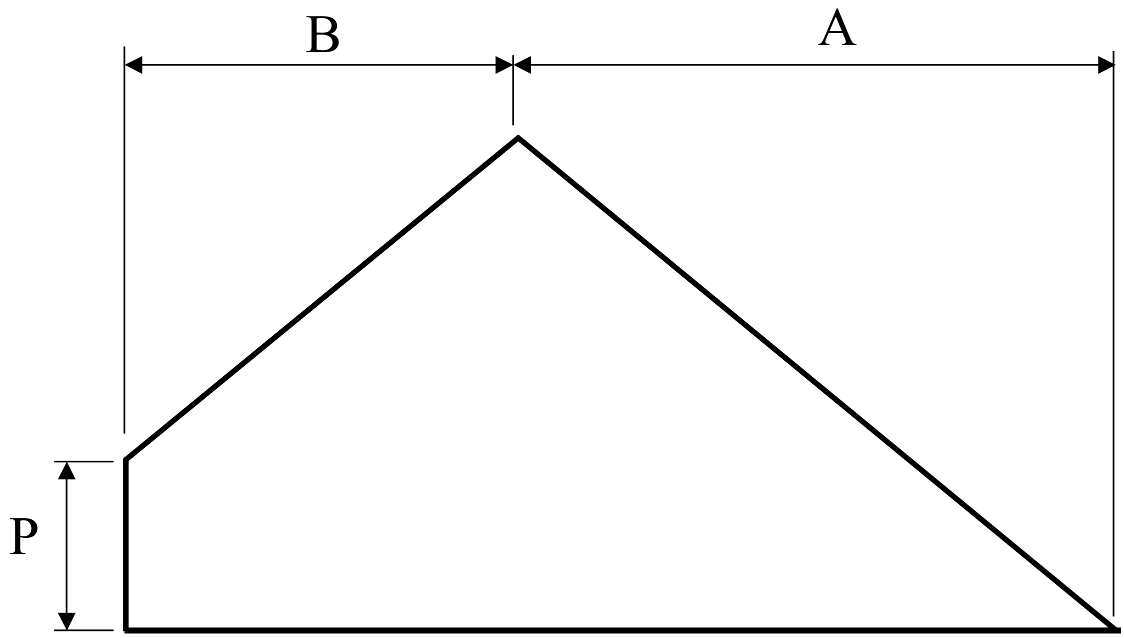

Figure A.1: **Axial force diagram for a short pipe with a unilateral restraint at the upstream end at the beginning of a cycle (ξ=0). (Line is fully cooled.).**

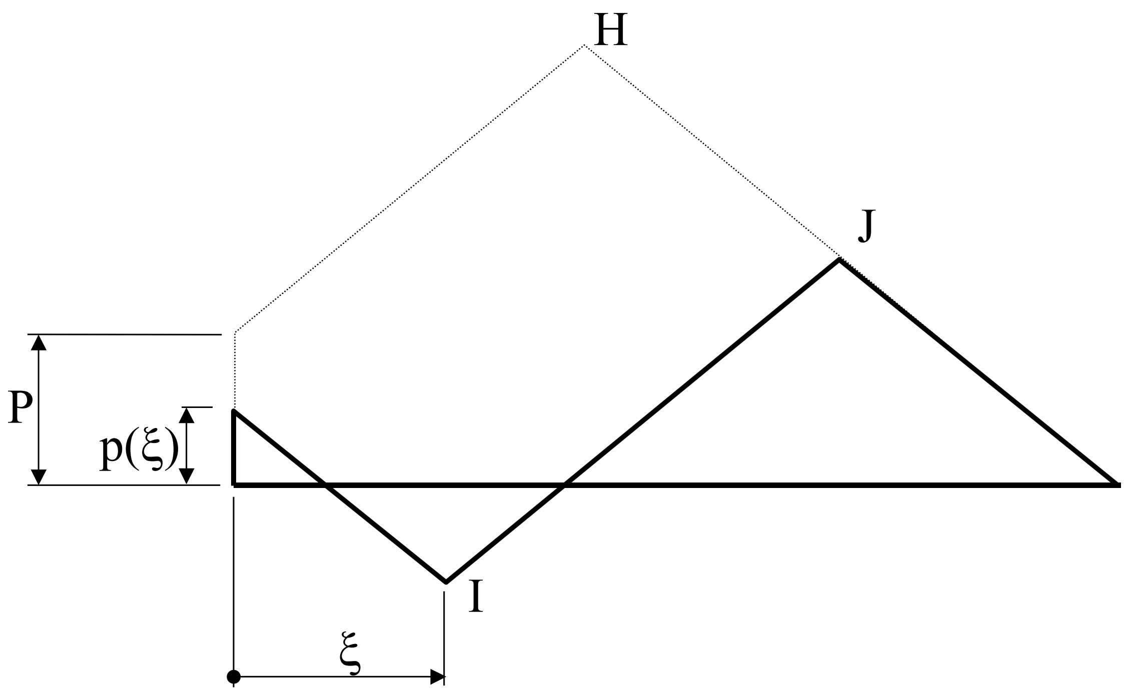

Figure A.2: **Axial force diagram during heating in the range $0 \leq \xi \leq c$.**

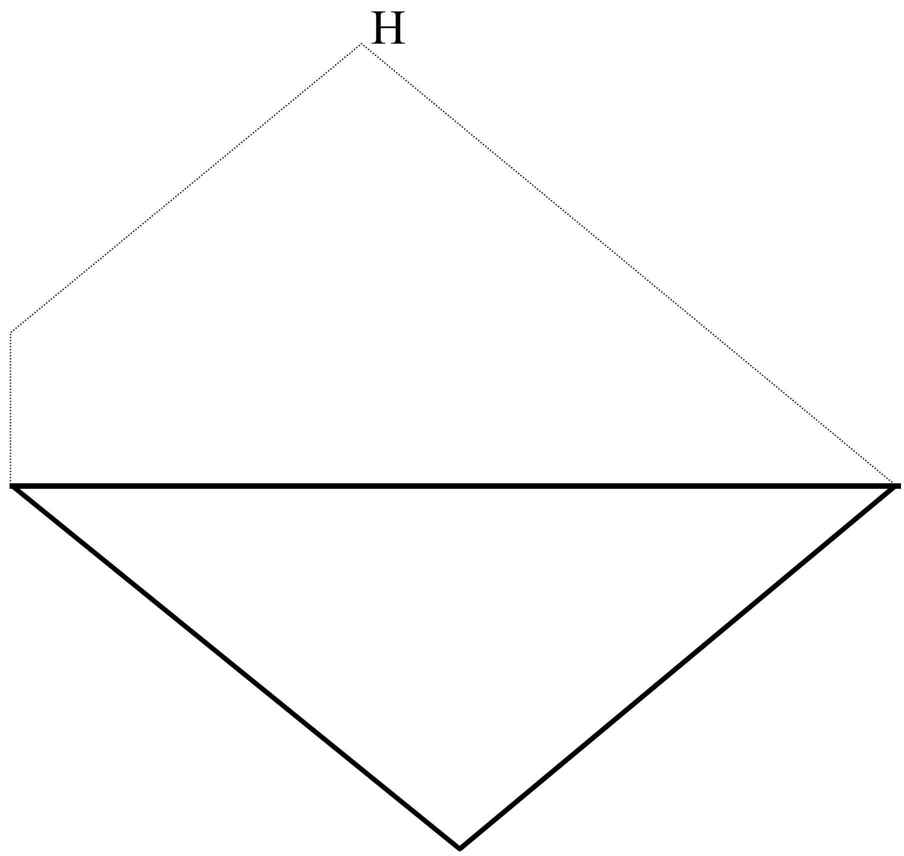

Figure A.3: Axial force diagram during heating in the range $L/2 \leq \xi \leq L$.

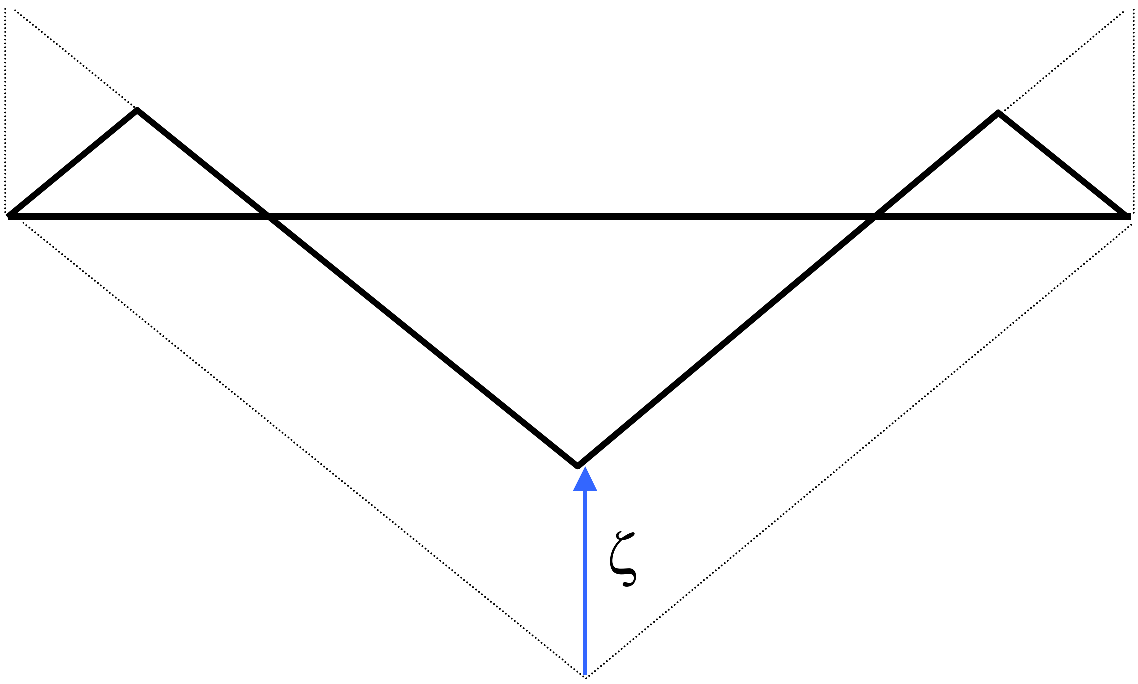

Figure A.4: Axial force diagram during cooling in the range $0 \leq \zeta \leq L$.

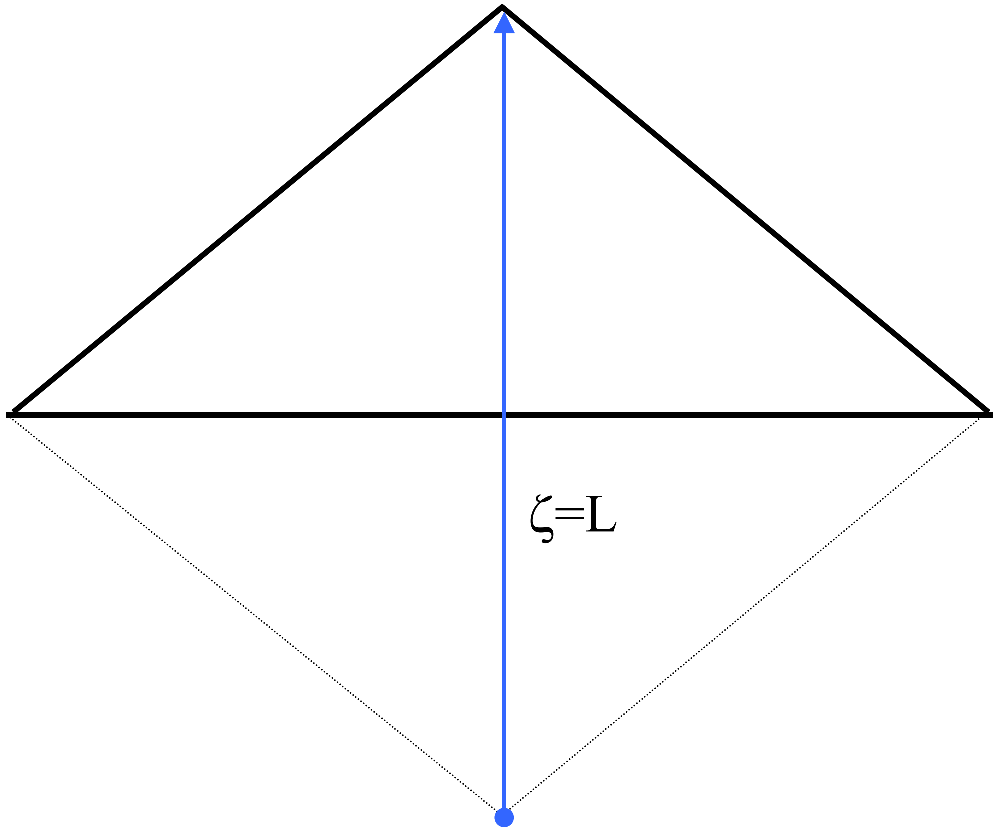

Figure A.5: Axial force diagram during cooling, when $\zeta = L$. (This AFD remains unchanged for $L \le \zeta \le \zeta_C$.).

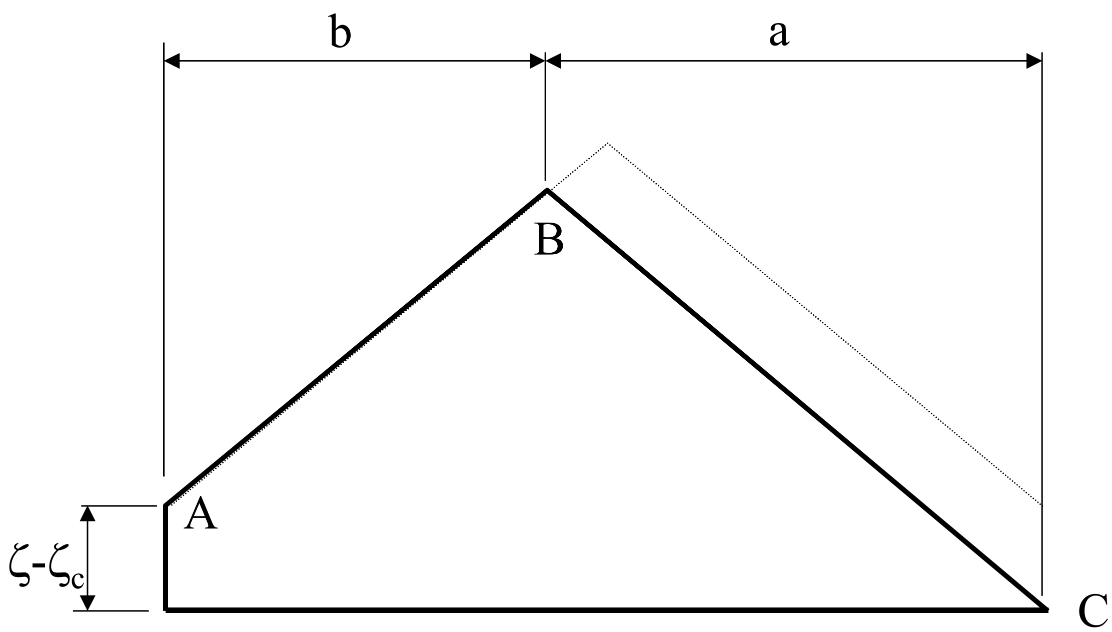

Figure A.6: Axial force diagram during cooling in the range $L \le \zeta \le \zeta_C$.

APPENDIX B. ANALYTICAL SOLUTION FOR UNILATERAL RESTRAINT AT OPTIMAL LOCATION

In this Appendix a steady-state analytical solution is derived, that satisfies the optimality condition stated in Section 6.2. This optimality condition is derived from observations from finite element solutions of Section 6, rather than from the analysis in this appendix. However this appendix does yield the "optimal"[vii] location of the restraint, and the force that the restraint must be able to resist.

The sequence of axial force diagrams that develops during the cycle is shown in Figures B.1 to B.8. Details of the analytical solution are given in separate sub-sections for each stage of the heating and cooling process. As before heating is by a temperature surge traveling down the line, and cooling is uniform. Furthermore the time-like parameters used are again ξ to denote the distance the temperature surge has traveled along the line during heating (ranging from $\xi=0$ to $\xi=L$), and ζ, which denotes the cooling fraction, and ranges from $\zeta=0$ for the fully hot line, to $\zeta=1$ for the fully cooled line. Throughout this Appendix all notation refers to the dimensionless values of the variables, as defined in Section 2.2.

Fully Cooled Line, $\xi = 0$ (Restraint Slack)

It is assumed that for the fully cooled line at the end of a steady-state cycle, there is a gap g at the restraint, and the Axial Force Diagram (AFD) is the triangular one of Figure B.1, involving a maximum axial tension of N= ½ L. The validity of these assumptions will be proven by showing that at the end of the cycle one returns to the same state.

The condition for a gap at the restraint can be written as

$$u = -g \quad \text{at} \quad x = L - h, \quad \xi=0 \tag{B.1}$$

where u is the displacement, g is the gap at the restraint at the start of the cycle (with $g>0$), and h denotes the distance from the restraint to the downstream end of the pipe. Thus the axial coordinate of the restraint is given by

$$x_r = L - h \tag{B.2}$$

It is assumed that the restraint is located downstream of the mid-line position (i.e. $h \le L/2$, $x_r \ge L/2$). This assumption will be confirmed in what follows by finding an optimal restraint location that lies within this range.

Heating, $0 \le \xi \le L/2$ (Restraint Slack)

The solution for this stage is a special case of the solution in Section 3 for the second heating cycle. This results in the AFD shown in Figure B.2.

At $\xi=L/2$, the slip front (point C in Figure B.2) reaches the end of the line, resulting in the AFD of Figure B.3. After $\xi=L/2$ further increases in the axial compressive force downstream of the restraint are not possible. Thus the optimality condition of Section 6.2 implies that the gap should close at $\xi=L/2$, i.e.,

$$u = 0 \qquad \text{at} \quad x = L - h, \quad \xi=L/2 \tag{B.3}$$

[vii] "Optimal" in the sense that the optimality condition of Section 6.2 is satisfied.

Since there is no slip at the downstream end, the increment in displacement at the restraint from $\xi=0$ to $\xi=L/2$ is given by

$$\Delta u_r = h^2 \qquad \text{(B.4)}$$

so that the total displacement at the restraint is

$$u = -g + h^2 \qquad \text{at} \quad x = L - h, \quad \xi=L/2 \qquad \text{(B.5)}$$

Thus the optimality condition yields

$$g = h^2 \qquad \text{(B.6)}$$

Heating, $L/2 \leq \xi \leq L - h$ (Restraint Active)

The heating front is now in-between the midline point and the restraint. Assuming again that the slip direction is away from the heating front results in the AFD shown in Figure B.4. Therein the restraint reaction $p=p(\xi)$ is the jump in axial force N at the restraint. It follows from the geometry of this AFD[viii] that the restraint reaction is given by

$$p = 2\,\xi - L \qquad \text{(B.7)}$$

Given that the displacement at the restraint must be zero, one can also integrate the axial force diagram (as described in Section 2.3) to obtain the following expression for the increment in displacements from time $\xi=L/2$ to the current value of ξ:

$$\begin{aligned}
\Delta u &= p\,(L-h-\xi) + (\xi-L/2)^2 - (\xi-x) && \text{for } 0 \leq x \leq L/2 \\
&= p\,(L-h-\xi) + (\xi-L/2)^2 - (x-L/2)^2 - (\xi-x) && \text{for } L/2 \leq x \leq \xi \\
&= p\,(L-h-x) && \text{for } \xi \leq x \leq L-h \\
&= 0 && \text{for } L-h \leq x \leq L \qquad \text{(B.8)}
\end{aligned}$$

By differentiating this expression with respect to ξ after substitution for $p=p(\xi)$ from Eq. B.7, it is readily verified that the required slip conditions are satisfied provided that $L\leq 1$. This validates the assumptions in regard to slip directions used to derive the AFD of Figure B.4.

When the heating front reaches the restraint ($\xi=L-h$), the AFD of Figure B.4 reduces to that of Figure B.5. Substituting $\xi=L-h$ into Eq. B.7 gives

$$P = L - 2h \qquad \text{(B.9)}$$

for the restraint force at $\xi=L-h$. It will seen that subsequent stages bring no further increase in restraint force, so that P is also the maximum restraint force.

Heating, $L-h \leq \xi \leq L$ (Active Restraint)

The heating front is now downstream of the restraint. This produces further downstream slip on the downstream side of the heating front, but no change in the AFD. Thus the AFD of Figure B.5 applies until the line is fully heated. There is also no change in the restraint force during this stage.

[viii] The change in the axial coordinate between points B and F in Fig. B.4 must be ½ p.

Cooling, $0 \leq \zeta \leq 2h$ (Active Restraint)

As before (in Section 3, and Appendix A), the AFD for uniform cooling can be obtained by moving the AFD for the fully heated line upwards (i.e. assuming no slip), and then adjusting the AFD for slip at the ends. This results in the AFD of Figure B.6. The restraint remains active with no change in the restraint force throughout this stage.

At $\zeta = 2h$, the AFD reduces to that of Figure B.7.

Cooling, $2h \leq \zeta \leq L$ (Active Restraint)

With cooling beyond ζ=2h, the force in the restraint begins to drop from the maximum value P to a value denoted by $p=p(\zeta)$ in Figure B.8. Slip towards the mid-line point continues in regions AG and EC (Figure B.8), but with no slip in GF. From the geometry of the changes in the AFD (Figure B.8), one obtains a restraint force (jump in the AFD at the restraint) of

$$p = p(\zeta) = L - \zeta \qquad \text{(B.10)}$$

The total displacement increments during cooling so far implied by the AFD of Figure B.8 are

$$\begin{aligned} \Delta u &= (x - \tfrac{1}{2}\zeta)^2 && \text{for } 0 \leq x \leq \tfrac{1}{2}\zeta \\ &= 0 && \text{for } \tfrac{1}{2}\zeta \leq x \leq L - h \\ &= -(\zeta - 2h)[x - (L\text{-}h)] - [x - (L\text{-}h)]^2 && \text{for } L - h \leq x \leq L \qquad \text{(B.11)} \end{aligned}$$

By differentiating these expressions with respect to ζ to obtain the velocities, one can verify that the slip directions are consistent with those assumed in the derivation of the AFD, as they must be to validate the solution.

At the end of this stage (ζ=L), the AFD is back to the triangle of the beginning of the cycle (Figure B.1), and the restraint force p has reduced to zero.

Cooling, $L \leq \zeta \leq 1$ (Slack Restraint)

Cooling beyond ζ=L produces no change in the AFD. The cooling is accommodated by slip towards the mid-line point. Thus the displacement increment from ζ=L to the current value of ζ is

$$\Delta u = (\zeta - L)(L/2 - x) \qquad \text{(B.12)}$$

In particular the gap that opens up at the restraint by the time the line is fully cooled is given by

$$g^* = (1 - L)(L/2 - h) \qquad \text{(B.13)}$$

Optimal Restraint Location

For steady-state conditions the gap g at the beginning of the cycle (from Eq. B.6) must be equal to the gap g^* at the end of the cycle (from Eq. B.13). This gives the following equation for the optimal restraint location:

$$h^2 = (1 - L)(L/2 - h) \qquad \text{(B.14)}$$

which can be solved for h to obtain

$$h = \tfrac{1}{2} \{ (1-L^2)^{1/2} + L - 1 \} \quad \text{(B.15)}$$

Correspondingly the value of the axial coordinate x at the optimal restraint location is

$$x_{r,opt} = L - h$$

$$= \tfrac{1}{2} \{ L + 1 - (1-L^2)^{1/2} \} \quad \text{(B.16)}$$

and the maximum value of the restraint force for this optimal location of the restraint is given by

$$P = 1 - (1-L^2)^{1/2} \quad \text{(B.17)}$$

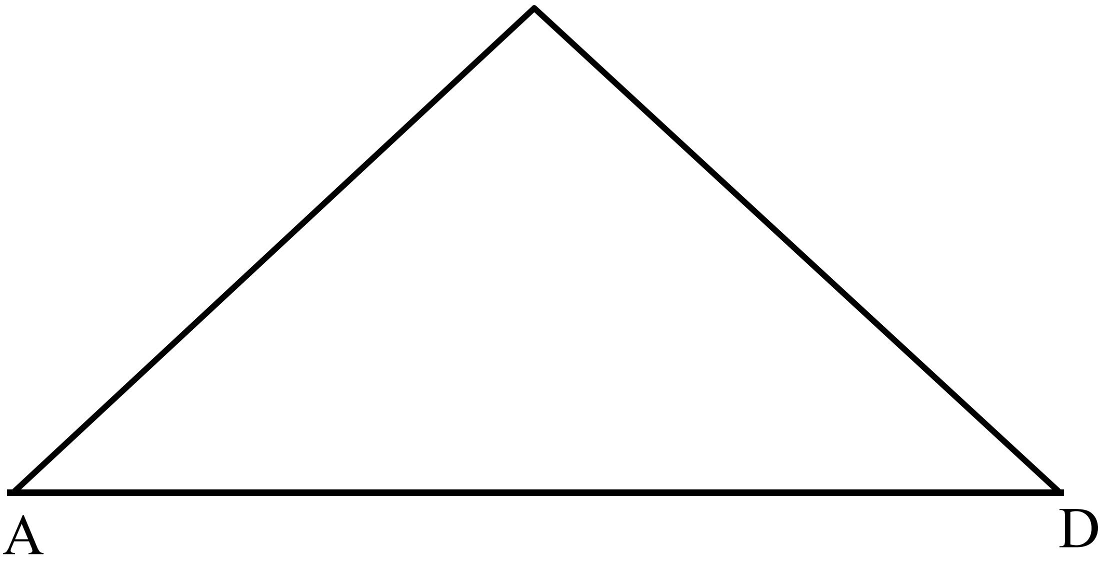

Figure B.1: **Axial Force Diagram at beginning and end of a steady-state cycle for a short ($L \leq L_{anchor}$) line with a unilateral restraint at the optimal location. (A is the upstream end, D the downstream end.)**

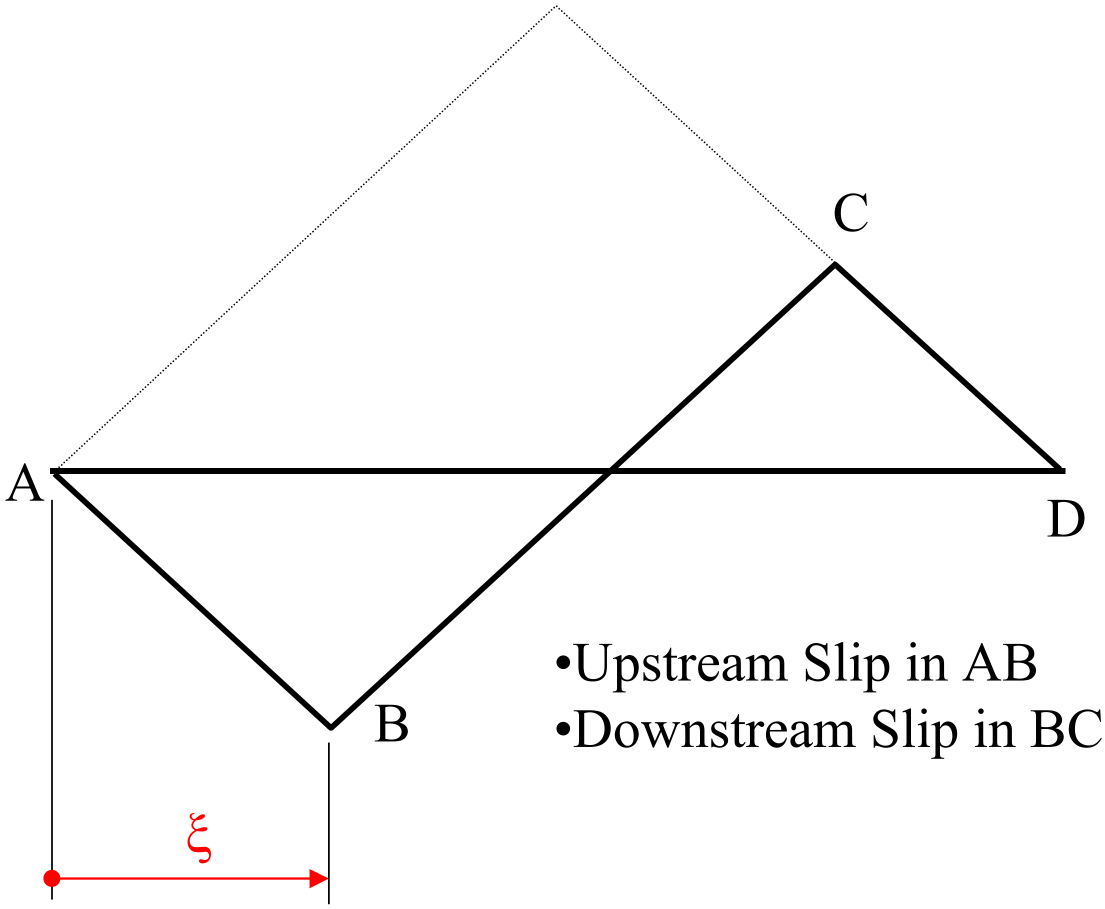

Figure B.2: **Axial force diagram during heating with $0 \leq \xi \leq L/2$.**

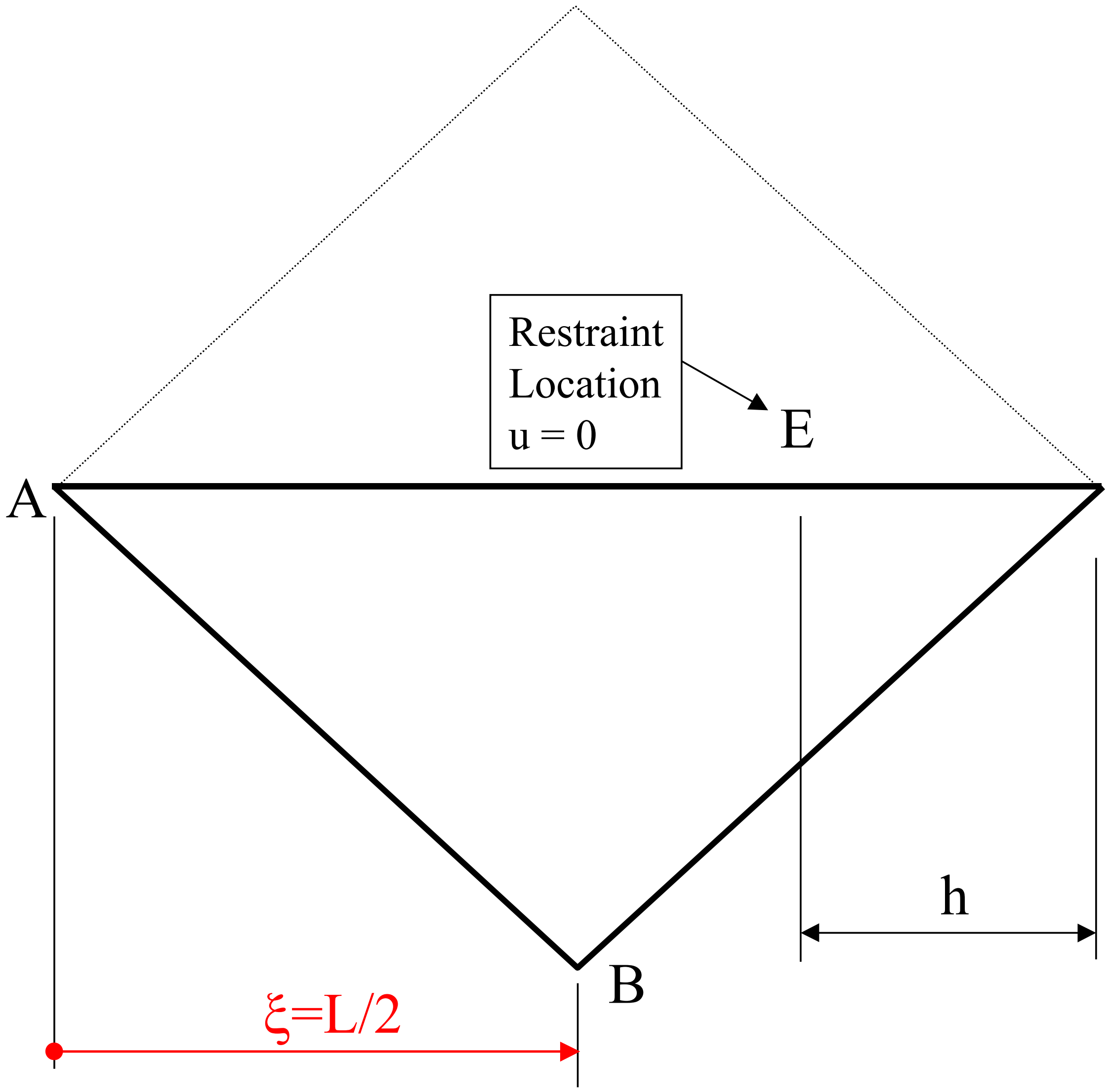

Figure B.3: **Axial force diagram during heating at ξ = L/2 (Temperature surge is at mid-line. Axial force downstream of the restraint location has reached its maximum possible value.).**

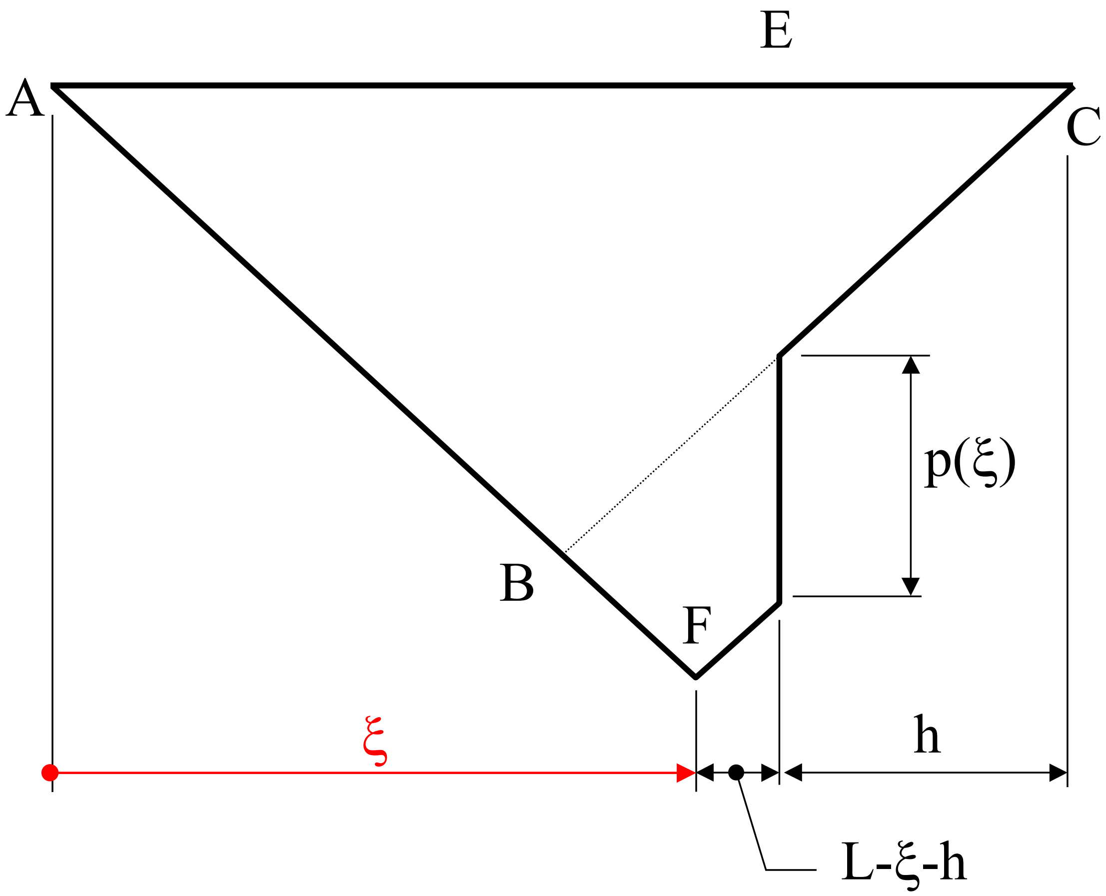

Figure B.4: **Axial force diagram during heating for $L/2 \leq \xi \leq L\text{-}h$. (Temperature front is in between the mid-line point and the restraint. Restraint is active, exerting a force $p=p(\xi)$ onto the line in the upstream direction.).**

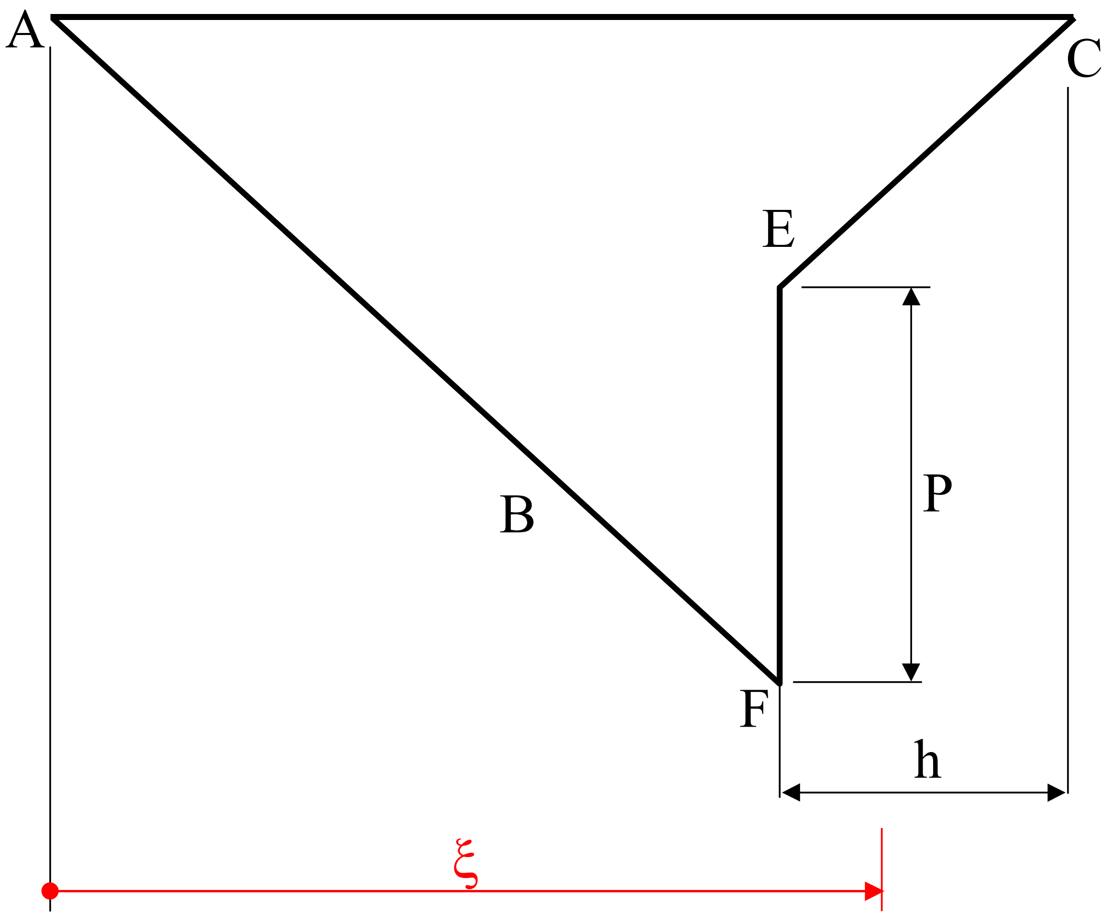

Figure B.5: **Axial force diagram during heating with L-h ≤ ξ ≤ L. (Temperature front is downstream of the restraint. There is no change in the axial forces, since the maximum possible axial compressive forces on the downstream side of the restraint have already been reached by the time the temperature front reached the restraint.).**

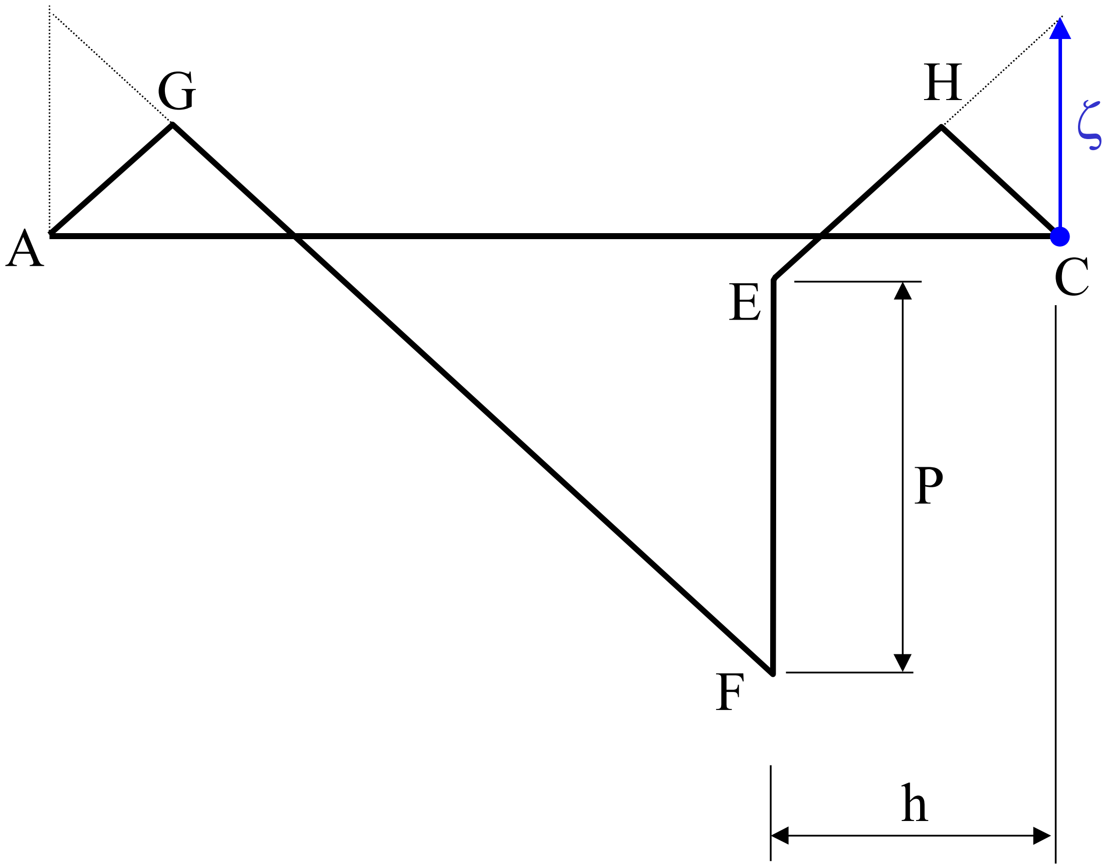

Figure B.6: **Axial force diagram during cooling with $0 \leq \zeta \leq 2h$. (Inward slip occurs in regions AG and HC only.).**

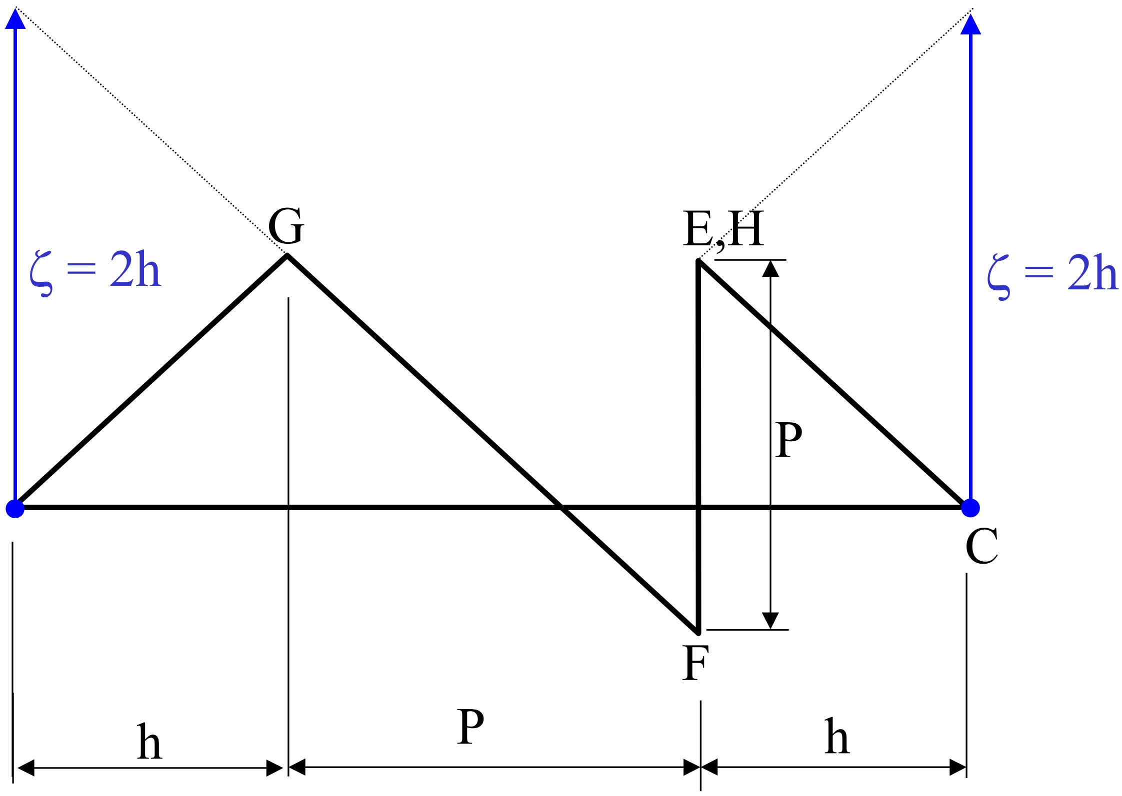

Figure B.7: **Axial force diagram during cooling at $\zeta = 2h$.**

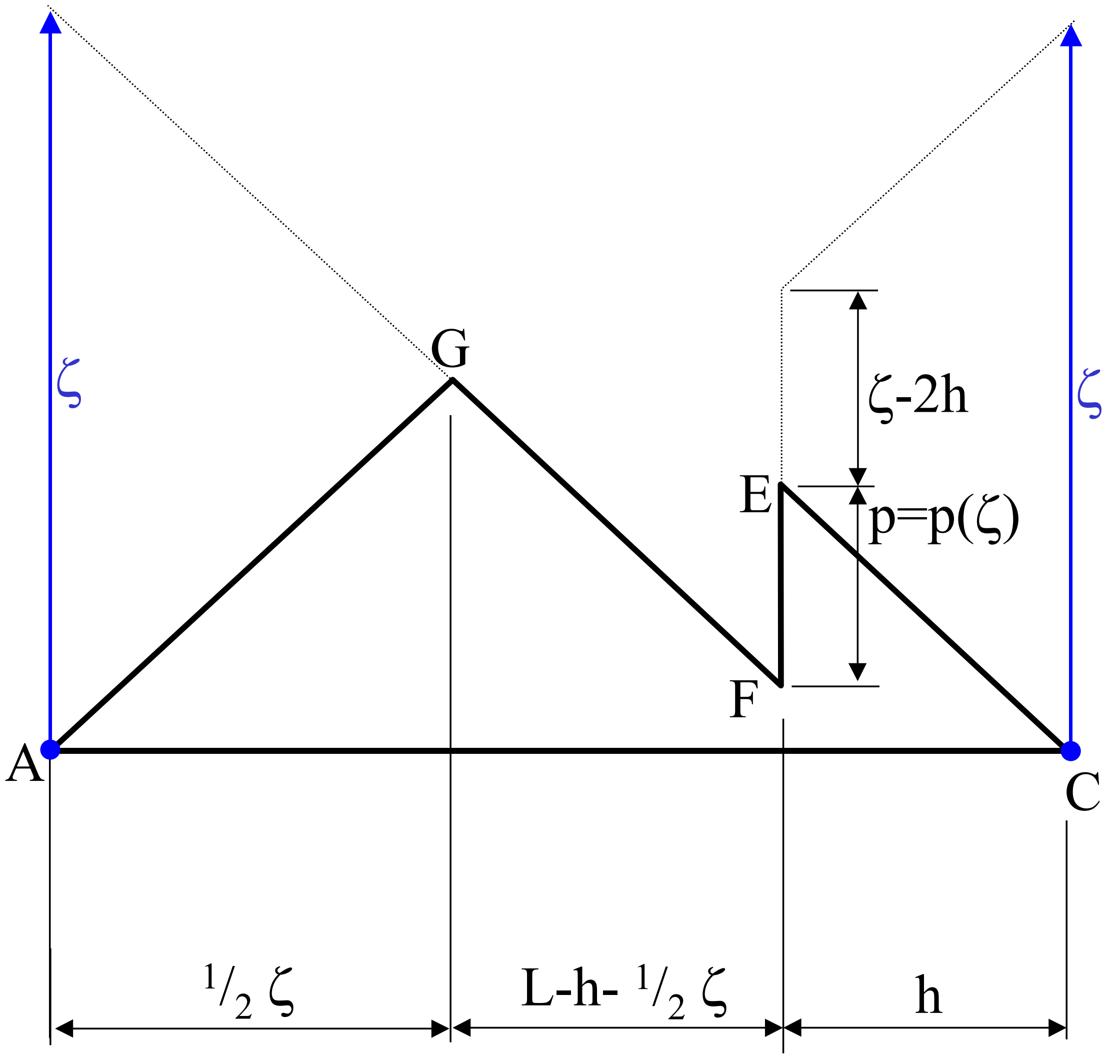

Figure B.8: Axial force during cooling in the range $2h \leq \zeta \leq L$.

APPENDIX C. FORTRAN SOURCE CODE FOR FINITE ELEMENTS USED IN SIMULATION OF PIPE CRAWL

A general purpose modular program npex developed at the University of Michigan is used for the finite element analyses reported in this report. For every type of element that is available to this program two subroutines are needed. One to read the required element properties from an input file, and another to calculate the element tangent stiffness matrix and nodal forces representing the resistance to deformation of the element. This appendix contains the source code of the element routines.

```
C
C Element for simulation dimensionless axial ratchetting problem.
C Assumptions:
C   Elastic pipe with axial deformations only.
C   Soil Friction model with linear pre-mobilisation response.
C   Travelling heat ramp over distance XRISE
C   Uniform colling between time THOT and TCOLD
C   Periodic temperature with period TCOLD.
C
      SUBROUTINE RELPROP_20(AELPROP,IELPROP,     !arrays
C input/output -->           o       o
     &   IEXFLAG,IU9STAT,NAELDAT1,NIELDAT1,      !scalars
C        i       i&o     i        i
     &   NEN,NAELPAR,NAELPROP,NDOF1,NIELPAR,NIELPROP,NSD1) !scalars
C        o   o       o        o     o       o        o
      IMPLICIT REAL*8 (A-H,O-Z)
      DIMENSION IELPROP(NIELDAT1),AELPROP(NAELDAT1)
C
C Read Element Data:
      WRITE(6,'(2X/
     &"  Element 20: dimensionless pipe axial ratchetting problem."/
     &"  unit values:"/
     &"    unit of axial force:         No"/
     &"    unit of length:              No/f"/
     &"    unit of axial displacement:  No^2/(f EA)"/
     &"  in which"/
     &"    No  = constrained axial force for max temp. change"/
     &"    f   = axial friction force per unit length"/
     &"    EA  = axial rigidity of pipe"/
     &"  "/
     &"  Element Properties are:"/
     &"    UMOB = dimensionless mobilisation displacement"/
     &"    XRISE = time & distance over which temperature rises"/
     &"    THOT  = max X plus Xrise"/
     &"    TCOLD = time when uniform cooldown is complete")')
      CALL RDRECNA(AELPROP,'UMOB,XRISE,THOT,TCOLD',21,IU9STAT,4)
      NEN=2                 !number of element nodes used
      NAELPAR=1             !number of real element parameters needed
      NAELPROP=4            !number of element properties needed (defined above)
      NDOF1=1               !number of degrees of freedom per node needed
      NIELPAR=0             !number of integer element parameters needed
      NIELPROP=0            !number of integer element properties needed (defined above)
      NSD1=1                !number of coordinates per node used by element
C
C Check storage requirements:
      CALL CHKINT(NIELPROP,NIELDAT1,'NIELPROP in nelmt20',19)
      CALL CHKINT(NAELPROP,NAELDAT1,'NAELPROP in nelmt20',19)
      RETURN
      END
C End of subroutine RELPROP_20
C
C
      SUBROUTINE GENELKP_20(AELPAR,AELPROP,
     &   ELK,ELP,ELP_L,
     &   ID,IELPAR,IELPROP,
     &   IEN,LM,
     &   U,UB_L,U0,X,
     &   IEL,IELFLAG,IGRP,ISTEP,NAELPAR,NAELPROP,NDOF,NDOF4BC,
     &   NELDOF,NELDOFI,
     &   NEN,NIELPAR,NIELPROP,NNODES,NSD,TIME,TIME0)
      IMPLICIT REAL*8 (A-H,O-Z)
      DIMENSION AELPAR(NAELPAR),AELPROP(NAELPROP),
     & ELK(NELDOF,NELDOF),ELP(NELDOF),ELP_L(NELDOF),
     & ID(NDOF4BC,NNODES),IELPAR(NIELPAR),IELPROP(NIELPROP),
```

```
     & IEN(NEN),LM(NELDOF),
     & U(NDOF,NNODES),UB_L(NDOF,NNODES),U0(NDOF,NNODES),X(NSD,NNODES)
C
C Local declarations:
      LOGICAL LF_INDIC
      DIMENSION UELB_L(2)
C
C Nodal quantities:

      NODE2=IEN(2)
      XX2=X(1,NODE2)
      UU2=U(1,NODE2)
      U02=U0(1,NODE2)
      UELB_L(2)=UB_L(1,NODE2)
      LM(2)=ID(1,NODE2)

      NODE1=IEN(1)
      XX1=X(1,NODE1)
      UU1=U(1,NODE1)
      U01=U0(1,NODE1)
      UELB_L(1)=UB_L(1,NODE1)
      LM(1)=ID(1,NODE1)

      NELDOFI=2

C
C Extract element properties & parameter:
      UMOB=AELPROP(1)
      XRISE=AELPROP(2)
      THOT=AELPROP(3)
      TCOLD=AELPROP(4)
      FF0=AELPAR(1)
C
C Element length (CLL), strain (EPS), and displ incr at Gaussian pt (DUG):
      CLL=XX2-XX1
      XXG=0.5D0*(XX2+XX1)
      EPS=(UU2-UU1)/CLL
      DUG=0.5D0*(UU2+UU1-U02-U01)
C
      IF(LF_INDIC(IELFLAG,4)) THEN  !===== fourier modes 4FM
        WRITE(6,'(2X/
     &"  **** Fourier Modes are not Available for This Element ****")')
        STOP
      ENDIF  !====LF_INDIC(IELFLAG,4)
C
C Compute Element out-of-balance load vector:
C   Calculation of temperature (TT) & time derivative (TT_L):
      TIME1=DMOD(TIME,TCOLD)
      IF(TIME1.GT.THOT) THEN
        TT_L=1.D0/(THOT-TCOLD)
        TT=TT_L*(TIME1-TCOLD)
      ELSE
        XI=(XXG-TIME1)/XRISE
        IF(XI.GT.0.D0) THEN
          TT=0.D0
          TT_L=0.D0
        ELSE IF(XI.LT.-1.D0) THEN
          TT=1.D0
          TT_L=0.D0
        ELSE
          TT=-XI
          TT_L=1.D0/XRISE
        ENDIF
      ENDIF
```

```
C   Calculation of axial force (CNN) and friction force (FF):
      CNN=EPS-TT
      SK0=1.D0/UMOB
      FF=FF0+SK0*DUG
      IF(FF.GT.1.D0) THEN
        FF=1.D0
        SK=0.D0
      ELSE IF(FF.LT.-1.D0) THEN
        FF=-1.D0
        SK=0.D0
      ELSE
        SK=1.D0/UMOB
      ENDIF
      TST=0.5D0*CLL*FF
      ELP(2)=-CNN-TST
      ELP(1)= CNN-TST
C
      IF(LF_INDIC(IELFLAG,1)) THEN
C  Calculate ELK:
        TST1=1.D0/CLL
        TST2=0.25D0*CLL*SK
        TST3=TST2+TST1
        TST4=TST2-TST1
        ELK(1,1)=TST3
        ELK(1,2)=TST4
        ELK(2,2)=TST3
        ELK(2,1)=TST4
C  Compute partial derivative ELP_L:
        ELP_L(1)=-ELK(1,1)*UELB_L(1)-ELK(1,2)*UELB_L(2)-TT_L
        ELP_L(2)=-ELK(2,1)*UELB_L(1)-ELK(2,2)*UELB_L(2)+TT_L
      ENDIF  !LF_INDIC(IELFLAG,1)
C
C Update element parameter if applicable:
      IF(LF_INDIC(IELFLAG,2)) AELPAR(1)=FF
C
C Print stresses in element:
      IF(LF_INDIC(IELFLAG,3)) THEN
        WRITE(6,'(" XXG,CNN,FF,TT",4G14.5)') XXG,CNN,FF,TT
      ENDIF   !LF_INDIC(IELFLAG,3)
      RETURN
      END
```

DISTRIBUTION

Report number	:	OP 02-30011
Title	:	Crawling of Pipelines under Cyclic Thermal Loading
Date of issue	:	January 2002
Author(s)	:	R. Peek
Reviewed by	:	P.R. Paslay and W.T. Jones
Owner/Custodian	:	R. Peek OGUP
		responsible for approving contents and distribution of report:
Project number	:	(remove field if not applicable)
Activity code	:	(remove field if not applicable)
Sponsor/customer	:	(remove field if not applicable)
Keywords	:	(remove field if not applicable)
Electronic file	:	(remove field if not applicable)
Issuing Library	:	Shell Global Solutions Int. B.V. The Hague
Distribution	:	**Shell Global Solutions Int. B.V. The Hague**

OGF/3 (Reports Library)	7
Michael Eckstein SDS, Woodcreek	1
Frans Kopp SDS, Woodcreek	1
Andries Otter SDS, Woodcreek	1
Ian Gardiner, SDS, Woodcreek	1
Uche Okonkwo SDS, Woodcreek	1
Ralf Peek, SGS NL	1
Paul R. Paslay	1
810 Bienville Street, Apt. 211	
New Orleans, LA 70112-3153	
USA	
Warren Jones, SGS US, Bellaire	1

Restrictions on distributions	:	US Export control applicable.
Additional distribution	:	Any additional distribution (outside the above mentioned distribution list) can only be effected with special permission of owner/custodian (see above).